

Terrestrial and Aquatic Nitrous Oxide Emissions

A DISSERTATION
SUBMITTED TO THE FACULTY OF
UNIVERSITY OF MINNESOTA
BY

Peter August Turner

IN PARTIAL FULFILLMENT OF THE REQUIREMENTS
FOR THE DEGREE OF
DOCTOR OF PHILOSOPHY

Timothy J. Griffis

October 2016

© Peter August Turner 2016

Acknowledgements

First, I would like to thank my advisor Dr. Tim Griffis whose guidance and support shaped this dissertation. Tim continually encouraged me to push my writing and research one-step further and for that, I am grateful. I am also appreciative of the feedback and tremendous advice provided by my committee members, including Drs. John Baker, Rod Venterea, and David Mulla.

I am thankful for the helpful discussions with Drs. Xuhui Lee, Jeff Wood, John Crawford, and Luke Loken. Further, all of the following projects were made possible with the technical and logistical support graciously provided by Bill Breiter, Matt Erickson, Mike Dolan, and Joel Fassbinder. Lastly, I am continually impressed by the level of collaboration and support by all those affiliated with the Biometeorology Group – including Zichong Chen, Ke Xiao, Kendall King, Natalie Schultz, Lucas Rosen, Ming Chen, Cody Winker, Cheng Hu, Peter Ganzlin, Michelle Dobbratz, and Meishan Roen. I am grateful for the private landowners, especially Mark Bauer, who allowed my access to their fields, all those affiliated with UMore Park in Rosemount, MN, and the USDA-ARS.

Special thanks to my parents and family for encouraging this endeavor and to those at the Willow Lake Farm for their stimulating agroecological insights. Lastly, big thanks to Kelly Zimmerman for the support and patience throughout.

Abstract

Agriculture has emerged as the foremost source of nitrous oxide (N_2O), a potent greenhouse gas and the dominant ozone depleting substance, in response to the widespread application of nitrogen (N) fertilizer. Globally, the magnitude of this source is well constrained based on long-term trends in atmospheric N_2O [Crutzen *et al.*, 2008]. However, large uncertainties remain at regional-scales where discussions around the development of scalable mitigation practices and policies will be implemented.

To estimate national or regional emissions, bottom-up emission inventories are created that predict N_2O losses by applying an emission factor (EF) to individual land-use activities. However, recent top-down validation exercises – performed using tall towers and aircraft, have determined that regional bottom-up models significantly underestimate North American agricultural emissions. As a result, benchmarking the success of widespread mitigation practices is hampered. The goals of this dissertation are, therefore, twofold: 1) isolate and revise the EF that is responsible for biasing the bottom-up N_2O emission inventory; and, 2) identify the underlying mechanisms that control emissions to help guide mitigation practices.

The emission factor for N leaching and runoff from agricultural fields (EF_{5r}) is one of the most uncertain components included in bottom-up inventories. Here, a full stream network approach shows that N_2O emissions decline exponentially with increasing Strahler stream order. This function was used to upscale emissions and revise the EF_{5r} , which determined that the default EF_{5r} had been underestimated by as much as 9-fold in bottom-up emission inventories. This correction brings regional bottom-up

inventories in line with top-down models, improving our confidence in these budgets when the riverine component is properly accounted.

However, uncertainty remains in the river biochemical conditions necessary to promote high aquatic emissions. Towards this end, data were collected using a novel gas equilibrator coupled to flow-through water quality sensors [Crawford *et al.*, 2015] to identify complex biochemical relationships. This freshwater data set, the world's largest and the first measurements from the Mississippi River, shows that dissolved N₂O concentrations plateau at high nitrate (NO₃⁻) concentrations. The decreasing N₂O response at higher NO₃⁻ concentrations is likely the result of environmental limitations on N processing – including, turbidity, dissolved oxygen, and carbon. However, this relationship suggests that if river models are accurate, the projected doubling of riverine NO₃⁻ export could amplify N₂O emissions by as much as 40%. Yet, this response could be diminished if environmental limits on N processing were imposed – including, decreased turbidity, highlighting an important tool to mitigate indirect N₂O emissions.

Mitigation of direct emissions from soils, the largest single component of the agricultural source, have been heavily discussed in the literature. However, due to the variability of N₂O production, the success of practices designed to mitigate emissions have been mixed. Here, two techniques to mitigate direct emissions were assessed. The first explored the effect that a kura clover living mulch had on N₂O emissions in a corn – soybean rotational field. Alternative management practices are becoming more common, yet their impact on N₂O emissions is not well understood. As a legume, kura clover provides a N-credit to the crop, allowing farmers to reduce their application of synthetic

fertilizer, which may reduce N₂O losses. Contrary to our hypothesis, elevated emissions from the kura clover treatment during periods of soil disturbance, plant stress, and post-anthesis significantly increased N₂O losses relative to the non-kura clover treatment.

Lastly, the importance of emission “hotspots” in the field-scale N₂O budget was assessed by resolving N₂O emissions at a high spatial resolution using geospatial analyses. These data and analyses determined that hotspots were responsible for a disproportionate share of the field-scale emissions, despite occupying a limited area of the field. From these measurements, targeted management of N₂O hotspots could be used to efficiently reduce field-scale emissions by as much as 17%. The findings presented here provide a roadmap for policy makers and farm managers to proactively address and mitigate agricultural N₂O emissions.

Table of Contents

Acknowledgements.....	i
Abstract.....	ii
List of Tables	ix
List of Figures.....	x
Chapter 1: Introduction.....	1
Chapter 2: Indirect nitrous oxide emissions from streams within the US Corn Belt scale with stream order	7
Overview.....	8
Significance.....	9
Introduction.....	9
Results and Discussion	12
Materials and Methods.....	20
N ₂ O Flux Sampling.....	20
Upscaling	21
Acknowledgements.....	22
Appendix.....	27
Chapter 3: Regional-scale controls on dissolved nitrous oxide in the Upper Mississippi River.....	31
Overview.....	32
Introduction.....	32
Materials and Methods.....	34

Site Description.....	34
Water Sampling	35
Ensemble Regression Trees	39
Results and Discussion	39
Conclusions.....	43
Acknowledgments.....	44
Chapter 4: The Impact of Kura Clover Living Mulch on Nitrous Oxide Emissions in a Corn/Soybean System.....	49
Overview.....	50
Introduction.....	51
Methods and Materials.....	53
Site Description and Experimental Design.....	53
Nitrous Oxide Emissions	55
Climate, Soil, and Plant Analyses.....	56
Data Analysis and Statistics.....	57
Results and Discussion	58
2013 – Corn.....	58
2014 – Soybeans	59
Prior to Strip-Tillage.....	59
Strip-Tilling and Planting	60
Mowing.....	60
Suppression Spraying.....	61

Fertilizer Application	62
Post-Anthesis Mineralization.....	62
Irrigation	63
Indirect Emissions.....	64
Conclusions.....	64
Acknowledgements.....	65
Chapter 5: A geostatistical approach to identify and mitigate agricultural nitrous oxide	
emission hotspots	69
Highlights.....	70
Overview.....	70
Introduction.....	71
Materials and Methods.....	73
Site Description and Experimental Design.....	73
Nitrous Oxide Measurements	76
Soil Analyses	77
Geostatistical Analyses	78
Results and Discussion	79
Meteorology and Soil Characteristics.....	79
N ₂ O Emissions.....	80
Conclusions.....	86
Acknowledgements.....	87
Appendix.....	94

Chapter 6: Conclusion.....	95
Future Research Directions.....	99
“Legacy” Nitrogen.....	99
Machine Learning Applications.....	99
Agricultural Drainage.....	100
Moving Forward.....	100
References.....	103

List of Tables

Table 2.1. The daily average N₂O flux (mg N₂O-N m⁻² d⁻¹), NO₃⁻ concentrations (mg NO₃⁻ kg⁻¹), and moisture content.

Table 3.1. The mean (SD) of N₂O_{sat}, N₂O_{FLUX} (nmol N₂O-N m⁻² s⁻¹), NO₃⁻ (mg N L⁻¹), DO (% Saturation), Chl-*a* (RFU), Turbidity (FNU), *f*DOM (QSU), and temperature (°C) during each sample campaign.

Table 4.1. The cumulative emissions and results from statistical analyses from each activity period during the two sample years. The numbered intervals correspond to Figure 4.1. Sample size (*n*) excludes instrument downtime. The total emissions during a measurement interval are reported while the difference between treatments (kura clover – corn-soybean) has been given. Significance was determined using paired *t*-tests were performed on the log-transformed emissions over the listed DOY range.

List of Figures

Figure 2.1. The relation between N₂O flux and the Strahler stream order in southeastern Minnesota. The black line represents the best fit of an exponential function to the mean flux values measured at each stream order. Red lines represent the 95% confidence interval of the model fit and error bars indicate one standard deviation from the mean.

Figure 2.2. Results from upscaling N₂O emissions. a) A comparison of local indirect N₂O-N sources from default IPCC EFs and our scaling method. b) Total US Corn Belt emissions from the three methods. c) The flux densities from the tall-tower source footprint for each method.

Figure 2.3. The first-order default EF_{5r} underestimation from the Corn Belt region. The bias is defined as the difference between IPCC EF_{5r} emissions and the results from stream order scaling.

Figure 3.1. The seasonal and spatial dynamics of N₂O_{sat} in Pool 8 of the UMR in a) April ($n = 298$), b) August ($n = 828$), and c) October ($n = 514$).

Figure 3.2. Inset) Agricultural land use within the UMR basin. Row-crop (brown) and pasture (yellow) were drawn using information from the National Land Cover Database (2011). a). The regional-scale variability of N₂O_{sat} in the UMR ($n = 1,553$). Hotspots and coldspots of b) N₂O_{sat} and c) NO₃⁻.

Figure 3.3. Relative predictor importance (RPI) determined using ensemble ($n = 500$) regression trees to predict N₂O_{sat} observations. Red and blue bars denote positive and negative relationships, respectively. The variable importance describes the explanatory power of a predictor on the N₂O_{sat} response. The pseudo R^2 was determined from an

observed $\text{N}_2\text{O}_{\text{sat}}$ vs. predicted $\text{N}_2\text{O}_{\text{sat}}$ determined from the ensemble regression model.

Each value was normalized to the most important predictor in each system where a) is the RPI of the regional-scale measurements, b) is the seasonal (April, August, October) RPI from Pool 8.

Figure 3.4. Measurements of N_2O and NO_3^- from the UMR basin. The dashed line is the Michaelis-Menten function derived from the regional-scale campaign ($n = 1,553$).

Figure 4.1. Daily area-scaled N_2O fluxes (symbols) and cumulative emissions (lines) for (A) 2013 and (B) 2014 averaged ($n = 4$) by treatment. Missing data due to instrument downtime were not gap filled. Cumulative emissions represent the sum of treatment daily averaged fluxes throughout the measurement period. Dotted vertical lines and numbers correspond with emission intervals described in Table 4.1.

Figure 5.1. Boxplots of a) NO_3^- concentration ($\text{mg NO}_3^- \text{ kg}^{-1}$), b) gravimetric moisture content (%), and c) N_2O flux density ($\text{mg N}_2\text{O-N m}^{-2} \text{ d}^{-1}$). Red points designate outliers.

Figure 5.2. Plotted relationships between topographic indices and soil characteristics ($n = 129$). Top row). Mean soil NO_3^- concentration (blue dots); mean gravimetric water content (θ ; green triangles). Bottom row). Integrated soil NO_3^- ($\text{NO}_3^-_{\text{int}}$; blue dots); integrated gravimetric water content (θ_{int} ; green triangles).

Figure 5.3. Plotted relationships between mean N_2O fluxes (a, b, and c) and cumulative N_2O emissions (d, e, and f) over the measurement period against topographic indices ($n = 60$). Lines of linear best fit (red lines) for each graph are included.

Figure 5.4. The Wetland Probability Index (WPI) overlain with chamber measurements (blue circles) and soil samples (red diamonds). Results are presented from the N_2O

ordinary cokriging model, which interpolated mean flux density and cumulative emissions at a 1-m spatial resolution.

Figure 5.5. The relationship between cumulative N₂O emissions and the soil characteristics, NO₃⁻_{int} and θ_{int}. A linear line of best fit is included (red).

Figure 5.6. Results from the Getis Ord Gi* statistic that was used to identify the spatial distribution of hotspots and coldspots. Intermediate locations are transparent.

Chapter 1

Introduction

Advancements in technology have stimulated global crop productivity to unprecedented levels that are now capable of supporting the basic needs of more than seven billion people annually. One innovation, the manufacture of synthetic nitrogen (N) fertilizers *via* the Haber-Bosch process, has been credited with averting a *Malthusian* crisis [Trewavas, 2002] by removing the N limitation and thereby promoting high yielding crops. Despite modernization efforts that have made food production more efficient than ever, global demand for N continues to rise at rate of 1.8 Tg N yr⁻¹ [FAO, 2015]. Agroecosystems also receive N from atmospheric deposition and organic sources, such as manure and legume species. Cumulatively, these sources (synthetic + organic) exceed 170 Tg N yr⁻¹ globally [Smil, 1999]. However, as much as 70% can be lost to the water and atmosphere [Galloway *et al.*, 2003], of which 4% [Crutzen *et al.*, 2008] is converted to nitrous oxide (N₂O), a powerful greenhouse gas [Hartmann *et al.*, 2013] and stratospheric ozone depleting substance [Ravishankara *et al.*, 2009].

Consequently, the ambient concentration of N₂O has risen steadily, up 20% from the pre-industrial estimate [Hartmann *et al.*, 2013]. This rise is largely attributed to agricultural systems, which account for between 60-80% of the anthropogenic N₂O emission budget [Davidson, 2009; Davidson and Kanter, 2014; US Department of State, 2014]. Therefore, strong emissions occur where climate allows for efficient crop production. For instance, the United States Corn Belt, one of the most intensively cultivated areas on Earth, produces 40% of the world's grain [NRCS, 2012] and consumes nearly 60% (7 Tg N yr⁻¹) of the national fertilizer budget. Here, measurements from tall-towers note ambient N₂O concentrations that are up to 3 ppb greater than non-

cultivated locations [Griffis *et al.*, 2013]. The agricultural signal can also be seen globally; a latitudinal tropospheric N₂O gradient has emerged whereby Northern Hemisphere concentrations are 2 ppb higher than those in the Southern Hemisphere [Hartmann *et al.*, 2013] in response to the strong agricultural sources in North America, Europe, and Asia.

Signatories to the United Nations Framework Convention on Climate Change are obligated to create a national N₂O emission inventory. These “bottom-up” inventories are generated using emission factors (EFs)¹ to estimate the cumulative emissions given a limited set of activity data [De Klein *et al.*, 2006]. These EFs have been constrained from field and laboratory experiments with national-scale integration in mind. Because bottom-up emission inventories are necessary tools for treaty benchmarking and objective policy assessment, their accuracy is essential. However, top-down emission constraints – including those from tall-towers [Miller *et al.*, 2012; Griffis *et al.*, 2013; Zhang *et al.*, 2014; Chen *et al.*, 2016] and aircraft [Kort *et al.*, 2008], indicate that bottom-up emission inventories significantly underestimate the agricultural N₂O source. To reconcile bottom-up and top-down inventories, many hypothesize that one or more EFs are underestimated [Griffis *et al.*, 2013; Zhang *et al.*, 2014]. Yet, the episodic and spatially variable nature of N₂O fluxes has made the determination of which EF is biased, and to what extent, challenging.

¹ Emission factors provide a first-approximation of annual N₂O emissions given known land-use and activity data.

The goals of this dissertation are therefore to: 1) quantify the strength of indirect N₂O emissions from leaching and runoff and revise the EF (EF₅) accordingly; and, 2) identify the underlying mechanisms that control direct and indirect emissions in order to help guide N₂O mitigation practices. The findings presented here provide a roadmap for policy makers and farm managers to address agricultural N₂O.

In Chapter 2, the indirect emission factor for leaching and runoff (EF₅), the most uncertain EF included in bottom-up inventories [Nevison, 2000], is assessed. This EF describes the quantity of N₂O emitted offsite in response to agriculturally linked N that flows through groundwater (EF_{5g}), rivers (EF_{5r}), and eventually into estuaries (EF_{5e}). Of these components, the accuracy of the EF_{5r} is the most contentious, as some suggest it may underestimate N₂O emissions in agricultural areas [Beaulieu *et al.*, 2011; Outram and Hiscock, 2012]. The large uncertainty in the EF_{5r} has been caused by a paucity of studies [Clough *et al.*, 2006] and a wide range of river morphology types [Beaulieu *et al.*, 2008]. Although river morphology, semi-quantitatively described by the Strahler stream order, directly effects the turbulent exchange of mass across the air – water interface [Butman and Raymond, 2011], its relationship with the flux of N₂O has not yet been assessed. Here, a portable floating chamber system is used to measure emissions across a Strahler stream order gradient in a dense agricultural region. These measurements, coupled with high-resolution stream network and fertilizer data sets, are used to provide a robust revision of the EF_{5r}. This chapter concludes with an upscaling exercise to estimate total riverine emissions from the United States Corn Belt.

Constraining which variables regulate N₂O emissions from agriculturally impacted rivers in the United States Corn Belt is a necessity for policy and emission model forecasting. This heavily modified agricultural region is largely drained by the Upper Mississippi River. Consequently, the effects of excess nitrate (NO₃⁻) here have been studied extensively [Turner and Rabalais, 1991], yet N₂O dynamics in the Upper Mississippi River have not yet been observed. Towards this end, data collected using a novel flow-through sensor platform are presented in Chapter 3 to describe regional N₂O patterns and their biochemical controls in the Upper Mississippi River. These data and analyses provide insight into mechanisms that may limit indirect N₂O emissions and provides insights regarding future emissions given specific NO₃⁻ modelling projections and policy targets.

Chapter 4 addresses direct N₂O emissions from agricultural soils, one of the largest individual sources included in bottom-up emission inventories [Davidson, 2009]. The mitigation of direct emissions generally focuses on improving field-scale nitrogen management practices, including fertilizer timing and source optimization. Although alternative management practices, like living mulches, which provide N benefits are experiencing greater use. A living mulch is a technique whereby a perennial cover crop is grown with the crop, and is capable of reducing NO₃⁻ leaching [Ochsner *et al.*, 2010] while fixing additional N [Baker, 2012]. However, N₂O measurements from these systems are rare and must be explored so farmers can manage with respect to N₂O emissions. Here, the first N₂O measurements from a kura clover based living mulch are reported, which allow for a thorough exploration of direct emissions in these systems.

Static chambers are the most common method to measure soil N₂O emissions, yet the accuracy of a field-scale budget is limited by N₂O production mechanisms that vary widely throughout a field. As a result, N₂O measurement campaigns yield a high degree of uncertainty, due in large part to emission “hotspots”. Such sources generally appear in low-lying areas [*Ambus and Christensen, 1995*] where flow paths converge [*McClain et al., 2003*] to support disproportionately high rates of denitrification. In Chapter 5, emission and soil sample data sets are coupled with geospatial analyses, to resolve N₂O emissions at a high-spatial resolution. These data and analyses highlight the options available to mitigate agricultural N₂O hotspots and an estimation of their potential emission benefits.

Chapter 2

Indirect nitrous oxide emissions from streams within the US

Corn Belt scale with stream order

Peter A. Turner, Timothy J. Griffis, Xuhui Lee, John M. Baker, Rodney T. Venterea, and Jeffrey D. Wood (2015), *Proceedings of the National Academy of Sciences*, (112), 32, 9839-9843, doi: 10.1073/pnas.1503598112

© National Academy of Sciences

Overview

Nitrous oxide (N₂O) is an important greenhouse gas and the primary stratospheric ozone depleting substance. Its deleterious effects on the environment have prompted appeals to regulate emissions from agriculture, which represents the primary anthropogenic source in the global N₂O budget. Successful implementation of mitigation strategies requires robust bottom-up inventories that are based on emission factors (EFs), simulation models, or a combination of the two. Top-down emission estimates, based on tall-tower and aircraft observations, indicate that bottom-up inventories severely underestimate regional and continental scale N₂O emissions, implying that EFs may be biased low. Here, we measured N₂O emissions from streams within the US Corn Belt using a novel chamber-based approach and analyzed the data as a function of Strahler stream order (S). N₂O fluxes from headwater streams often exceeded 29 nmol N₂O-N m⁻² s⁻¹ and decreased exponentially as a function of S . This relation was used to scale up riverine emissions and to assess the differences between bottom-up and top-down emission inventories at the local to regional scale. We found that the Intergovernmental Panel on Climate Change (IPCC) indirect EF for rivers (EF_{5r}) is underestimated up to 9-fold in southern Minnesota, which translates to a total Tier 1 agricultural underestimation of N₂O emissions by 40%. We show that accounting for zero-order streams as potential N₂O “hotspots” can more than double the agricultural budget. Applying the same analysis to the US Corn Belt demonstrates that the IPCC EF_{5r} underestimation explains the large differences observed between top-down and bottom-up emission estimates.

Significance

N₂O emissions from riverine systems are poorly constrained, giving rise to highly uncertain indirect emission factors that are used in bottom-up inventories. Using a novel, non-steady-state flow-through chamber system, N₂O fluxes were measured across a stream order gradient within the US Corn Belt. The results show that N₂O emissions scale with the Strahler stream order. This information was used to estimate riverine emissions at the local and regional scales and demonstrates that previous bottom-up inventories based on the IPCC default values have significantly underestimated these indirect emissions.

Introduction

N₂O is projected to remain the dominant stratospheric ozone depleting substance of the 21st century [Ravishankara *et al.*, 2009] and is a powerful greenhouse gas (GHG) that currently accounts for about 6% of the net radiative forcing associated with long-lived anthropogenic GHGs [Hartmann *et al.*, 2013]. The detrimental environmental impacts of N₂O have stimulated appeals to regulate emissions from agricultural lands [Ravishankara *et al.*, 2009; Kanter *et al.*, 2013], which account for nearly 80% of the global anthropogenic N₂O budget [Crutzen *et al.*, 2008; Davidson, 2009]. The successful regulation and mitigation of N₂O emissions requires a sound understanding of the direct and indirect emission processes and reduced uncertainty regarding the emission factors (EFs) [Shcherbak *et al.*, 2014].

The IPCC Tier 1 approach uses EFs to provide first-order approximations of

annual N₂O emissions based on mechanistic and empirical information that have been constrained by field studies. These EFs are widely used in bottom-up inventories such as the Emission Database for Global Atmospheric Research² (EDGAR) and the Global Emissions Initiative³ (GEIA). These inventories are essential tools for tracking country specific emission trends, assessing thresholds for international treaties, and for evaluating the impacts of mitigation policies. Recent independent top-down estimates note large discrepancies with these bottom-up inventories.

Tall-tower and aircraft-based top-down studies use atmospheric concentration data to estimate landscape N₂O fluxes. Several studies using these approaches demonstrate that bottom-up inventories underestimate N₂O emissions by up to 9-fold in the Midwest United States Corn Belt [*Kort et al.*, 2008; *Miller et al.*, 2012; *Griffis et al.*, 2013; *Zhang et al.*, 2014], implying that some EFs are too small. An important problem, therefore, is determining which EFs are biased low and how to reduce their uncertainty.

Bottom-up N₂O emission inventories include direct and indirect emission pathways. Direct emissions describe the loss of N₂O produced in soils by microbial processes (e.g. nitrification and denitrification). This source is arguably well-constrained as a consequence of more than 1000 chamber-based emission studies [*Stehfest and Bouwman*, 2006; *Shcherbak et al.*, 2014]. Plant N₂O fluxes, although neglected in direct emissions inventories, appear to be negligible [*Zhang et al.*, 2014]. The relatively low direct emission uncertainty range (0.4 – 3.8 Tg N yr⁻¹) [*Nevison*, 2000] suggests that this

² European Commission (2011), Joint Research Centre/Netherlands Environmental Assessment Agency. Emissions database for Global Atmospheric Research, v.4.2, <http://edgar.jrc.ec.europa.eu>

³ IGAC/iLEAPS/AIMES (2014), Global Emissions Initiative (GEIA), <http://www.geiacenter.org>

EF (0.003 – 0.03) [De Klein *et al.*, 2006] is well constrained.

Indirect emissions represent the aggregate of N₂O production from leaching and runoff, human sewage, and atmospheric deposition of reactive nitrogen. Global indirect emission estimates range from 0.23 – 11.9 Tg N yr⁻¹ [Mosier *et al.*, 1998] and represent nearly two thirds of the uncertainty in the total global N₂O budget [Nevison, 2000]. In fact, the EF for leaching and runoff (IPCC emission factor: EF₅), which includes emissions from groundwater (EF_{5g}), rivers (EF_{5r}), and estuaries (EF_{5e}), is the single largest source of uncertainty in the bottom-up inventory [Nevison, 2000]. In the 2006 IPCC Emission Guidelines report, the EF₅ value was reduced from 0.025 to 0.0075 by reducing both the EF_{5g} and EF_{5r} to 0.0025 in response to two studies from New Zealand and the United Kingdom [De Klein *et al.*, 2006]. Although recent studies [Beaulieu *et al.*, 2011; Outram and Hiscock, 2012; Hinshaw and Dahlgren, 2013; Yu *et al.*, 2013] suggesting riverine N₂O loss is underestimated by up to 3-fold notably contradict the EF_{5r} reduction.

Uncertainty in the EF_{5r} can be attributed to a scarcity of studies [Clough *et al.*, 2006, 2007], poorly constrained water-air gaseous exchange relationships [Cole and Caraco, 1998; Beaulieu *et al.*, 2012], and high variability in river morphology [Beaulieu *et al.*, 2008; Wang *et al.*, 2009]. Further, the EF_{5r} assumes a linear relation between nitrate in water and N₂O emissions [Nevison, 2000], the validity of which is the subject of considerable debate [Rosamond *et al.*, 2011, 2012; Xia *et al.*, 2013; Venkiteswaran *et al.*, 2014]. Finally, N₂O fluxes derived from simple gas exchange models have been shown to underestimate the flux if stream channel hydraulics (i.e. stream flow velocity) are

ignored [Reay *et al.*, 2003], highlighting that stream chemistry alone is not an accurate predictor of N₂O fluxes.

We posit that the indirect N₂O fluxes in agricultural landscapes are highly dependent on stream hierarchy, which is semi-quantitatively represented with the Strahler stream order (S), a numerical classification system. Here, we demonstrate that with detailed knowledge of S , N₂O fluxes can be scaled up to the region and help to resolve the discrepancy between top-down and bottom-up N₂O emission estimates in the US Corn Belt.

Results and Discussion

N₂O fluxes in southeastern Minnesota were measured in streams of varying S over a two year period. A total of nineteen stream systems, representing nine stream orders, were sampled. An exponential function was used to describe the relationship between observed N₂O fluxes (F , nmol N₂O-N m⁻² s⁻¹) and S ,

$$F = b_0 \exp(-b_1 * S) \quad (\text{Equation 2.1})$$

where $b_0 = 34 \pm 10.2$ (95% confidence interval), $b_1 = 0.73 \pm 0.2$, with $R^2 = 0.95$ and 0.58 for binned ($n = 9$) and raw data ($n = 200$), respectively (Figure 2.1). Fluxes ranged from below the chamber system detection limit of 0.018 nmol N₂O-N m⁻² s⁻¹ (i.e. for the Mississippi River; $S = 9$) to a maximum observed flux of 34.5 nmol N₂O-N m⁻² s⁻¹ in a headwater stream ($S = 1$). A Kruskal-Wallis significance test revealed a significant mean rank difference ($p < 0.05$) in fluxes for headwater streams versus all other stream orders. Further, there was a significant rank difference between fifth – ninth-order streams while

there was no rank difference detected in second – fifth-order streams. The differences were greatest when testing non-sequential stream orders.

We hypothesize that the exponential decline in N₂O flux is the result of both weakened concentration gradient and lower piston velocities (*k*) in higher order streams. Riverine N₂O fluxes are a product of the concentration gradient between the surface water and the overlying atmosphere and a physical gas transfer coefficient [Raymond and Cole, 2001]. We propose two possible mechanisms underlying the emergent pattern shown in Figure 2.1 including: 1. Decreased *in-situ* N₂O production and loading; and, 2. Decreased gas exchange rates.

Mechanism 1: Headwater streams form from surface and subsurface runoff that, in regions with a high density of row crop agriculture, have high nitrate and ammonium loads and as a consequence, approximately 45-50% of a watershed's inorganic nitrogen transport can occur in these systems [Peterson *et al.*, 2001; Alexander *et al.*, 2007]. Nitrogen is rapidly transformed *via* nitrification and removed through denitrification [Mulholland *et al.*, 2008] in headwater streams [Peterson *et al.*, 2001] and these processes can quickly produce a surplus of N₂O in the water column. However, the average first-order rate of nitrogen loss within stream channels declines by as much as 90% down the stream order continuum [Alexander *et al.*, 2000]. Therefore, production potential declines as stream order increases. Accordingly, we observed a decline in surface water N₂O concentrations from super-saturated (>1000%) in second-order streams to near equilibrium with atmospheric N₂O in fourth-order streams. Groundwater dissolved gas inputs are an additional N₂O source and are most impactful in low flow

headwater systems [Jones and Mulholland, 1998]. However, groundwater loading has less of an effect on stream water chemistry with rising stream order (i.e. due to the water volume dilution effect) [Jones and Mulholland, 1998]. Collectively, with increasing stream order, N₂O production potential and loading progressively decline, which could account for the pattern shown in Figure 2.1.

Mechanism 2: Exchange across the water-atmosphere interface of supersaturated gases is governed by k , which describes the turbulent nature of the stream. An inverse relationship between $k\text{CO}_2$ and S has been observed [Butman and Raymond, 2011; Raymond et al., 2012, 2013; Crawford et al., 2013] and as a consequence, the highest $k\text{CO}_2$ values are frequently observed in headwater streams [Butman and Raymond, 2011; Wallin et al., 2011; Crawford et al., 2013; Raymond et al., 2013]. The same relationship after adjusting for the Schmidt number should be applicable to N₂O, implying that $k\text{N}_2\text{O}$ increases with declining stream order. Localized areas with high k values (i.e. riffles) have been shown to be strong emission sources [Reay et al., 2003] if streams are supersaturated (e.g. Mechanism 1). However, if the stream is not supersaturated, a high k value alone cannot generate a large flux. Further, a lower k implies a longer total residence time (age) and therefore, a greater probability of N₂O reacting with nitrous oxide reductase (*nos*), the enzyme that catalyzes the final step in the denitrification reaction sequence – the reduction of N₂O to N₂ [Maier et al., 2009]. Although this has not been documented in river systems, this potential mechanism merits further research to determine its importance and its ability to weaken the water-atmosphere N₂O concentration gradient. We posit that these two mechanisms, individually or combined,

account for the relationship observed in Figure 2.1 and require further study in order to elucidate their relative importance.

In our study, the variability of N₂O flux (i.e. the standard deviation) scaled with stream order, leading to a tightly constrained relation for high order systems (Figure 2.1). These observations imply a robust constraint on high order (fifth-order and higher) emissions and that this pattern could be applied to similar systems [Beaulieu *et al.*, 2010]. Conversely, much larger uncertainty in low ordered systems [Hasegawa *et al.*, 2000; Harrison and Matson, 2003] exists, indicating that caution must be taken before generalizing our scaling function outside of the US Corn Belt. Headwater streams displayed the greatest uncertainty and their high variability has also been noted in CO₂ evasion work [Crawford *et al.*, 2013]. Low order streams receive tile drainage outflow and groundwater from springs giving rise to localized “hotspots” of N₂O loss [Hasegawa *et al.*, 2000], similar to those seen in methane evasion work [Crawford *et al.*, 2013].

To test the appropriateness of the default IPCC EF_{5r} value, we used Equation 1 to up-scale emissions within the observed concentration footprint (50 km radius) of our tall-tower N₂O flux station [Griffis *et al.*, 2013]. Land use in this study area consists of 70% crops and pasture, 14% mixed vegetation, 11% forest, 3% developed, 2% open water and is representative of the US Corn Belt. Streams in the area represent only a small fraction (0.16%) of the total surface area. Using default IPCC EFs for direct and indirect emissions, we provide a conservative estimate of the local agricultural N₂O budget in addition to our up-scaled riverine emissions.

Whole-river emissions are the product of our scaling function and river area over a predicted ice-free period. We estimated the annual riverine N₂O loss by coupling Equation 1 with detailed geospatial datasets on stream length and width. Headwater streams ($S = 1$) were the strongest sources, emitting 60% of the riverine budget. The remaining streams in the study area ($S = 2$ through 5) contributed 14%, 8%, 10%, and 8% to the up-scaled riverine emission budget, respectively. This disproportionate flux distribution was a result of a 3-fold greater mean flux density from headwater streams ($17.1 \text{ nmol N}_2\text{O-N m}^{-2} \text{ s}^{-1}$) than second-order streams ($5.7 \text{ nmol N}_2\text{O-N m}^{-2} \text{ s}^{-1}$).

Using the IPCC Tier 1 methodology [De Klein *et al.*, 2006], the total agricultural (direct + indirect) N₂O emissions from the tall-tower footprint were $0.2 \text{ Gg N}_2\text{O-N yr}^{-1}$ which corresponds to a flux density of $0.25 (0.08 - 0.6) \text{ nmol N}_2\text{O-N m}^{-2} \text{ s}^{-1}$. Indirect and direct sources contributed 22% and 78%, respectively to the Tier 1 budget. Here, the default EF_{5r} predicts that rivers emitted $0.01 \text{ Gg N}_2\text{O-N yr}^{-1}$, which represents just over 5% of the total N₂O-N emissions. Our scaling method predicted a riverine source of $0.09 (0.04 - 0.18) \text{ Gg N}_2\text{O-N yr}^{-1}$ (Figure 2.2a), an estimate that is 9 times greater than the source predicted by the default EF_{5r}, signaling a significant bottom-up bias in the EF_{5r}. Replacing the EF_{5r} with our scaling function suggests that the total Tier 1 bottom-up agricultural emissions have been underestimated by 40%. Accounting for this potential bias increases the predicted bottom-up flux density within the tall-tower source footprint to $0.36 \text{ nmol N}_2\text{O-N m}^{-2} \text{ s}^{-1}$ (Figure 2.2c). This estimate is in excellent agreement with the top-down tall-tower measured ensemble flux of $0.35 (0.3 - 0.4) \text{ nmol N}_2\text{O-N m}^{-2} \text{ s}^{-1}$ [Griffis *et al.*, 2013], indicating that top-down and bottom-up budgets can be reconciled

by applying our stream order scaling function. Our study suggests that an appropriate EF_{5r} for the tall-tower source footprint should be closer to 2%, assuming the average application rate of nitrogen fertilizer⁴ (88.8 kg N ha⁻¹), which is in agreement with a recent independent investigation [Outram and Hiscock, 2012].

Based on the Tier 1 methodology, we estimated the agricultural N₂O budget of the US Corn Belt at 58 (15 – 256) Gg N₂O-N yr⁻¹, of which 6% or 3.5 Gg N₂O-N yr⁻¹ emanates from rivers (Figure 2.2b). In this region, watersheds with high agricultural land use (>40%) occupy 93 million ha (58 million ha under active row-crop cultivation). Applying Equation 1 to these watersheds and using river area data, we obtained a riverine emission of 19.5 (9.3 – 41.2) Gg N₂O-N yr⁻¹. Our findings suggest that riverine N₂O emissions are underestimated by at least 16 Gg N₂O-N yr⁻¹ for the Corn Belt and on average by 29 kg N₂O-N km⁻² yr⁻¹ in watersheds whose cropland fractions are greater than 40% (Figure 2.3). This translates to a 27% increase in the total Tier 1 emission estimate from 58 to 75 Gg N₂O-N yr⁻¹ (Figure 2.2b). These results indicate that a more appropriate regional EF_{5r} is closer to 1.5% (0.7% - 3%) if the average nitrogen inputs, agricultural coverage⁵, and runoff scaling factor [De Klein et al., 2006] are used.

⁴ Potter P, Ramankutty N, Bennett EM, Donner SD (2011) Global Fertilizer and Manure, Version 1: Nitrogen Fertilizer Application. Palisades, NY: NASA Socioeconomic Data and Applications Center (SEDAC). <http://dx.doi.org/10.7927/H4Q81B0R>. Accessed 29 August 2014.

⁵ Fry J, et al. 2011 Completion of the 2006 National Land Cover Database for the Conterminous United States, *PE&RS*, Vol. 77(9):858-864.

It is important to note that our revised EF_{5r} may not be applicable to areas that are nitrogen limited. Our conservative land use threshold of > 40% cropland was chosen because the corn and soybean systems prevalent in the US Corn Belt indirectly identify areas of high nitrogen loading. While average nitrogen application rates vary, from 1994-2001 the average applied to all arable lands within the US Corn Belt was 48 kg N ha^{-1} [Potter *et al.*, 2011]. As such, we propose that agriculturally dominated watersheds receiving rates greater than 48 kg N ha^{-1} will be subject to similar indirect emissions and emission factors as observed in this study. We believe that the majority of the annual riverine N_2O budget will originate from those watersheds and that their total area globally exceeds 235 million ha. Following the United States (93 million ha), the largest regions meeting these criteria are China (69 million ha), Europe (43 million ha), and India (30 million ha). The remaining watersheds are likely to be small N_2O sources and the default 2006 IPCC EF_{5r} value should be appropriate for these cases [Dong *et al.*, 2004].

The application of our methodology to the global scale is limited by two main factors. First, the scaling relation described in Figure 2.1 is likely applicable to watersheds that are dominated by cropland systems with nitrogen inputs greater than 48 kg N ha^{-1} . Second, our stream order width was estimated using methodologies limited to the contiguous United States and Africa [Downing *et al.*, 2012]. At this time, we are unaware of an existing accurate global river width dataset and this represents an important limitation for application of our method to other regions. We believe this is an important research need, especially in countries with significant agricultural production including corn (e.g. China, India, Brazil, and others).

The above analyses did not consider the role of fine-scale drainage features. Zero-order streams, or microflow stream channels, extend upland of headwater streams, are highly episodic, and are likely “hotspots” of nitrogen processing [McClain *et al.*, 2003]. Zero-order stream systems form at the intersection of terrestrial and aquatic environments. However, because of their episodic nature and low spatial coverage, N₂O flux observations are severely lacking. Advancements in LiDAR remote sensing have made it possible to identify episodic microflow paths that may activate following snowmelt and precipitation events. The microflow paths are produced from high resolution (1 m) elevation maps that predict surface water movement. From these data, zero-order streams represent the most common stream order. We estimate that their length is 33 times that of first-order streams in the tall-tower footprint. By extrapolating Equation 1 to include zero-order streams, we suggest that they exert a significant influence on the N₂O budget by increasing the local emissions to 0.41 Gg N₂O-N yr⁻¹ in the tall-tower footprint, or 101% greater than the default IPCC estimate. Scaling zero-order streams to the Corn Belt increases indirect emissions to 82 Gg N₂O-N yr⁻¹ while the total emissions double to 129 Gg N₂O-N yr⁻¹. However, the uncertainty in N₂O emissions related to zero-order streams is large because we lack direct observational data, the reactivation timing is uncertain, and the microscale watershed threshold necessary to form a zero-order stream is highly variable. Regardless, there appears to be growing evidence of their importance in closing the gap between bottom-up and top-down emission estimates for the US Corn Belt.

Materials and Methods

N₂O Flux Sampling

N₂O fluxes were measured in the field using a flow-through non-steady-state chamber system adapted for deployment in rivers. The floating chamber consisted of an aluminum lid with a pressure equilibration vent buoyed by foam insulation and covered with reflective material. The chamber enclosed a surface area of 0.145 m² with a headspace volume of approximately 0.0147 m³.

Headspace gas was pulled through a Teledyne gas filter correlation N₂O analyzer (Model M320EU2, Teledyne Instruments API, City of Industry, California, USA) and the dry mole fraction was recorded at a sampling frequency of 1 Hz using a data-logger (model 23X, Campbell Scientific Inc., Logan, Utah, USA). The analyzer was powered in the field by deep cycle 12 VDC batteries wired in parallel to a DC-to-AC inverter. The chamber system has a minimum detectable flux of 0.028 nmol N₂O m⁻² s⁻¹ [Fassbinder *et al.*, 2013]. The analyzer was calibrated at the beginning of the season using an analytical grade standard and zeroed two times per month using N₂ gas. The concentration precision of the analyzer was 1.5 nmol mol⁻¹ and the flux measurement precision was 0.003 nmol m⁻² s⁻¹ [Fassbinder *et al.*, 2013].

The raw data were processed in Matlab (Matlab, Version R2012a, Mathworks, Natick, Massachusetts, USA). Fluxes were calculated according to:

$$F = \frac{\rho V \Delta}{A} \quad (\text{Equation 2.2})$$

where ρ (mol m^{-3}) is the molar density of dry air, A (m^2) is the surface area enclosed by the chamber, V (m^3) is the chamber volume, and Δ ($\text{nmol N}_2\text{O mol}^{-1} \text{s}^{-1}$) is the rate of change of N_2O concentration in the chamber headspace determined from linear regression [Fassbinder *et al.*, 2013]. Prior to calculating the chamber N_2O fluxes, a wavelet de-noising technique was applied to the raw concentration data. This reduced the effect of instrument noise and improved the signal to noise ratio [Fassbinder *et al.*, 2013]. We eliminated all chamber flux data when the linear regression R^2 value was less than 0.9.

Upscaling

Nonlinear regression analysis was performed using the “fitnlm” function in Matlab. Local stream order data were downloaded from the Minnesota Department of Natural Resources. Mean North American stream order width [Downing *et al.*, 2012] was used to generate stream area. Stream order areal estimates were applied to our nonlinear function to predict river emissions over a 214 day period (DOY 91-305).

The extent of the Corn Belt is subjective and lacks boundaries. Our definition was determined by selecting HUC12 sub-watersheds[¶] with greater than 40% agriculture from 13 states in the Midwest (ND, SD, NE, KS, MN, IA, MO, AR, WI, IL, OH, IN, MI). Regional stream order data (NHDPlus) was used in our nonlinear model. The regional dataset is at a lower resolution than the local stream order and as a consequence

[¶] NHDPlus V.2, Horizon Systems Corp., Herndon, Virginia, USA, <http://www.horizon-systems.com/NHDPlus/>

underestimated stream length. A comparison of Minnesota streams determined a scaling factor (1.4) was appropriate to apply to the regional data to correct for this underestimation.

Default Tier 1 IPCC methodologies were used to estimate N₂O emissions [*De Klein et al.*, 2006]. This budget included direct emissions from soils from synthetic and organic nitrogen application, indirect emissions from the volatilization of synthetic and organic fertilizer, rivers, and groundwater. We did not account for emissions from natural systems, industry, grazing livestock, organic soils, crop residues and legumes. Annual rates of synthetic and organic fertilizer application were used.

Zero-order streams were estimated from LiDAR data provided by the Minnesota Geospatial Information Office that was processed using ArcMap. A threshold of 250 m² was set before a stream would “activate”. We assumed a period of 2 months of active emissions which would include spring thaw and periodic precipitation events. Zero-order width was estimated using a regression equation from North American stream width data [*Downing et al.*, 2012].

Acknowledgements

We thank Joel Fassbinder, Matt Erickson, Mike Dolan, William Breiter, Kendall King, and Natalie Schultz for field and laboratory assistance and support provided by the United States Department of Agriculture, Grant Number: USDA-NIFA 2013-67019-21364 (TG and XL), USDA-ARS, NOAA (grant no. NA13OAR4310086), and the

Minnesota Supercomputing Institute for Advanced Computational Research
(<https://www.msi.umn.edu/>).

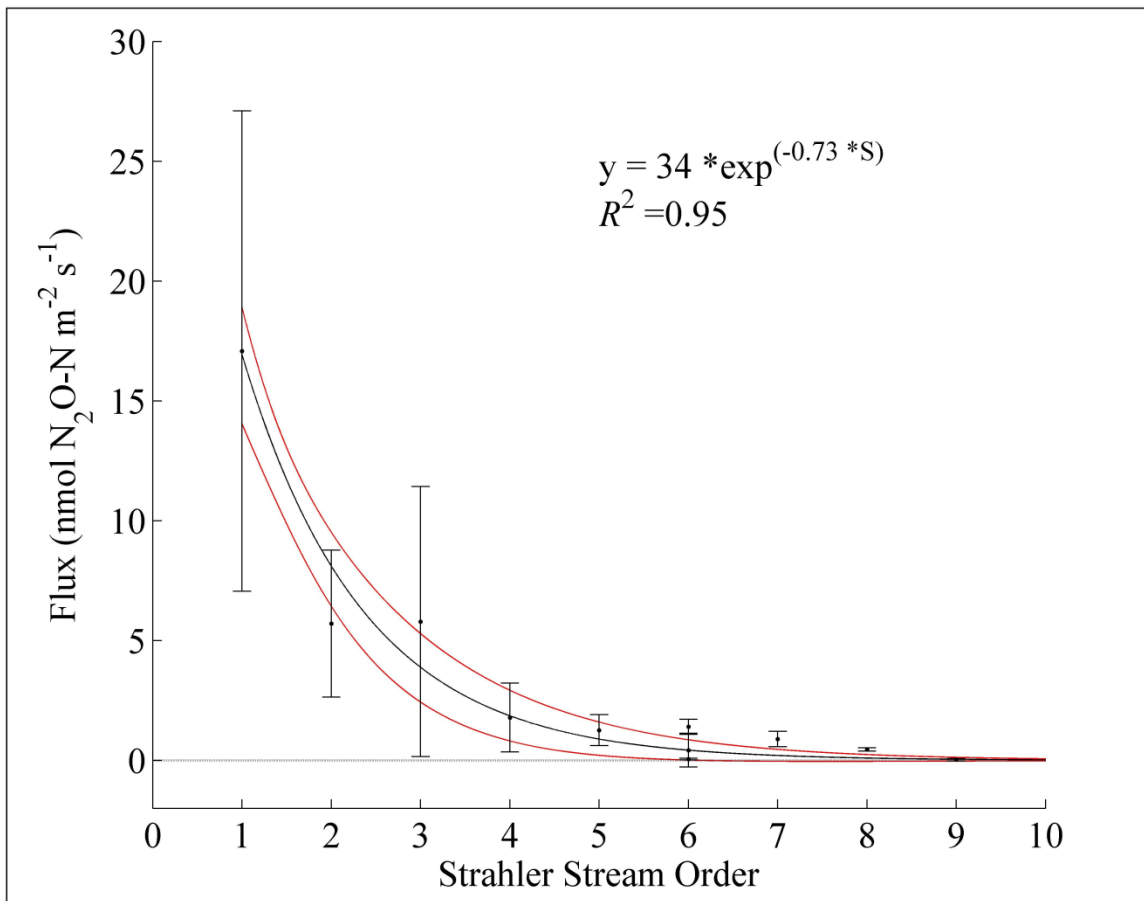


Figure 2.1. The relation between N₂O flux and the Strahler stream order in southeastern Minnesota. The black line represents the best fit of an exponential function to the mean flux values measured at each stream order. Red lines represent the 95% confidence interval of the model fit and error bars indicate one standard deviation from the mean.

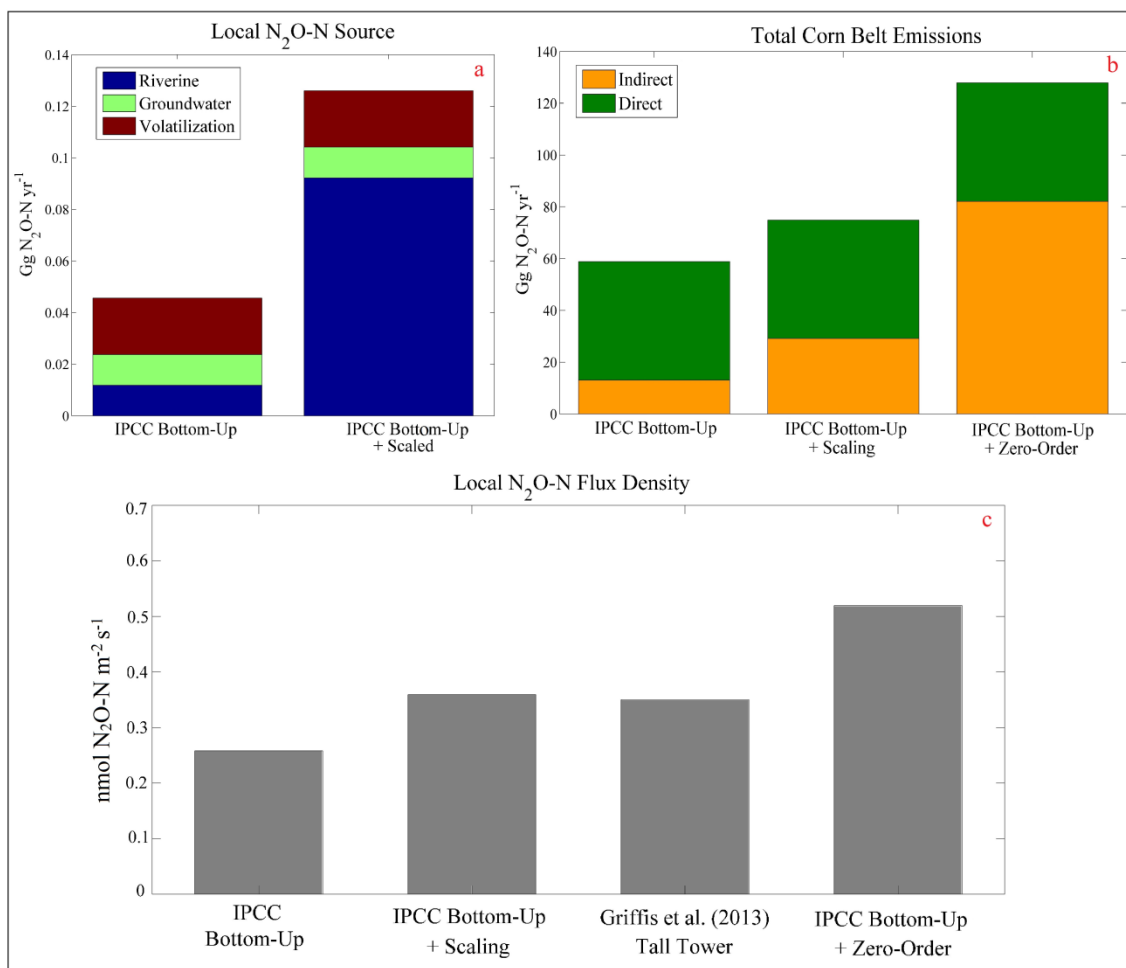


Figure 2.2. Results from upscaling N₂O emissions. a) A comparison of local indirect N₂O-N sources from default IPCC EFs and our scaling method. b) Total US Corn Belt emissions from the three methods. c) The flux densities from the tall-tower source footprint for each method.

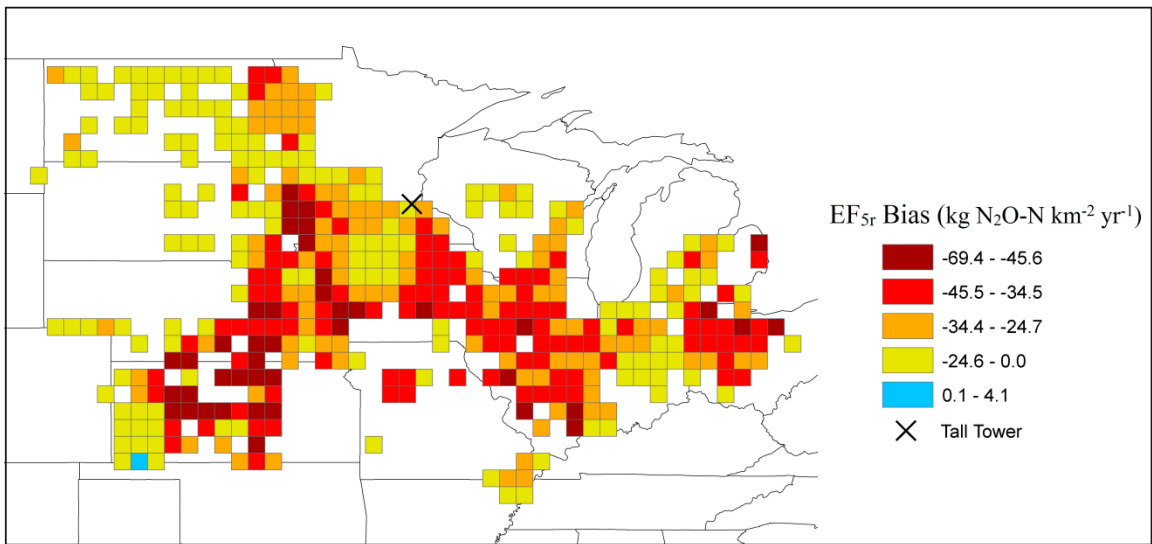


Figure 2.3. The first-order default EF_{5r} underestimation from the Corn Belt region. The bias is defined as the difference between IPCC EF_{5r} emissions and the results from stream order scaling.

Appendix

Stream N₂O flux observations were taken from locations scattered throughout southern Minnesota, U.S.A. during the 2013-2014 ice-free seasons. The seasonal and spatial distribution of sample dates and sites are described below.

Latitude	Longitude	Date	Stream
44.696	-93.076	06 17 2013	1st Order
44.696	-93.076	06 17 2013	1st Order
44.696	-93.076	06 17 2013	1st Order
44.696	-93.076	06 17 2013	1st Order
44.696	-93.076	06 17 2013	1st Order
44.696	-93.076	06 17 2013	1st Order
44.696	-93.076	06 17 2013	1st Order
44.695	-93.075	06 17 2013	1st Order
44.695	-93.075	06 17 2013	1st Order
44.695	-93.075	06 17 2013	1st Order
44.695	-93.075	06 17 2013	1st Order
44.674	-93.076	06 17 2013	1st Order
44.674	-93.076	06 17 2013	1st Order
44.674	-93.076	06 17 2013	1st Order
44.674	-93.076	06 17 2013	1st Order
44.590	-93.116	06 20 2014	1st Order
44.590	-93.116	06 20 2014	1st Order
44.590	-93.116	06 20 2014	1st Order
44.590	-93.116	06 20 2014	1st Order
44.361	-93.204	07 03 2013	1st Order
44.361	-93.204	07 03 2013	1st Order
44.361	-93.204	07 03 2013	1st Order
44.360	-93.204	07 03 2013	1st Order
44.360	-93.204	07 03 2013	1st Order
44.360	-93.204	07 03 2013	1st Order
44.361	-93.204	07 12 2013	1st Order
44.361	-93.204	07 12 2013	1st Order
44.361	-93.204	07 12 2013	1st Order
44.360	-93.204	07 12 2013	1st Order
44.360	-93.204	07 12 2013	1st Order
44.360	-93.204	07 12 2013	1st Order
44.360	-93.204	07 12 2013	1st Order

Latitude	Longitude	Date	Stream
44.360	-93.205	07 12 2013	1st Order
44.360	-93.205	07 12 2013	1st Order
44.360	-93.205	07 12 2013	1st Order
44.360	-93.205	07 12 2013	1st Order
44.360	-93.205	07 12 2013	1st Order
44.360	-93.205	07 12 2013	1st Order
44.022	-94.319	08 29 2013	1st Order
44.022	-94.319	08 29 2013	1st Order
44.022	-94.319	08 29 2013	1st Order
44.022	-94.319	08 29 2013	1st Order
44.539	-93.100	06 20 2014	2nd Order
44.539	-93.100	06 20 2014	2nd Order
44.539	-93.100	06 20 2014	2nd Order
44.572	-93.024	06 24 2014	2nd Order
44.572	-93.024	06 24 2014	2nd Order
44.572	-93.024	06 24 2014	2nd Order
44.486	-93.215	07 15 2014	2nd Order
44.486	-93.215	07 15 2014	2nd Order
44.486	-93.215	07 15 2014	2nd Order
44.539	-93.100	07 18 2014	2nd Order
44.539	-93.100	07 18 2014	2nd Order
44.539	-93.100	07 18 2014	2nd Order
44.539	-93.100	07 18 2014	2nd Order
44.539	-93.100	06 20 2014	3rd Order
44.539	-93.100	06 20 2014	3rd Order
44.539	-93.100	06 20 2014	3rd Order
44.539	-93.100	06 20 2014	3rd Order
44.555	-92.975	06 24 2014	3rd Order
44.555	-92.975	06 24 2014	3rd Order
44.555	-92.975	06 24 2014	3rd Order
44.522	-93.247	07 15 2014	3rd Order
44.522	-93.247	07 15 2014	3rd Order
44.522	-93.247	07 15 2014	3rd Order
44.539	-93.100	07 18 2014	3rd Order
44.539	-93.100	07 18 2014	3rd Order
44.539	-93.100	07 18 2014	3rd Order
44.539	-93.100	07 18 2014	3rd Order
44.507	-93.130	06 20 2014	4th Order
44.507	-93.130	06 20 2014	4th Order

Latitude	Longitude	Date	Stream
44.515	-93.232	07 15 2014	4th Order
44.515	-93.232	07 15 2014	4th Order
44.515	-93.232	07 15 2014	4th Order
44.507	-93.130	07 18 2014	4th Order
44.507	-93.130	07 18 2014	4th Order
44.507	-93.130	07 18 2014	4th Order
44.093	-94.108	08 29 2013	Blue Earth River
44.093	-94.108	08 29 2013	Blue Earth River
44.093	-94.108	08 29 2013	Blue Earth River
44.093	-94.108	08 29 2013	Blue Earth River
44.488	-93.128	08 01 2013	Cannon River
44.489	-93.119	08 01 2013	Cannon River
44.492	-93.113	08 01 2013	Cannon River
44.495	-93.108	08 01 2013	Cannon River
44.496	-93.100	08 01 2013	Cannon River
44.499	-93.093	08 01 2013	Cannon River
44.506	-93.074	08 01 2013	Cannon River
44.509	-93.065	08 01 2013	Cannon River
44.510	-93.059	08 01 2013	Cannon River
44.513	-93.056	08 01 2013	Cannon River
44.515	-93.050	08 01 2013	Cannon River
44.516	-93.020	08 01 2013	Cannon River
44.640	-93.757	08 20 2013	Minnesota River
44.644	-93.758	08 20 2013	Minnesota River
44.645	-93.749	08 20 2013	Minnesota River
44.649	-93.734	08 20 2013	Minnesota River
44.659	-93.716	08 20 2013	Minnesota River
44.668	-93.710	08 20 2013	Minnesota River
44.672	-93.695	08 20 2013	Minnesota River
44.683	-93.684	08 20 2013	Minnesota River
44.684	-93.683	08 20 2013	Minnesota River
44.694	-93.657	08 20 2013	Minnesota River
44.695	-93.646	08 20 2013	Minnesota River
44.899	-93.191	08 15 2013	Mississippi River
44.895	-93.186	08 15 2013	Mississippi River
44.894	-93.179	08 15 2013	Mississippi River
44.894	-93.171	08 15 2013	Mississippi River
44.896	-93.161	08 15 2013	Mississippi River
43.783	-92.032	08 28 2013	Root River

Latitude	Longitude	Date	Stream
43.783	-92.032	08 28 2013	Root River
43.783	-92.032	08 28 2013	Root River
43.783	-92.032	08 28 2013	Root River
43.783	-92.032	08 28 2013	Root River
43.840	-92.197	08 28 2013	Root River
43.840	-92.197	08 28 2013	Root River
44.674	-93.075	06 20 2013	Vermillion River
44.674	-93.075	06 20 2013	Vermillion River
44.674	-93.075	06 20 2013	Vermillion River
44.026	-94.229	08 29 2013	Watonwan River
44.022	-94.319	08 29 2013	Watonwan River
44.046	-94.195	08 29 2013	Watonwan River
44.047	-94.168	08 29 2013	Watonwan River
44.047	-94.168	08 29 2013	Watonwan River
44.319	-92.701	08 27 2013	Zumbro River
44.319	-92.701	08 27 2013	Zumbro River
44.306	-92.761	08 27 2013	Zumbro River
44.306	-92.761	08 27 2013	Zumbro River
44.257	-92.494	08 27 2013	Zumbro River
44.257	-92.494	08 27 2013	Zumbro River
44.257	-92.493	08 27 2013	Zumbro River
44.320	-92.127	08 27 2013	Zumbro River
44.320	-92.127	08 27 2013	Zumbro River

Chapter 3

**Regional-scale controls on dissolved nitrous oxide in the Upper
Mississippi River**

Peter A. Turner, Timothy J. Griffis, John M. Baker, Xuhui Lee, John T. Crawford, Luke C. Loken, and Rodney T. Venterea (2016), *Geophysical Research Letters*, 43 (9), 4400-4407, doi: 10.1002/2016GL068710

© American Geophysical Union

Overview

The U.S. Corn Belt is one of the most intensive agricultural regions of the world and is drained by the Upper Mississippi River (UMR), which forms one of the largest drainage basins in the U.S. While the effects of agricultural nitrate (NO_3^-) on water quality in the UMR have been well documented, its impact on the production of nitrous oxide (N_2O) has not been reported. Using a novel equilibration technique, we present the largest dataset of freshwater dissolved N_2O concentrations and examine the controls on its variability over a 350-km reach of the UMR. Driven by a supersaturated water column, the UMR was an important atmospheric N_2O source that varies non-linearly with NO_3^- , which should be considered in emission inventories. Our analyses indicated that a projected doubling of NO_3^- by 2050 would cause dissolved N_2O concentrations and atmospheric emissions to increase by about 40%.

Introduction

The Upper Mississippi River (UMR) drains nearly 492,000 km^2 of the U.S. Corn Belt [NRCS, 2012], one of the most intensively cultivated regions on the planet. Within the UMR basin, more than half of the U.S. share of nitrogen (N) fertilizers are applied [Griffis *et al.*, 2013; FAO, 2015] to produce 40% of the nation's corn [NRCS, 2012]. These activities have amplified river N loading, mainly as nitrate (NO_3^-) [Turner and Rabalais, 1991; Panno *et al.*, 2006]. Much effort has focused on the effects of excessive N on water quality [Rabalais, 2002] and the ability of the UMR to reduce downstream

transport [Richardson *et al.*, 2004; Strauss *et al.*, 2004, 2011] to estuary systems. However, measurements of nitrous oxide (N₂O), the dominant stratospheric ozone depleting substance [Ravishankara *et al.*, 2009] and an important greenhouse gas [Hartmann *et al.*, 2013], in the UMR are conspicuously absent in the literature, representing a significant knowledge gap in our understanding of the regional controls on dissolved N₂O concentrations and emissions in heavily modified agricultural rivers.

Rivers are globally significant sources of N₂O to the atmosphere [Beaulieu *et al.*, 2011; Turner *et al.*, 2015], responsible for 10% – 17% of the anthropogenic budget [Beaulieu *et al.*, 2011; Syakila and Kroeze, 2011]. Yet, rivers remain one of the most uncertain N₂O sources [Nevison, 2000], largely due to low spatiotemporal sampling resolution that is unable to resolve the high variability of surface water N₂O concentrations caused by dynamic production and consumption processes. Nitrous oxide production *via* denitrification and nitrification in the water column [Beaulieu *et al.*, 2010] and sediments [Boyer *et al.*, 2006; Marzadri *et al.*, 2014] causes rivers to become saturated with N₂O that is emitted to the atmosphere. Generally, the degree of N₂O saturation increases with the concentration of NO₃⁻ and ammonium (NH₄⁺), indicating that emissions from large rivers are derived from *in-situ* N₂O production [Beaulieu *et al.*, 2010], rather than terrestrial delivery. Global model simulations suggest a doubling of N loading in rivers by the year 2050 [Seitzinger *et al.*, 2002], implying that N₂O emissions from rivers, including the UMR, will likely increase. However, the relationship between dissolved N₂O concentrations in rivers and N loading is poorly constrained because

obtaining these types of data is logistically challenging and, consequently, observations are very limited.

Recent studies indicate that surface water N₂O concentrations behave non-linearly, plateauing in response to a number of environmental drivers, including dissolved oxygen concentration [Rosamond *et al.*, 2012] and water temperature [Venkiteswaran *et al.*, 2014]. Observations that N₂O concentrations increase at a decreasing rate is likely caused by the inverse relation between N loading and removal efficiency [Mulholland *et al.*, 2008]. This non-linearity implies that N₂O emissions will not increase proportionally with N loading projections, especially as a river becomes N-saturated. Characterizing the N₂O:NO₃⁻ mass ratio should provide an upper constraint on N₂O concentrations in N-rich systems and provide insights regarding how these rivers may respond under business-as-usual nitrogen use scenarios.

Here, we present the largest freshwater dissolved N₂O concentration dataset to date and the first N₂O surface water concentration measurements from the UMR to: 1) explore the biochemical factors that control the degree of riverine N₂O saturation; 2) identify N₂O hotspots; and 3) predict how N₂O concentrations will respond to future N loading.

Materials and Methods

Site Description

For this study, we considered a portion of the UMR that extends from Minneapolis, MN through Pool 8 (near La Crosse, WI). Along this stretch, eight lock

and dam combinations have been installed to facilitate navigation. The river is organized into pools to describe river sections between two neighboring dams. In addition to the main channel, a pool includes impounded waters, side channels, and backwaters [*Strauss et al.*, 2011]. The seasonal (10 April, 16 June, 4 August, and 13 October) and spatial dynamics of N₂O concentration were observed in Pool 8, a 104 km² section of the UMR upstream of Lock and Dam 8. From 1-3 August 2015, a 350 km reach from Minneapolis, Minnesota to Pool 8 provided a regional-scale assessment of N₂O concentration patterns in the UMR.

Water Sampling

We used a boat-mounted flow-through sampling system [*Crawford et al.*, 2015] to continually measure surface water N₂O and other limnological parameters. In brief, we pumped surface water (0.3-m) to a series of sensors and stripped the dissolved gases using a sprayer-type equilibration device [*Crawford et al.*, 2015]. This type of equilibrator has a fast response time [*Santos et al.*, 2012; *Yoon et al.*, 2016] and has been used in oceanic N₂O campaigns [*Bange et al.*, 1996; *Arévalo-Martínez et al.*, 2013, 2015; *O'Reilly et al.*, 2015] but has never been used to measure N₂O in freshwater systems. Equilibrator headspace air was drawn through a desiccant tube before entering a Teledyne gas filter correlation N₂O analyzer (Model M320EU2; Teledyne Instruments, City of Industry, CA, USA) [*Fassbinder et al.*, 2013; *Turner et al.*, 2015]. A circular loop was created by returning sample air back to the equilibrator device. A data-logger

(Model 23X; Campbell Scientific, Logan, UT, USA) stored the N₂O analyzer output at 1 Hz for processing.

This system, the Fast Limnology Automated Measurement (FLAMe) platform has been used extensively to monitor dissolved CO₂ and CH₄ on the Mississippi River [Crawford *et al.*, 2016]. The FLAMe instrument panel consisted of a YSI sonde (Model EXO2; Yellow Springs, OH, USA), an optical NO₃ sensor (Model SUNA V2, Satlantic, Halifax, NS, Canada), and a GPS device. The FLAMe platform measured water temperature (T), dissolved oxygen (DO), pH, turbidity, specific conductivity, Chl-*a*, and fluorescent dissolved organic matter (fDOM). Higher fDOM values are related to terrestrially derived organic matter [Spencer *et al.*, 2013] and are a proxy for dissolved organic carbon [Crawford *et al.*, 2015]. Spatial coordinates were recorded semi-continuously at 1 Hz while measurements of NO₃⁻ were stored at 0.1 Hz.

Data Processing

The raw N₂O concentration data ($n = 101,862$) were processed using Matlab (R2013b; Mathworks, Natick, MA, USA) software. To georeference the FLAMe and N₂O data, we determined the hydraulic and sensor response time lags using a series of step-change experiments [Crawford *et al.*, 2015]. The hydraulic and sensor lag describes the time required for the instrument to detect a step change (42.3-s) caused by tube length, instrument responsivity, and equilibrators lag. The sensor responsivity of the N₂O analyzer was estimated using an equilibrators time constant τ (61.6-s) that describes the time required for a 63% step change to occur. A wavelet denoising technique was

applied to the N₂O concentration data to improve the signal to noise ratio of the instrument [Fassbinder *et al.*, 2013]. For convenience of data processing and statistical analyses, all of the data streams were subjected to 30-s block averaging resulting in a data series of $n = 3,667$.

The surface water [N₂O] (mol N₂O L⁻¹) was calculated from:

$$[\text{N}_2\text{O}] = [\text{N}_2\text{O}_*] \times F(T, p) \quad (\text{Equation 3.1})$$

where [N₂O_{*}] is the equilibrator concentration, and F(T, p) is the solubility function at the given surface water temperature (T) and pressure (p) [Weiss and Price, 1980; Grefe and Kaiser, 2014]. The theoretical equilibrium N₂O concentration ([N₂O_{amb}], mol N₂O L⁻¹) assuming water-atmosphere equilibrium was calculated similarly:

$$[\text{N}_2\text{O}_{\text{amb}}] = [\text{N}_2\text{O}_{\text{amb}*}] \times F(T, p) \quad (\text{Equation 3.2})$$

where [N₂O_{amb*}] is the ambient atmospheric concentration reading by the N₂O analyzer, and T and p are ambient water temperature and air pressure, respectively at the time of measurement. The ambient concentration was measured every 2-hrs. The analyzer was zeroed and spanned using analytical grade standards (Specialty Gases of America, Toledo, OH, USA) before each measurement campaign. The concentration precision of the analyzer after wavelet denoising is 1.5-nmol mol⁻¹ [Fassbinder *et al.*, 2013]. These two metrics, [N₂O] and [N₂O_{amb}], are water temperature dependent. Therefore, we use their ratio to standardize the measurements with respect to the in-situ water temperature:

$$\text{N}_2\text{O}_{\text{sat}} = \frac{[\text{N}_2\text{O}]}{[\text{N}_2\text{O}_{\text{amb}}]} \quad (\text{Equation 3.3})$$

A novel aspect of the FLAMe platform is its capacity to incorporate spatial coordinates to identify spatial patterns driving N_2O_{sat} across large spatial distances. A Getis-Ord G^* analysis of each dataset identified clustering of statistically significant high and low N_2O_{sat} and NO_3^- values relative to neighboring points [Ord and Getis, 2010]. A 99% significance threshold was used to determine N_2O_{sat} and NO_3^- hotspots and coldspots (Arcmap v.10.3; ESRI, Redlands, CA, USA).

Using CO_2 piston velocity (k) measurements from the UMR [Crawford *et al.*, 2016], we estimated the mean ($n = 22$) k using the temperature adjusted N_2O Schmidt number [Wanninkhof, 1992]. Nitrous oxide fluxes ($\text{nmol } N_2O\text{-N } m^{-2} s^{-1}$) from the UMR were calculated as:

$$\text{Flux}_{N_2O} = k \times ([N_2O] - [N_2O_{\text{amb}}]) \quad (\text{Equation 3.4})$$

We assumed that variations in the evasion coefficient would be negligible within the UMR because of minimal channel geometry change and consequently, N_2O_{sat} and Flux_{N_2O} would be most sensitive to in-situ production and consumption mechanisms. We estimated that N_2O_{sat} ratios greater than 1.2 and less than 0.8 were indicative of active production and consumption zones, respectively, while N_2O_{sat} values within this window were classified as zones of negligible production and consumption [Beaulieu *et al.*, 2015].

Ensemble Regression Trees

The controls on riverine $\text{N}_2\text{O}_{\text{sat}}$ were identified independently for each river section using ensemble ($n = 500$) binary bagged regression trees with the Matlab *fitensemble* function (v.2015.b, Mathworks, Natick, MA, USA). This supervised learning method does not require an assumption of normality and the bootstrap aggregation technique reduces prediction variance [De'ath and Fabricius, 2000; Sutton, 2005] making it a powerful tool for better understanding the controls on N_2O saturation [Baulch et al., 2011; Venkiteswaran et al., 2014; Lundy et al., 2015]. The relative predictor importance (RPI) of each explanatory variable on the corresponding $\text{N}_2\text{O}_{\text{sat}}$ response was computed by summing the change in mean square error from splitting each predictor and dividing by the number of nodes. The importance was normalized with respect to the largest value [Lundy et al., 2015]; a response of 1 recognizes the independent variable with the greatest impact on the $\text{N}_2\text{O}_{\text{sat}}$ and a value of zero indicates no influence. The variance of the ensemble regression model was determined by calculating the pseudo R^2 value of model predicted and observed $\text{N}_2\text{O}_{\text{sat}}$ concentrations.

Results and Discussion

The UMR was supersaturated with N_2O throughout the ice-free measurement period, indicating it was an important atmospheric source (Figure 3.1, 3.2a). Across all sampling locations and dates, the mean (standard deviation) $\text{N}_2\text{O}_{\text{sat}}$ was 2 (0.9) times the atmospheric saturation (Table 3.1). The regional mean flux was 0.5 (0.3) $\text{nmol N}_2\text{O-N m}^{-2} \text{ s}^{-1}$, which is comparable to observations from nearby corn fields [Griffis et al., 2013]

and within the range observed in other large rivers [McMahon and Dennehy, 1999; Cole and Caraco, 2001; Hinshaw and Dahlgren, 2013]. Since groundwater and most tributary flows are negligible in a river of this size, and because of the short residence time of upstream dissolved gases, our data indicate that the UMR actively produces N₂O throughout the year.

During the June Pool 8 campaign, an instrument issue prevented N₂O_{sat} measurements greater than 4.8. Since we can only state that N₂O_{sat} was equal to or above 4.8, they were not included in the following analyses. However, the high N₂O_{sat} in Pool 8 in June is consistent with recent top-down measurements and modeling that found total emissions (direct + indirect) [Miller *et al.*, 2012; Griffis *et al.*, 2013] and indirect emissions from leaching and runoff [Chen *et al.*, 2016] to be highest during this period, likely because of the recent application of N fertilizers.

Spatial analyses, based on the Getis-Ord G* statistic [Ord and Getis, 2010], identified four N₂O_{sat} hotspots along this section of the UMR (Figure 3.2b). Hotspots were generally within close proximity to municipal wastewater treatment plants (WWTP). These hotspots dissipated rapidly, presumably because of dilution, over relatively short distances suggesting that care should be taken when sampling nearby. The strength of these hotspots reflects differences in effluent discharge and river volume. Since NO₃⁻ hotspots were not observed downstream of each WWTP (Figure 3.2c), it is likely that N₂O was produced during wastewater processing prior to discharge into the UMR [Kampschreur *et al.*, 2009]. However, WWTPs are relatively minor contributors to the total N in the UMR, with greater than 70% being from agricultural sources [Wall *et*

al., 2013]. Our analyses identified five $\text{N}_2\text{O}_{\text{sat}}$ coldspots along this reach that were collocated with NO_3^- coldspots (Figure 3.2c), indicating that NO_3^- concentrations are an underlying requirement for N_2O production.

Overall, the surface water NO_3^- (RPI = 1) concentration was the most important explanatory variable driving regional fluctuations in UMR $\text{N}_2\text{O}_{\text{sat}}$ (Figure 3.3a), whereas across seasons, temperature (RPI = 1) and NO_3^- (RPI = 0.86) were the most important predictors (Figure 3.3b). The strong relation with NO_3^- throughout the UMR was expected because it is linked to both nitrification and denitrification. These processes are well documented in rivers [*Strauss et al.*, 2002; *Beaulieu et al.*, 2011], lakes [*Wang et al.*, 2009], reservoirs [*Beaulieu et al.*, 2015], and estuaries [*Owens*, 1986; *Murray et al.*, 2015]. In a well-oxygenated river such as the UMR, the strong relation between NO_3^- and $\text{N}_2\text{O}_{\text{sat}}$ suggests that nitrification is a likely N_2O production pathway [*Beaulieu et al.*, 2015]. Further, we argue that the NO_3^- concentration in the surface water is also an indirect measure of the NO_3^- available for diffusion into hypoxic sediments [*Rosamond et al.*, 2012], i.e. the sediment denitrification potential. However, the kinetics of NO_3^- processing and concurrent N_2O production are affected by secondary environmental factors – including turbidity (RPI = 0.4), pH (RPI = 0.3), fDOM (RPI = 0.18), and DO (RPI = 0.14) that may limit or enhance reaction rates (production *via* nitrification and consumption *via* denitrification).

We posit that these secondary factors indirectly dampen the $\text{N}_2\text{O}_{\text{sat}}$ response by reducing the efficiency of NO_3^- removal (i.e. N_2O production potential) at high solute concentrations [*Mulholland et al.*, 2008]. This response has been attributed to limits on

denitrification – including, dissolved oxygen and carbon [Mulholland *et al.*, 2008] that were also identified by our ensemble regression tree model. These data also classified pH as an important predictor, likely because it affects the rates of denitrification [Knowles, 1982] and nitrification [Strauss *et al.*, 2004]. We hypothesize that the positive relation identified between turbidity and N_2O_{sat} in the model reflects the fact that nitrifying bacteria bind to suspended particles in the water column [Beaulieu *et al.*, 2010]. Together, these factors affect the fraction of NO_3^- converted to N_2O at N saturation [Beaulieu *et al.*, 2011] that underlies the horizontal asymptote observed for dissolved N_2O concentrations in the UMR (Figure 3.4).

Using Michaelis-Menten kinetics [García-Ruiz *et al.*, 1998; Boyer *et al.*, 2006], we describe the weakening N_2O response to N saturation as:

$$[N_2O] = \frac{V_{max} \times [NO_3^-]}{K_m + [NO_3^-]} \quad (\text{Equation 3.5})$$

with the parameters estimated using a nonlinear least squares fitting function (*enzkin*; v.R2013B; Mathworks, Natick, MA, USA). Here, the $[N_2O]$ (mg N_2O -N L^{-1}) can be derived from the $[NO_3^-]$ (mg NO_3^- L^{-1}) with a V_{max} of 0.0011 (95% CI; $\pm 4.1 \times 10^{-5}$) mg N_2O -N L^{-1} and a K_m of 1.36 (± 0.11) mg NO_3^- L^{-1} . The V_{max} represents the system's maximum $[N_2O]$ and the K_m is the $[NO_3^-]$ required to reach 50% of the V_{max} . The non-linearity of Figure 3.4 implies that increasing NO_3^- concentrations will have a progressively weaker effect on N_2O concentrations in the UMR. In North America, river models project a doubling of the NO_3^- exported to estuaries by the year 2050 [Seitzinger *et al.*, 2002]. Using the relation shown in Figure 3.4, a doubling of NO_3^- would increase

N₂O emissions from the UMR by about 42% (95% CI; 32-52%). Conversely, the U.S. Environmental Protection Agency has established a goal to reduce N export by 45% by 2035. If this goal were achieved, N₂O concentrations in the UMR would be decreased by about 32% (26-38%), implying a significant reduction in N₂O emissions. However, because our regression tree models indicated that N₂O_{sat} was influenced by secondary factors, these forecasts could be diminished – for instance, a reduction in turbidity (decreased substrate for nitrifying bacteria) would lower N₂O_{sat} and therefore these forecasts should represent an upper estimate.

While automated soil N₂O measurement systems have become more common in recent years, techniques for continuous measurement of riverine N₂O concentrations have lagged behind. The techniques applied in this study have potential to address this problem worldwide and could significantly reduce the uncertainty in riverine N₂O emissions and the riverine emission factor (EF_{5r}) provided by the Intergovernmental Panel on Climate Change (IPCC). For instance, stationary *in-situ* sampling platforms located at strategic locations within a stream network could be used for emission upscaling [Turner *et al.*, 2015] to develop regionally appropriate, Tier II EF_{5r} values. Further, such data could be used to improve our understanding of the inter-annual variability and long-term dynamics of dissolved riverine N₂O and emissions.

Conclusions

Our data and analyses demonstrate that the UMR is supersaturated with N₂O during the ice-free period and is an important source of atmospheric N₂O. The regression

tree models evaluated in this study indicate that NO_3^- is the dominant control on N_2O concentrations, but that other environmental variables may limit NO_3^- processing. Given the significant non-linear relation between NO_3^- and N_2O in the UMR, we expect that a doubling of N loading is likely to cause a substantial (32-52%) rise in dissolved N_2O concentrations and atmospheric emissions.

Acknowledgments

We thank William Breiter, Michael Dolan, Mark Dornblaser, and Matt Erickson for field and laboratory assistance. This work was supported by the US Department of Agriculture, Grant Number: USDA-NIFA 2013-67019-21364, USDA-ARS, and the U.S. Geological Survey's LandCarbon program. Data are hosted at <http://www.biometeorology.umn.edu/research/data-archives>. Any use of trade or product names is for descriptive purposes only and does not imply endorsement by the U.S. Government.

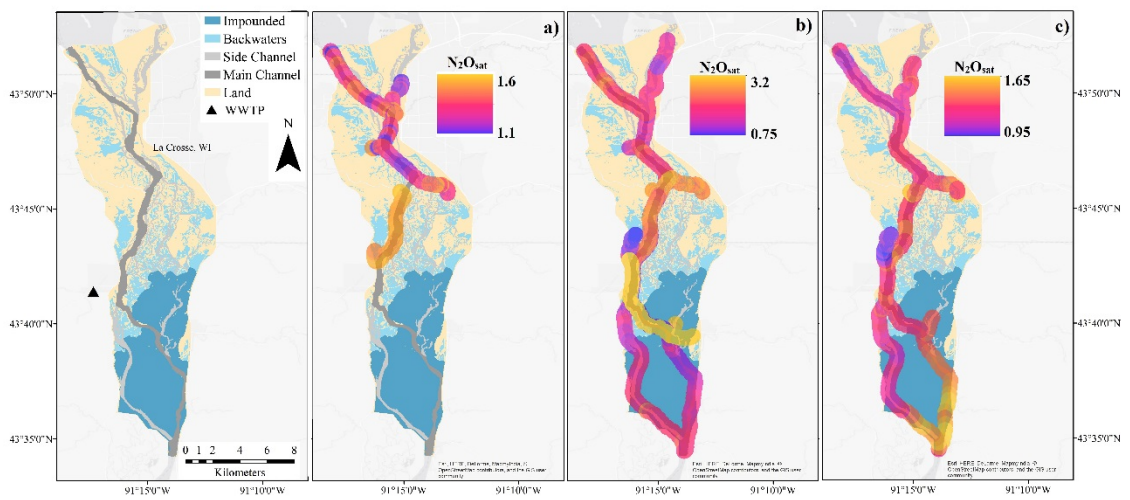


Figure 3.1. The seasonal and spatial dynamics of N_2O_{sat} in Pool 8 of the UMR in a) April ($n = 298$), b) August ($n = 828$), and c) October ($n = 514$).

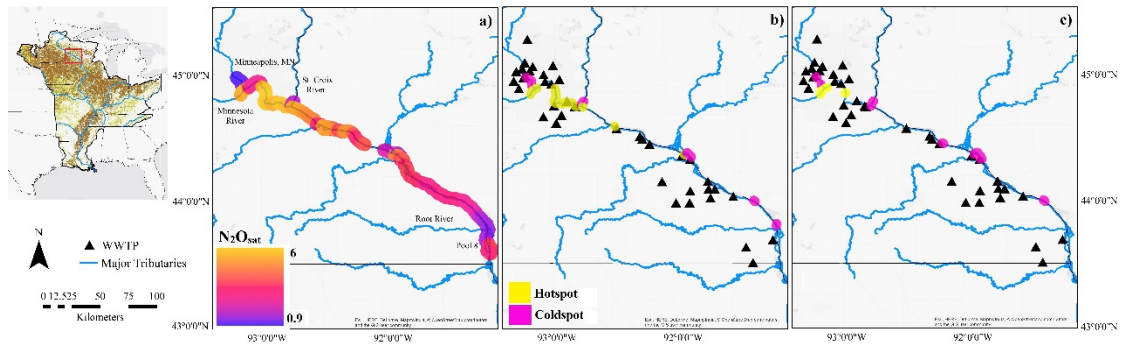


Figure 3.2. Inset) Agricultural land use within the UMR basin. Row-crop (brown) and pasture (yellow) were drawn using information from the National Land Cover Database (2011). a). The regional-scale variability of N_2O_{sat} in the UMR ($n = 1,553$). Hotspots and coldspots of b) N_2O_{sat} and c) NO_3^- .

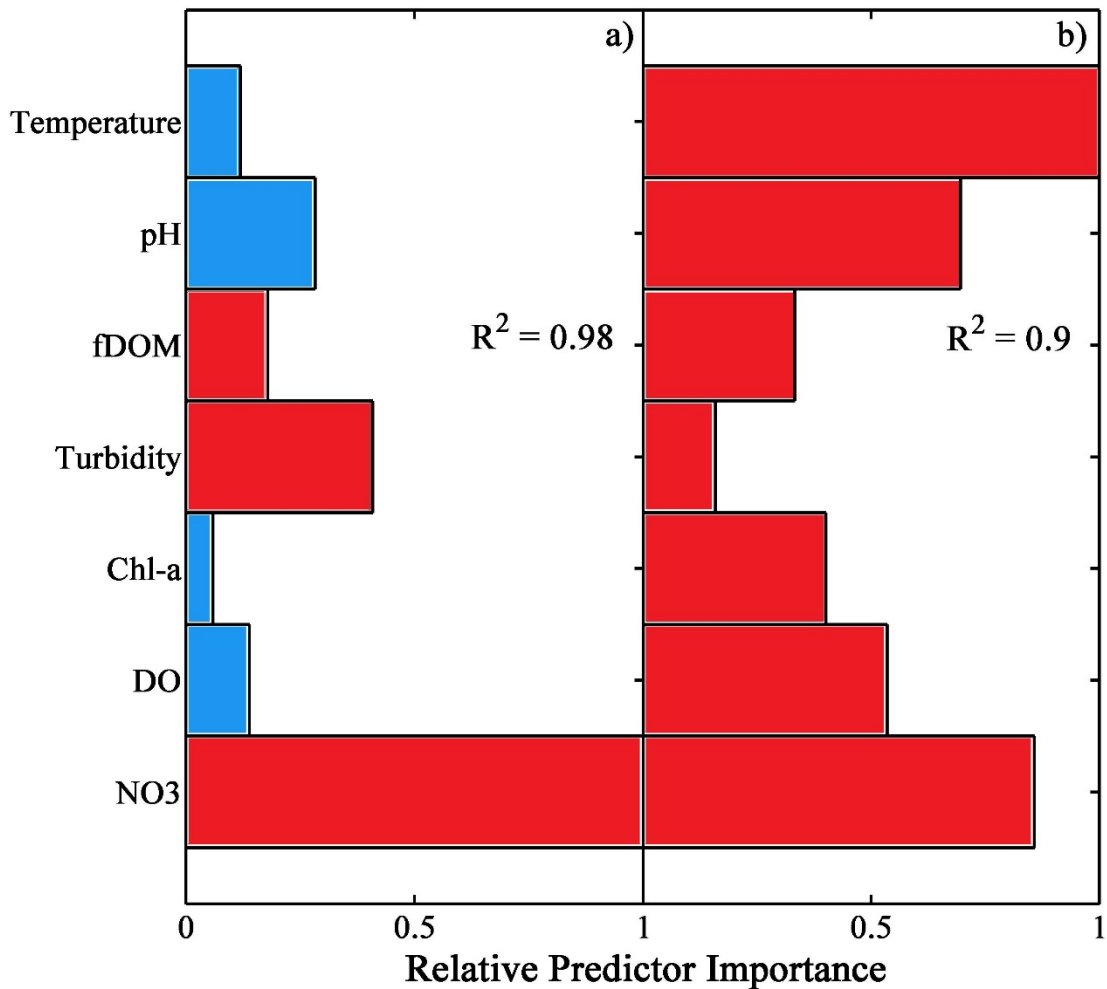


Figure 3.3. Relative predictor importance (RPI) determined using ensemble ($n = 500$) regression trees to predict N_2O_{sat} observations. Red and blue bars denote positive and negative relationships, respectively. The variable importance describes the explanatory power of a predictor on the N_2O_{sat} response. The pseudo R^2 was determined from an observed N_2O_{sat} vs. predicted N_2O_{sat} determined from the ensemble regression model. Each value was normalized to the most important predictor in each system where a) is the RPI of the regional-scale measurements, b) is the seasonal (April, August, October) RPI from Pool 8.

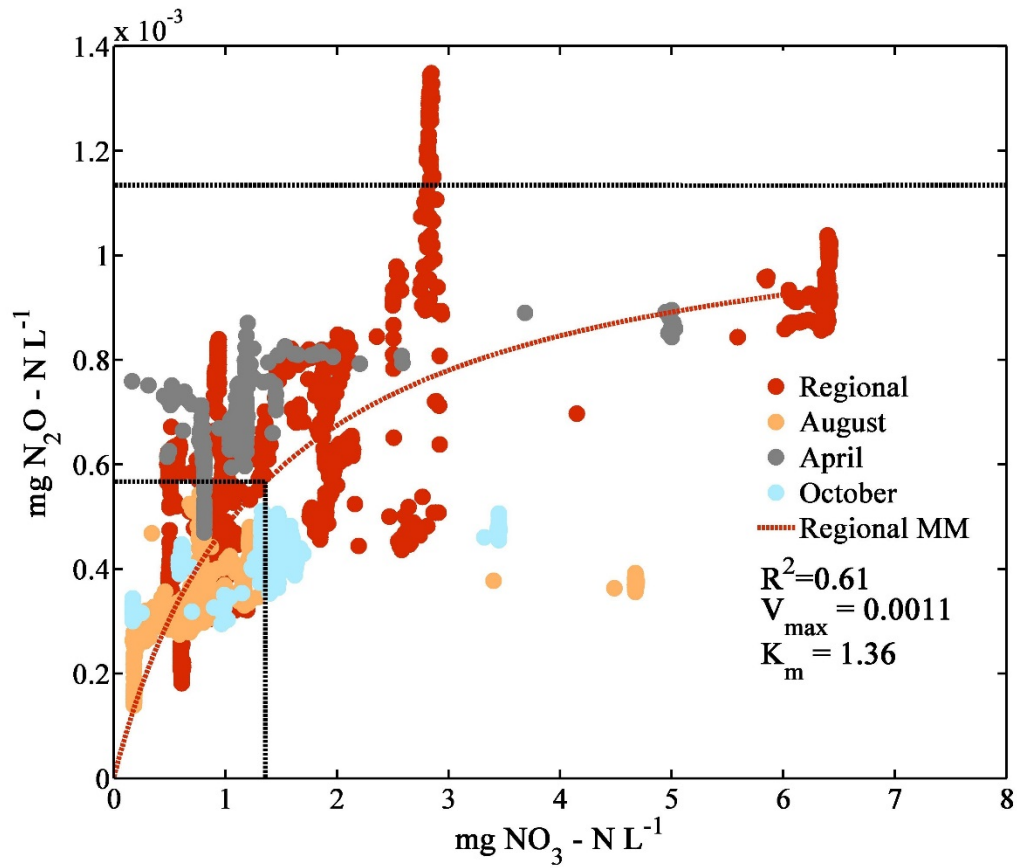


Figure 3.4. Measurements of N_2O and NO_3^- from the UMR basin. The dashed line is the Michaelis-Menten function derived from the regional-scale campaign ($n = 1,553$).

Chapter 4

The Impact of Kura Clover Living Mulch on Nitrous Oxide Emissions in a Corn/Soybean System

Peter A. Turner, John M. Baker, Timothy J. Griffis, and Rodney T. Venterea (2016),
Journal of Environment Quality, (45), 1782-1787, doi: 10.2134/jeq2016.01.003

© American Society of Agronomy, Crop Science Society of America, and Soil Science
Society of America

Overview

Nitrous oxide (N₂O), produced primarily in agricultural soils, is a potent greenhouse gas and the dominant ozone depleting substance. Efforts to reduce N₂O emissions are underway, but mitigation results have been inconsistent. The leguminous perennial kura clover (*Trifolium ambiguum* M. Bieb.) can grow side-by-side with cash crops in rotational corn (*Zea mays* L.) – soybean (*Glycine max* L.) systems. With biological nitrogen fixation, kura clover (KC) provides land managers an opportunity to reduce external fertilizer inputs, which may diminish problematic N₂O emissions. To investigate the effect of a KC living mulch on N₂O emissions, automated soil chambers coupled to a N₂O analyzer were used to measure hourly fluxes from April through October in a 2-yr corn-soybean rotation. Emissions from the KC treatment were significantly greater than those from the conventional corn-soybean (CS) treatment, despite the fact that the KC treatment received substantially less inorganic nitrogen (N) fertilizer. A seasonal tradeoff was observed with the KC treatment wherein emissions prior to strip-tillage were reduced but were surpassed by high losses following strip-tillage and also post-anthesis. These results represent the first-reported measurements of N₂O emissions from a KC -based living mulch. The findings cast doubt on the efficacy of KC for mitigating N₂O loss in corn-soybean systems. However, if KC reduces nitrate leaching losses, as has been reported elsewhere, it may result in lower indirect (offsite) N₂O emissions.

Introduction

Nitrous oxide (N₂O) is an important greenhouse gas [Hartmann *et al.*, 2013] and the primary ozone depleting substance [Ravishankara *et al.*, 2009]. In the United States, approximately 74% of the anthropogenic N₂O source is linked to agriculture [USEPA, 2015], placing tremendous pressure on the agricultural community to reduce N₂O emission while simultaneously increasing grain yields. Most often, the discussion to reduce N₂O emission revolves around modifying traditional crop and N management practices. Efforts have included optimizing fertilizer timing [Venterea and Coulter, 2015] source [Halvorson *et al.*, 2014], and depth of application [Maharjan and Venterea, 2014]; amendments of biochar [Lin *et al.*, 2014]; and alternative tillage techniques [Bavin *et al.*, 2009; Jin *et al.*, 2014]. However, the success rates of these practices have been inconsistent and conflicting, in part because of the complex site specific soil and meteorological interactions governing N₂O production [Decock, 2014].

Because N fertilizers stimulate N₂O production, the N rate is often the best predictor of N₂O emissions [Stehfest and Bouwman, 2006]. Notably, recent work suggests that emissions may respond exponentially to increasing N application rates [Hoben *et al.*, 2011; Shcherbak *et al.*, 2014], especially beyond the agronomic optimum application rate [van Groenigen *et al.*, 2010]. Correspondingly, N₂O emissions can be reduced most effectively by simply reducing the N rate, but this practice can reduce yield. To minimize yield loss in response to N rate reduction, a legume can be used to supplant N through biological nitrogen fixation (BNF). This process releases N over time and at lower concentrations than those initially observed following fertilizer application that

could improve synchronization with crop N needs [*Crews and Peoples, 2004*] while affecting N₂O emissions. Commonly grown legumes include soybeans and cover crop (CC) species such as alfalfa, red clover, and hairy vetch. A long-term alternative is a perennial living mulch management system. This approach provides the BNF benefit of a leguminous CC, minimizing the need for external N fertilizers, which could concurrently reduce N₂O emissions without harming yields.

A living mulch is an alternative cropping system in which a CC grows year round with a commodity crop planted into it. Living mulches provide numerous environmental benefits to the community and land managers by reducing soil erosion [*Wall et al., 1991*], increasing soil organic matter [*Farahbakhshazad et al., 2008*], reducing nitrate (NO₃⁻) leaching [*Ochsner et al., 2010*], and improving the field's pest resilience [*Enache and Ilnicki, 1990*]. The leguminous perennial KC can grow alongside corn and, when managed correctly, may only minimally impact grain yield [*Zemenchik et al., 2000*]. We have successfully grown soybeans interseeded into KC as well [*Baker, 2012*], so it has the potential to be a perennial living mulch for corn-soybean rotational systems. However, for farmers to make informed management decisions relative to total environmental impact, the N₂O advantages or disadvantages of living mulches must also be considered.

The impacts of CCs on agricultural N₂O emissions are poorly understood because studies have been sparse and conflicting [*Basche et al., 2014*]. Leguminous CCs have been reported to either increase [*Gomes et al., 2009*] or have no effect [*Alluvione et al., 2010; Barton et al., 2011*] on the N₂O budget. Leguminous production of N₂O is driven

by the decomposition of N-rich residues [Rochette and Janzen, 2005], rather than the process of BNF [Zhong *et al.*, 2009]. Residues of legume CC species generally have low (< 25:1) carbon (C):N ratios [Gomes *et al.*, 2009] that permit rapid decomposition and nitrification of biotic N, creating an abundance of NO_3^- for N_2O production. Because living mulch systems are not terminated, proper management of these perennial systems could curtail the N_2O losses observed following the termination of a CC [Basche *et al.*, 2014], which are amplified at low C:N residue ratios [Huang *et al.*, 2004]. However, the effects of KC management and root turnover on N_2O emissions are unknown. There is hope that agricultural producers can play an important role in climate change mitigation, but that requires a better understanding of the impact of alternative management practices on greenhouse gas emissions. Toward that end, our objective was to compare N_2O emission budgets from a conventional CS system to one that included a KC living mulch in a strip-tilled, irrigated field over two growing seasons.

Methods and Materials

Site Description and Experimental Design

The experiment was conducted in a 17-ha field on the University of Minnesota Rosemount Research and Outreach Center near Rosemount, MN (44°42' N 93°06' W) over the 2013 and 2014 growing seasons. The soil is a Waukegan silt loam consisting of a silt loam surface layer of 0.4 - 0.7-m depth overlying a layer of outwash sand and gravel > 20-m thick. It is well drained and the surface layer has an organic matter content

of 5.2% and a pH of 6.4 [Baker, 2012]. This location has been under nearly continuous cultivation for 125 years, primarily in corn and soybeans since the 1950's [Griffis *et al.*, 2007].

Kura clover was established vegetatively in the summer of 2010, with the primary intent of comparing corn and soybean production in a living mulch versus conventional production [Baker, 2012]. The field is equipped with a center pivot. The field was split into four blocks (quartered), and each block was subdivided into four 1-ha plots: irrigated CS, irrigated KC, rain-fed conventional CS, and rain-fed KC. Our instruments were housed on the border between an irrigated CS plot and an irrigated KC plot.

Measurements reported here were taken only from the irrigated plots. For the past four years, the entire field has been in a corn-soybean rotation, with soybean in even years and corn in odd. Each year the entire field is strip-tilled immediately before planting using an Othman 6-row unit. This implement has a single shank with fluted row cleaners in front of the shank and wavy coulters on either side.

Glyphosate (N-(phosphonomethyl)glycine)-resistant seed was planted on DOY 154 (Corn; Pioneer P9917R) and 151 (Soybean; Pioneer 22T69R) in 2013 and 2014, respectively. In late spring following strip-tillage and planting, during the crucial germination and early growth period for corn and soybeans, the KC remaining in the inter-row grows vigorously, competing with the young crop for light and resources [Baker, 2012]. To minimize these impacts, the KC was mowed to a height of 0.05-m shortly after planting on DOY 165 and DOY 163 in 2013 and 2014, respectively, with the residue left to decompose [Baker, 2012]. Weed control in both treatments was

accomplished with a glyphosate application at a rate of 1.04 kg ae ha⁻¹ on DOY 176 and 175 in 2013 and 2014, respectively. This rate has been tailored to suppress rather than to kill the KC [Zemenchik *et al.*, 2000], while also controlling weeds. To minimize water stress, the field received 12.5-mm from the center pivot irrigator on 7 and 3 occasions in 2013 and 2014, respectively.

To capitalize on the BNF benefit provided by the KC, the N rate was reduced (-43%) during the corn phase (2013) in the KC relative to the CS treatment. We anticipated that labile KC residues created by tillage and mowing would release mineralizable N in the root zone to support crop requirements. On DOY 154, a broadcast pre-plant N, P, K starter fertilizer (9-18-9) provided 6.7 kg N ha⁻¹ to the entire field. The whole field was side-dressed with a 28% urea and ammonium nitrate (UAN) solution at a rate of 57.1 kg N ha⁻¹ on DOY 171. The remainder, 76.2 (DOY 200) and 15.7 (DOY 203) kg N ha⁻¹, was applied to the CS and KC treatment, respectively as 28% UAN through the center pivot irrigator. Fertilizer was not applied to the soybean crop in 2014.

Nitrous Oxide Emissions

Soil N₂O fluxes were measured with automated soil chambers (Model LI8100-104; Li-Cor Inc., Lincoln, NE, USA) controlled by a datalogger (Model 23X; Campbell Scientific, Logan, UT, USA) connected to a multiplexer controlling two sets of solenoids (Clippard Inc., Cincinnati, OH, USA) [Fassbinder *et al.*, 2013; Baker *et al.*, 2014]. All soil chambers ($n = 8$) were vented, finished with white enamel to minimize solar heating, and installed onto PVC collars. The collars were placed at the center of the inter-row and

inserted 0.05-m into the soil. A rubber gasket and weather stripping prevented ambient dilution during chamber closure. Each chamber was activated for 7-min at one hour intervals during which headspace air was pulled through a column of desiccant before entering a N₂O analyzer (Model M320EU2; Teledyne Instruments API, San Diego, CA, USA). A nafion dryer within the Teledyne removes remaining H₂O vapor before the sample air enters the measurement cell. Fluxes ($n = 31,539$ and $28,972$ for 2013 and 2014, respectively) were calculated using:

$$F = \frac{PV\Delta}{ART} \quad (\text{Equation 4.1})$$

P is air pressure (Pa), V is the chamber volume (0.004 m^3), A is the chamber footprint (0.032 m^2), R is the molar gas constant ($\text{J mol}^{-1} \text{ }^\circ\text{K}^{-1}$), T is the air temperature at the time of measurement ($^\circ\text{K}$), and Δ is the slope of N₂O concentration change over time in the chamber headspace. Prior to slope calculation, the raw N₂O concentration data were passed through a wavelet de-noising algorithm to improve the signal to noise ratio [Fassbinder *et al.*, 2013]. The slope was calculated from a 90-s window beginning 150-s after chamber closure. All data were processed using Matlab software (Version R2013b; Mathworks, Natick, MA, USA).

Climate, Soil, and Plant Analyses

Precipitation was measured at a micrometeorology tower located 1.6-km east of the experimental field. Soil temperature and volumetric water content were measured in each plot at 0.05, 0.1, 0.2, 0.3, and 0.4-m (5TM; Decagon Devices Inc, Pullman, WA, USA) at 30-min intervals (EM-50; Decagon Devices Inc, Pullman, WA, USA). Each

chamber was equipped with a thermocouple (Type E) to measure soil temperature at 0.05-m depth. In August 2015, aboveground KC biomass was collected and samples ($n = 21$) were dried and pulverized before total carbon and nitrogen were calculated with an elemental analyzer (VarioMax; Elementar, Hanau, Germany). At crop maturity, corn and soybean grain from 6-m row sections in each plot were hand-harvested, dried, and weighed to obtain grain yields.

Data Analysis and Statistics

The 24-h cumulative area-scaled N₂O emissions were determined by integration of the daily mean flux for each plot. The cumulative emission budget was calculated for each plot as the sum of the daily area-scaled emissions during the measurement periods (196 and 151-d in 2013 and 2014, respectively). Missing data due to instrument downtime (3% and 17% in 2013 and 2014, respectively) were not gap filled and therefore the cumulative emissions represent a conservative estimate. Yield-scaled emissions were determined by dividing the annual cumulative area-scaled emissions by the dry grain yield. Normality was evaluated using a Kolmogorov–Smirnov test. The daily cumulative area-scaled N₂O emissions were log transformed to improve normality [McSwiney *et al.*, 2010]. Treatment significance was assessed using a two-factor analysis of variance (ANOVA) [Jarecki *et al.*, 2009] of log transformed cumulative area-scaled daily N₂O emission data, treatment, and year. Automated chambers provide a temporally rich dataset that was used to evaluate emissions associated with different field activities (e.g., strip-tilling, mowing, and spraying) and periods (prior to strip-tilling and post-

anthesis) using paired *t*-tests ($\alpha = 0.01$) of log transformed daily area-scaled N₂O emissions. Photographs from 2013 were used to estimate the onset of crop anthesis (DOY 226). For consistency, DOY 226 was used in our 2014 analyses.

Results and Discussion

Overall, daily average N₂O fluxes were significantly influenced by the treatment (KC > CS; $p < 0.001$) and year (2013 > 2014; $p < 0.005$). The year effect is most likely a result of fertilizer application that only occurred during the corn phase (2013), rather than a meteorological difference. Average air temperature and precipitation during the measurement period in each year were 17°C and 606-mm and 17.5°C and 818-mm in 2013 and 2014, respectively (data not shown). Corn (2013; $p = 0.08$) yields were 11.1 ± 0.9 and 9.7 ± 0.9 Mg (dry) ha⁻¹ while soybean (2014; $p = 0.03$) yields were 2.51 ± 0.11 and 2.11 ± 0.18 Mg ha⁻¹ in the CS and KC treatments, respectively.

2013 – Corn

Presence of the KC living mulch significantly affected N₂O emissions during the corn phase (Figure 4.1). Cumulative area-scaled and yield-scaled emissions were, 2.3 ± 0.1 kg N ha⁻¹ and 233 ± 112 g N Mg⁻¹ grain, respectively in KC, and 1.3 ± 0.1 kg N ha⁻¹ and 118 ± 137.6 g N Mg⁻¹ grain in the CS, respectively. During the entire measurement period, the average volumetric water content and soil temperature at 0.05-m depth was 0.24 ± 0.02 and 16.5 ± 6.6 °C, respectively, from the KC treatment and 0.22 ± 0.02 and 14.5 ± 6.5 °C, from the CS respectively (data not shown).

2014 – Soybeans

The KC living mulch increased N₂O emissions during the soybean phase (Figure 4.1). Area-scaled and yield-scaled emissions were 1.6 ± 0.1 kg N ha⁻¹ and 765 ± 65 g N Mg⁻¹ grain, respectively from the KC treatment, and 0.7 ± 0.1 kg N ha⁻¹ and 291 ± 58 g N Mg⁻¹ grain from the CS treatment, respectively. Intermittent problems with our soil moisture and temperature probes prevented a full assessment of the treatment effects on the microclimate during 2014.

Prior to Strip-Tillage

The available data suggest that the KC living mulch may have marginally reduced N₂O emissions in the spring, prior to strip-tillage (Table 4.1). Although the treatment effect was not significant, the CS treatment emitted 9.3 mg N₂O-N m⁻² and 12 mg N₂O-N m⁻² more than the KC treatment in 2013 and 2014, respectively (Table 4.1). This trend may have resulted from greater residual soil N in the CS treatment, which the presence of a CC has been shown to reduce [Nair and Lawson, 2014]. This benefit, known as N “scavenging”, is the result of greater plant N demand, especially outside of the growing season. The KC living mulch removes N that would otherwise be available for N₂O production in the spring, contrary to the CS plots that were left fallow between growing seasons. The presence of an over-winter CC can result in lower spring N₂O emissions relative to fallow conditions [Wagner-Riddle and Thurtell, 1998]. The amount of residual N scavenged by a CC is variable and depends on the CC species [Nair and Lawson, 2014] and management decisions [Komatsuzaki and Wagger, 2015]. In Iowa,

uptake estimates of 20 kg N ha⁻¹ are common from rye CCs [Nair and Lawson, 2014] while rates as high as 80 kg N ha⁻¹ under legume CCs have been observed in the Philippines [George *et al.*, 1994]. Importantly, N scavenging can improve the field's overall nitrogen use efficiency by assimilating and recycling N [George *et al.*, 1994] that could be lost through leaching and runoff. In addition to N scavenging, the additional surface residue alters the KC soil microclimate by insulating the surface from solar radiation. However, we did not observe significant differences in soil temperature or volumetric water content between treatments during this period in 2013 (temperature: $p = 0.8$; moisture: $p = 0.5$) or 2014 (temperature: $p = 0.9$; moisture: N/A).

Strip-Tilling and Planting

Area-scaled N₂O emissions increased immediately after strip-tillage (Figure 4.1). Emissions from the KC treatment were up to 2.6-fold higher than the CS treatment in 2013 (Table 4.1). An even stronger N₂O emission response was observed in 2014 after tillage and planting where total N₂O losses from the KC treatment were 3.6-fold greater than the CS treatment (Table 4.1). Since strip-tillage and planting are disruptive activities, damage to the KC root system, coupled with incorporation of above-ground vegetation, may have caused the release of mineralizable N.

Mowing

Immediately following KC mowing, emissions were not significantly different between treatments in 2013 or 2014 (Table 4.1). However, cumulative N₂O emissions from the KC treatment were 1.5 and 1.6-fold larger than the CS treatment during 2013

and 2014, respectively (Table 4.1). This may represent a direct response of mowed KC residue mineralization as others have also observed high N₂O emissions coinciding with CC decomposition [Brozyna *et al.*, 2013; Mitchell *et al.*, 2013; Basche *et al.*, 2014]. The application of residue on the surface has resulted in a positive effect on N₂O emissions [Baggs *et al.*, 2003] that are amplified at low C:N residue ratios [Huang *et al.*, 2004]. Leaving the clippings in place can alleviate the denitrification carbon limitation creating an opportunity for high N₂O production [Mitchell *et al.*, 2013]. Kura clover biomass samples show that the C:N ratio was 14.4:1, which is considerably lower than corn stover (>50:1) [Baker *et al.*, 2014], with an average of 2.8% N. The low C:N ratio of the KC clippings would allow for rapid decomposition and nitrification, boosting soil NO₃⁻ content for N₂O production. Further, rapid decomposition would deplete oxygen, creating a more conducive environment for denitrification. Although CC residues may also immobilize soil N [McSwiney *et al.*, 2010], our results suggest that the KC clippings had a positive, but minor effect on N₂O emissions (Table 4.1).

Suppression Spraying

After herbicide application, N₂O emissions from the KC treatments were elevated (1.9-fold) above the CS treatments in 2013 (Table 4.1). Likewise, KC N₂O emissions were substantially greater (2.6-fold) in the period after suppression and prior to anthesis in 2014. The amplification of KC emissions following herbicide application may have been in response to KC mineralization. Suppression spraying can release N from the root system [Zemenchik *et al.*, 2000] that would be an important source of inorganic N for the

crop. Moreover, the mineralization of KC root exudates may partially explain the N₂O emission pulse observed on DOY 180 in 2013.

Fertilizer Application

The N₂O emissions from the KC treatment were 1.8-fold greater than the CS treatment following side-dressing, which was possibly bolstered by plant stress caused by KC mowing or the recent decomposition of mowed KC residue (Table 4.1). Similarly, plant stress brought about by the recent application of herbicides may partially explain why KC emissions were 3-fold greater than the CS treatment following fertigation (Table 4.1). By increasing N and C availability while depleting O₂, the rapid decomposition of residues and plant stress may enhance KC N₂O emissions, a response that becomes even more pronounced when N fertilization follows these events. Further, the comparatively low N₂O emission response from the CS treatment could indirectly signal optimal N application timing that facilitated rapid uptake by actively growing corn. A reduction in N₂O emissions has been observed in fertigated vegetable systems [Kennedy *et al.*, 2013] as N is applied more in line with crop needs.

Post-Anthesis Mineralization

In 2013 and 2014, a substantial proportion of the cumulative KC emissions occurred after anthesis (Figure 4.1). Emissions from the KC treatment were 2.4-fold greater than the CS treatment from DOY 226 through the end of the 2013 measurement campaign, likely in response to post-senescence kura mineralization (root turnover +

exudates). This late season pulse was responsible for 28% of the cumulative KC N₂O budget while 20% of the CS budget was lost during the same period (Table 4.1).

The post-anthesis burst in 2014 was sufficiently large to offset the significant modest early season N₂O reductions provided by KC N scavenging. Kura clover losses here accounted for 49% of the cumulative N₂O budget, but only 17% of losses from the CS (Table 4.1). Since we did not observe a similar pulse from the CS treatment, this would indicate that post-harvest mineralization of N from soybean residues must have been minimal. However, because measurements were seasonally limited to spring, summer, and fall, it is possible that low winter emissions from the KC treatment could counterbalance our observations [*Basche et al.*, 2014].

Irrigation

There were emission pulses following irrigation events in 2013 on DOY 186 (1st irrigation event) and DOY 233 (5th irrigation event), where the CS system lost 63 and 43% more N₂O, respectively than the KC treatment (data not shown). Greater levels of available N earlier in the season that are progressively depleted through the growing season may have been responsible for the pulse observed on DOY 186. The remaining five irrigation events in 2013 exhibited a negligible effect on emissions, possibly because either the standard 12.5-mm irrigation event was insufficient to saturate soils and promote denitrification or because of low residual N. Further, the emission response following irrigation on DOY 233 may have been made possible because an irrigation

event 5-d prior “primed” the soil microbe community. There was not an N₂O emission response to irrigation from either treatment during the 2014 (soybean) period.

Indirect Emissions

We did not consider the role of indirect N₂O emissions (i.e. through subsequent denitrification of NO₃⁻ lost in leaching and runoff) in our budget. Offsite nitrous oxide emissions associated with leaching and runoff have been identified as strong sources [Chen *et al.*, 2016], especially in agricultural regions [Griffis *et al.*, 2013; Turner *et al.*, 2015]. If perennial crops can consistently reduce NO₃⁻ leaching [Ochsner *et al.*, 2010], a necessary precursor for aquatic N₂O production [Turner *et al.*, 2016a], it is conceivable that groundwater and riverine emissions would be mitigated by increased use of KC living mulch systems, although indirect emissions are highly uncertain and much additional research is needed.

Conclusions

Perennial cover crops offer many environmental benefits to agricultural systems. However, reduction of N₂O emissions may not be one of them. We observed that even with a 43% reduced N application rate compared to a conventional corn-soybean system, the KC living mulch system increased direct N₂O emissions. Our data suggest an important trade-off in the KC system whereby emissions prior to strip-tilling may be lowered due to N scavenging, but strong emissions driven by post-anthesis mineralization offset this benefit. Lastly, because differences in corn grain yield were not significant, it

is possible that the N application rate could be reduced further to minimize N₂O emissions.

Acknowledgements

This work was supported by US Department of Agriculture Grant USDA-NIFA 2013-67019-21364 and by the USDA – Agricultural Research Service. We thank William Breiter, Jeffrey Coulter, Michael Dolan, and Joel Fassbinder for field, laboratory, and statistical assistance.

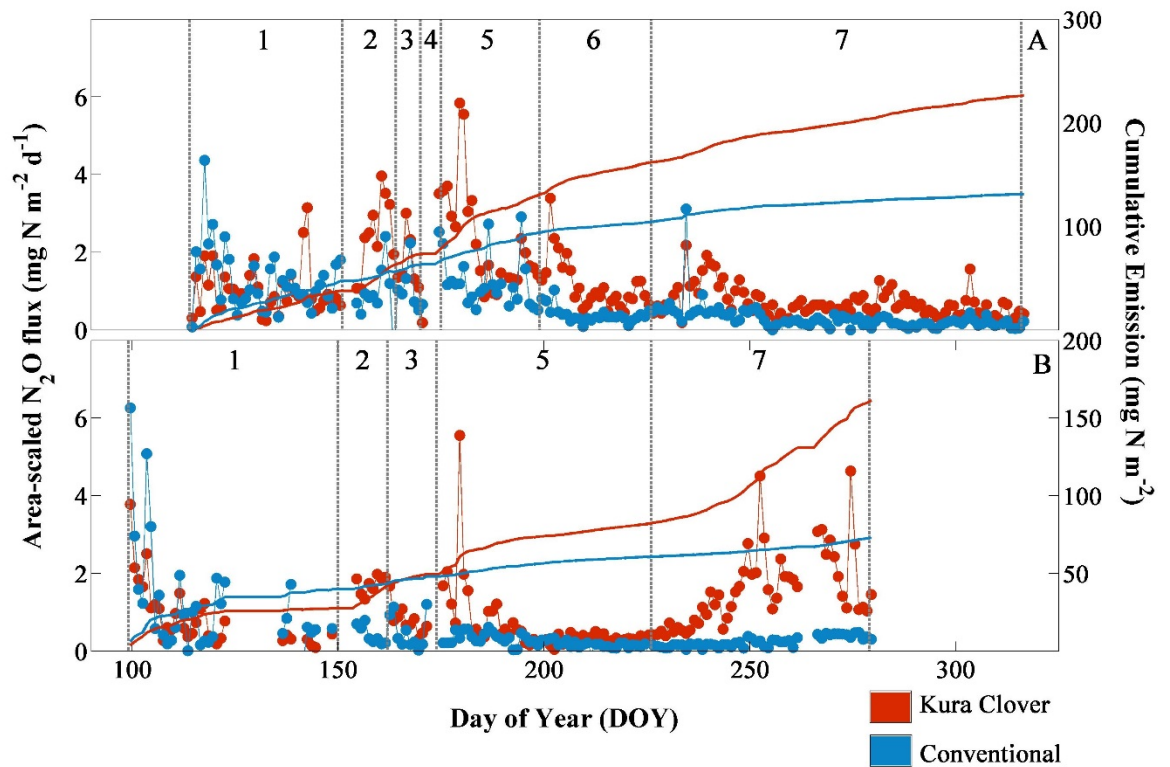


Figure 4.1. Daily area-scaled N_2O fluxes (symbols) and cumulative emissions (lines) for (A) 2013 and (B) 2014 averaged ($n = 4$) by treatment. Missing data due to instrument downtime were not gap filled. Cumulative emissions represent the sum of treatment daily averaged fluxes throughout the measurement period. Dotted vertical lines and numbers correspond with emission intervals described in Table 4.1.

Year		Prior to Field Activity 1	Tillage, Planting 2	Mowing 3	Side-Dressing 4	Spraying 5	Fertigation 6	Post Anthesis 7	Cumulative
2013	DOY Range	114-151 <i>n</i> = 37	152-164 <i>n</i> = 11	165-170 <i>n</i> = 6	171-175 <i>n</i> = 2	176-199 <i>n</i> = 23	200-226 <i>n</i> = 27	227-316 <i>n</i> = 90	114-316 <i>n</i> = 196
	Kura Clover Treatment (mg N m ⁻²)	37.8	26.2	9.4	7.1	51	30.6	64.4	226.5
	Conventional Treatment (mg N m ⁻²)	47.1	10	6.4	4.8	26.2	10.2	26.6	131.3
	Treatment Difference (mg N m ⁻²)	-9.3 <i>p</i> = 0.15	16.2 <i>p</i> < 0.01	3 <i>p</i> = 0.4	2.3 <i>p</i> = 0.02	24.8 <i>p</i> < 0.01	20.4 <i>p</i> < 0.01	37.8 <i>p</i> < 0.01	95.2 <i>p</i> < 0.01
2014	DOY Range	99-150 <i>n</i> = 32	151-162 <i>n</i> = 9	163-174 <i>n</i> = 9	N/A	175-226 <i>n</i> = 52	N/A	227-279 <i>n</i> = 49	99-279 <i>n</i> = 151
	Kura Clover Treatment (mg N m ⁻²)	27.7	15.5	6.4		32.9		78.8	161.3
	Conventional Treatment (mg N m ⁻²)	39.7	4.3	4		12.7		12.1	72.8
	Treatment Difference (mg N m ⁻²)	-12 <i>p</i> = 0.3	11.2 <i>p</i> < 0.01	2.4 <i>p</i> = 0.08		20.2 <i>p</i> < 0.01		66.7 <i>p</i> < 0.01	88.5 <i>p</i> < 0.01

Table 4.1. The cumulative emissions and results from statistical analyses from each activity period during the two sample years. The numbered intervals correspond to Figure 4.1. Sample size (n) excludes instrument downtime. The total emissions during a measurement interval are reported while the difference between treatments (kura clover – corn-soybean) has been given. Significance was determined using paired t -tests were performed on the log-transformed emissions over the listed DOY range.

Chapter 5

A geostatistical approach to identify and mitigate agricultural nitrous oxide emission hotspots

Peter A. Turner, Timothy J. Griffis, David J. Mulla, John M. Baker, and Rodney T.

Venterea (2016), *Science of the Total Environment*, (572), 442-449,

doi: 10.1016/j.scitotenv.2016.08.094

© Elsevier Ltd.

Highlights

1. Geospatial analyses resolved N₂O emissions at fine spatial scales
2. Hotspots emitted N₂O at rates more than 2-fold greater than non-hotspot locations
3. Targeted management of N₂O hotspots could reduce emissions by 17%

Overview

Anthropogenic emissions of nitrous oxide (N₂O), a trace gas with severe environmental costs, are greatest from agricultural soils amended with nitrogen (N) fertilizer. However, accurate N₂O emission estimates at fine spatial scales are made difficult by their high variability, which represents a critical challenge for the management of N₂O emissions. Here, static chamber measurements ($n = 60$) and soil samples ($n = 129$) were collected at approximately weekly intervals ($n = 6$) for 42-d immediately following the application of N in a southern Minnesota cornfield (15.6-ha), typical of the systems prevalent throughout the U.S. Corn Belt. These data were integrated into a geostatistical model that resolved N₂O emissions at a high spatial resolution (1-m). Field-scale N₂O emissions exhibited a high degree of spatial variability, and were partitioned into three classes of emission strength: hotspots, intermediate, and coldspots. Rates of emission from hotspots were 2-fold greater than non-hotspot locations. Consequently, 36% of the field-scale emissions could be attributed to hotspots, despite representing only 21% of the total field area. Variations in elevation caused hotspots to develop in predictable locations, which were prone to

nutrient and moisture accumulation caused by terrain focusing. Because these features are relatively static, our data and analyses indicate that targeted management of hotspots could efficiently reduce field-scale emissions by as much 17%, a significant benefit considering the deleterious effects of atmospheric N₂O.

Introduction

Nitrous oxide (N₂O) is a potent greenhouse gas [Hartmann *et al.*, 2013] and the leading cause of stratospheric ozone loss [Ravishankara *et al.*, 2009]. In response to its deleterious environmental effects, efforts to mitigate agricultural emissions, which account for nearly 75% of the national anthropogenic source [US Department of State, 2014], are in development. Such efforts often focus on N management improvements (e.g., optimizing the source, depth, and timing of fertilizer) at the field or farm scale. Yet, the findings from these mitigation strategies have been highly variable [Venterea *et al.*, 2016], in part because episodic and spatially variable emissions hinder accurate budget estimates [Velthof *et al.*, 2000; Mathieu *et al.*, 2006]. For instance, field-scale N₂O emission measurements with chambers can yield a coefficient of variation (CV) as high as 500% [Folorunso and Rolston, 1984; van den Pol-van Dasselaar *et al.*, 1998], suggesting that our ability to accurately determine the outcome of mitigation practices is cause for concern. At fine sub-field spatial scales (<1 m² to 1000 m²), N₂O “hotspots” appear to be disproportionately strong sources [Parkin, 1987; van den Heuvel *et al.*, 2009], yet their influence over cumulative field-scale emissions remains uncertain because high-resolution data are rarely available. For farmers to manage N₂O emissions

effectively, subfield-scale emission estimates are necessary to identify potential hotspots and to benchmark their effects on field-scale mitigation practices.

Light detection and ranging (LiDAR) digital elevation models (DEMs) are powerful tools that can help guide precision agriculture and conservation strategies [Galzki *et al.*, 2011; Wan *et al.*, 2014]. When coupled with geospatial techniques, this emerging technology helps generate high-resolution maps of agriculturally relevant information such as the presence of hydric soils [Fink and Drohan, 2016], moisture content [Moore *et al.*, 1993; Murphy *et al.*, 2009], and soil nitrogen status [Weintraub *et al.*, 2014] that allow farmers to focus extra attention and resources on critical areas. Furthermore, complex processes like methane emissions [Sundqvist *et al.*, 2015] have been characterized using DEMs, suggesting that this technology can better resolve the field-scale spatial distribution of N₂O emissions.

Indeed, differences in topography and landscape position have a strong influence on N₂O emissions [Ball *et al.*, 1997; Ambus, 1998] because terrain gradients redistribute moisture and nutrients that are necessary for the production of N₂O. Consequently, N₂O emission frequency distributions are typically positively skewed by a few strong sources [Parkin, 1987; Velthof *et al.*, 2000] observed at topographically low positions [Ambus, 1998]. Here, terrain focusing enables the development of hotspots by concentrating organic matter, moisture, and nitrate (NO₃⁻) into localized, but potentially predictable areas. Taken together, these soil characteristics can support disproportionately high rates of denitrification [Groffman *et al.*, 2009] that we posit are capable of sustaining high N₂O emissions. However, field-scale emission distribution maps remain coarse, since an

unrealistic number of static chambers are required to resolve the high variability, implying poor constraints on hotspots.

With the aid of DEMs and geospatial analyses, denitrification hotspots can be isolated and mapped by pinpointing locations with the highest probability of moisture and NO_3^- accumulation [Anderson *et al.*, 2015]. We propose that a similar approach can resolve the distribution of N_2O emissions at a high spatial resolution that will guide targeted mitigation practices. Here, we examine the spatial distribution of N_2O fluxes and cumulative emissions in a strip-tilled cornfield to address three questions: 1) can DEMs help predict where N_2O hotspots will develop on the landscape; 2) how significant are hotspots in the cumulative field-scale budget; and 3) how can DEMs be used to guide N management and N_2O mitigation?

Materials and Methods

Site Description and Experimental Design

The tile-drained, corn-soybean rotation research field (15.6-ha) was located on a private farm 11-km south of Northfield, Minnesota (44°21'37.2"N, 93°12'14.8"W). The predominant underlying soil is a Prinsburg silty clay loam (Typic Endoaquolls, USDA Classification) overlying a loam. Measurements were made during the corn (*Zea mays*, L.) phase in 2014 on DOY 126, 134, 150, 156, 161, and 168. The field was strip-tilled prior to planting and fertilized with 32% urea ammonium sulfate (UAS) on DOY 125 at a rate of 140 kg N ha⁻¹.

A 3-m micrometeorological tower was installed on the west side of the field to measure air temperature (VP-4; Decagon Devices, Pullman, WA, USA). Observations were recorded with a data logger at 5-min intervals and averaged hourly (Model EM50; Decagon Devices, Pullman, WA, USA).

All soil and chamber sample locations were georeferenced using a GPS device (GeoXH; Trimble, Sunnyvale, CA, USA) connected to a Mi-Fi mobile hotspot (model 2200; Verizon Wireless, Wallingford, CT, USA) that boosted the horizontal accuracy to 0.1 m. Spatial data were analyzed using ArcMap (ArcGIS v.10.2; ESRI Inc., Redlands, CA, USA).

To capture the effects of terrain on N₂O emissions and to ensure potential hotspots were included in the measurement campaign, a Wetland Probability Index (WPI) map was created (ArcGIS v.10.2; ESRI Inc., Redlands, CA, USA) to guide the experimental design. The WPI is a regression function of four factors: the presence of hydric soils, slope, profile curvature, and a compound topographic index (CTI) that is a function of flow accumulation and slope. The WPI provides a relative metric to describe the likelihood that water will pond at a specific location and has been used to identify areas for efficient wetland reclamation [Wan *et al.*, 2014]. The WPI was chosen rather than the widely used soil wetness index (SWI), because the WPI incorporates drainage (hydric soils), a recognized shortcoming of the idealized SWI [Murphy *et al.*, 2009]. In the context of N₂O production, field locations with wetland terrain characteristics are likely to accumulate moisture and nutrients and are thus candidates for hotspot formation. These areas are likely to experience more frequent and prolonged periods of soil

saturation than upland areas, in part because of low slopes and elevation. Using high-resolution (1-m) DEM data (Minnesota Geospatial Information Office) and soil survey information, each position on the landscape was assigned a relative WPI value of 0 to 1 [Wan *et al.*, 2014].

Since the natural movement of soil moisture is not confined to the explicit 1-m WPI grid, the highest spatial resolution is not necessarily appropriate for direct comparison with a dependent variable [Sørensen and Seibert, 2007]. For instance, contour cropping, crop residues, buffer strips and microtopography can affect the movement of moisture. To minimize these uncertainties, we have reduced the WPI resolution to 10-m [Zhang and Montgomery, 1994; Anderson *et al.*, 2015] for direct comparison of N₂O emission measurements and surface characteristics. All other analyses used the high-resolution WPI data set.

Because terrain differences can influence emissions, a stratified sampling design based on WPI was used to characterize emission heterogeneity. Groups ($n = 6$) of chambers ($n = 10$) were installed in the field across a range of WPI values on each of the sample dates. Measurements were taken at approximately weekly intervals for 42-d immediately after fertilization (DOY 125). Previous experiments in this field indicate that N₂O fluxes are highest in the 20 to 50-d following fertilization [Fassbinder *et al.*, 2013; Baker *et al.*, 2014]. Beyond this time frame, N₂O fluxes decline [Baker *et al.*, 2014; Turner *et al.*, 2016b] and as a result, the cumulative emission budget is most sensitive to loss during this brief period.

Nitrous Oxide Measurements

Soil N₂O fluxes were measured manually with non-flow-through non-steady-state chambers with a design that has been used extensively in agricultural systems [Maharjan and Venterea, 2014; Maharjan *et al.*, 2014; Venterea and Coulter, 2015]. Briefly, each chamber consisted of a stainless steel base inserted 0.05-m into the soil and a removable top (0.50 m x 0.29 m x 0.086 m). Weather stripping and spring clamps attached to opposing sides sealed the chamber headspace from ambient mixing. Each chamber top was vented and covered with an insulated, reflective material. Measurements were taken after at least 48-hr following chamber installation to avoid the potential influence of soil disturbance on the flux.

Gas samples were taken from between 0900 and 1500 local time at 0, 15, 30, and 45 minute intervals using a 12-mL polypropylene syringe inserted through a butyl rubber septum on the chamber lid. An ambient air sample was taken immediately after chamber closure. Samples were immediately transferred into glass vials sealed with butyl rubber septa and analyzed within one week using a headspace autosampler (Teledyne Tekmar; Mason, OH, USA) connected to a gas chromatograph (model 5990; Agilent/Hewlett-Packard, Santa Clara, CA, USA) equipped with an electron capture detector. Helium was used as the carrier gas in the GC analyses and the system was calibrated with analytical standards (Scott Specialty Gases, MI) [Bavin *et al.*, 2009]. Concentrations from the GC were converted into mass per volume units, assuming ideal gas relations and a known air temperature while sampling.

The slope of the chamber headspace gas concentration was determined using either a linear regression or a quadratic model depending on the curvilinearity of the slope [Parkin *et al.*, 2012; Venterea, 2013]. The linear slope was calculated using the SLOPE function (Excel v.2013; Microsoft, Redmond, WA) and the quadratic slope was estimated using the LINEST function at time zero. The quadratic model accounts for suppression of the concentration gradient in response to chamber closure, but is not always necessary. A linear slope was chosen if the second derivative of the quadratic equation was greater than zero [Maharjan *et al.*, 2014]. Soil fluxes were calculated using:

$$F = \frac{S \cdot V}{A} \quad \text{Equation 5.1}$$

where: S is the slope, V is the chamber volume (0.02-m³), and A (0.14-m²) is the chamber footprint. Cumulative N₂O emissions were calculated using trapezoidal integration that assumes linearity between sampling periods.

Soil Analyses

Within 24-hours of gas sampling, soil samples ($n = 129$) to a depth of 0.15-m were taken from a georeferenced 35-m grid using a hand corer. Soil samples were weighed within two hours. After drying at 105° C, gravimetric water content (θ) was determined. Using a 2 M KCl extraction, soil NO₃⁻ concentration was also determined [Maharjan and Venterea, 2014]. Extracts were filtered (Whatman no. 1) and NO₃⁻ was quantified using a flow-through injection analyzer (Lachat, Loveland, CO, USA). The NO₃⁻ intensity (NO₃⁻_{int}) was calculated using trapezoidal integration [Venterea *et al.*,

2011; *Maharjan and Venterea, 2014*], which assumes a linear slope between sample dates. Conceptually, $\text{NO}_3^-_{\text{int}}$ represents the cumulative exposure of soil microbes to NO_3^- . The θ intensity (θ_{int}) was calculated similarly. Stepwise regression models were used to identify any terrain indices that were significantly correlated with soil chemical variables.

Geostatistical Analyses

Interpolations of high-resolution N_2O flux and cumulative emission data were performed with ordinary cokriging (OC) in ArcMap (ArcGIS v.10.2; ESRI Inc., Redlands, CA, USA). Ordinary cokriging is a geostatistical approach that uses more frequently sampled secondary variables to improve prediction of the primary variable [*Vauclin et al., 1983*]. This method is useful when the primary attribute is costly or logistically more difficult to sample than other correlated variables.

Mean N_2O fluxes and cumulative emissions were interpolated at a resolution of 1-m with OC using an omnidirectional “stable” model. Soil NO_3^- and θ were used as secondary variables in this OC model. The sill (variance), nugget (estimate of independent or micro-scale errors), and range (maximum distance of autocorrelation) of each model were estimated from the semivariogram. The model parameters were optimized for estimation of the range value and neighborhood weights were based on distance. Cross validation was accomplished iteratively by comparing the observation to the OC model predicted value. All inputs were log transformed prior to OC to meet the assumption of normality.

A Getis-Ord G_i^* statistical test identified spatial clustering of high (hotspots) and low (coldspots) emissions at a 95% significance threshold [Ord and Getis, 2010]. The field was partitioned into three emission classes based on their respective z -score significance using ArcMap (ArcGIS v.10.2; ESRI Inc., Redlands, CA, USA). Locations with statistically significant high and low z -scores are referred to as emission hotspots and coldspots, respectively. All other values, i.e. those with insignificant ($p > 0.05$) z -scores, are considered “intermediate” locations. A Kruskal-Wallis significance test ($\alpha = 0.05$) was used to determine if there was a WPI difference among emission classes.

Results and Discussion

Meteorology and Soil Characteristics

Over the course of our measurement campaign, this field received 116.8 mm of precipitation and experienced a mean air temperature of 16.4°C. Across all sampling dates, the mean (range) soil NO_3^- concentration and θ content were 20.5 (0-107) mg NO_3^- kg^{-1} and 25% (12-50), respectively (Figure 5.1). Reported NO_3^- concentration and θ content frequency distributions were positively skewed on each sample date (data not shown), indicating the potential for nutrient processing hotspots. Following fertilization on DOY 125, the daily mean soil NO_3^- concentrations increased until DOY 157, after which they started declining, likely as a result of a combination of leaching, denitrification, and crop uptake.

Analyses indicated that the WPI (10-m) was significantly ($p < 0.05$) correlated with θ_{int} and $\text{NO}_3^-_{\text{int}}$ observations ($r^2 = 0.6$ and $r^2 = 0.14$, respectively) (Figure 5.2).

These relationships provide evidence of terrain focusing, implicit in the WPI calculation (e.g., elevation, slope). Indeed, measurements of θ_{int} were significantly ($p < 0.05$) and negatively correlated with both elevation ($r^2 = 0.6$) and slope ($r^2 = 0.4$). Observations of $\text{NO}_3^-_{\text{int}}$ were not as tightly coupled to elevation ($r^2 = 0.09$) or slope ($r^2 = 0.05$) as θ_{int} , probably because of the complex N cycling dynamics (i.e. including both production and consumption of NO_3^-) present in soils. Overall, the samples with the highest θ_{int} and $\text{NO}_3^-_{\text{int}}$ were observed in locations with the lowest slope and elevation (Figure 5.2), suggesting that the soil factors necessary to sustain high denitrification fluxes can become concentrated in predictable areas. This finding provides further support that remote sensing techniques can offer important insights into field-scale N processing dynamics by identifying locations that have an elevated likelihood of moisture and nutrient accumulation [Weintraub *et al.*, 2014; Anderson *et al.*, 2015].

N₂O Emissions

Temporal Dynamics

Across all chambers and sampling dates, the mean (range) N₂O flux was 1.7 (-1 – 32) mg N₂O-N m⁻² d⁻¹. The magnitude of N₂O fluxes ranged from 0.7 mg N₂O-N m⁻² d⁻¹ on DOY 126, within 24-hrs of fertilization, to a peak emission of 4.3 mg N₂O-N m⁻² d⁻¹ on DOY 157, and decreased to a value of 1.8 mg N₂O-N m⁻² d⁻¹ on DOY 168 (Figure 5.1). Over the sample period, the average N₂O flux was positively correlated ($r^2 = 0.06$; $p < 0.05$) to WPI (10-m), indicative of a terrain signal. Indeed, elevation ($r^2 = 0.12$; $p < 0.01$) and slope ($r^2 = 0.04$; $p = 0.06$) correlated with average N₂O fluxes (Figure 5.3)

These hourly mean flux density observations are comparable in strength to a previous study that used 6 automated chambers to estimate the annual N₂O budget at this field site during the 2010 corn phase [Fassbinder *et al.*, 2013]. Those investigators determined that N₂O emissions were elevated for 20 to 50 days after fertilization, but then losses declined precipitously and the average hourly standard deviation fell 14-fold, suggesting relatively low temporal measurement uncertainty beyond this brief period [Fassbinder *et al.*, 2013].

Spatial Dynamics

Trapezoidal integration of chamber data indicated that the mean (SD) cumulative N₂O emission was 69 (61) mg N₂O-N m⁻² during the 42-d sampling period. We calculated a field-scale CV of 88% from the cumulative chamber data, which is lower than some investigations [Folorunso and Rolston, 1984; Ambus and Christensen, 1995; Ball *et al.*, 1997; Jones *et al.*, 2011; Molodovskaya *et al.*, 2011] and significantly higher than others [Christensen *et al.*, 1996]. The reason for our comparatively low CV may have been because our sample size ($n = 60$) was relatively large compared to those previous studies and better captured the spatial heterogeneity. Contrary to our hypothesis, there was not a significant relationship ($r^2 = 0.03$; $p = 0.1$), between the WPI (10-m) and cumulative N₂O emissions (Figure 5.3). The low r^2 was probably the result of other factors that influence emissions but were not explicitly included in our model, e.g., pH, gas diffusivity, and sources of N₂O other than denitrification including nitrification [Kool *et al.*, 2011; Venterea *et al.*, 2015]. Similarly, slope ($r^2 = 0.04$; $p =$

0.08) was not a significant correlate with N₂O emissions either (Figure 5.3). However, elevation ($r^2 = 0.09$; $p < 0.05$) exhibited a negative, although weak relation to N₂O emissions (Figure 5.3), indicating that topographic position can affect N₂O production.

Based on *a priori* hypotheses, θ_{int} and $\text{NO}_3^-_{\text{int}}$ were included as secondary OC variables to improve the average N₂O flux and cumulative emission model prediction ($n = 156,190$). Cross-validation of cumulative emissions determined that an omnidirectional stable model was appropriate. Stable model semivariograms indicate that the sill, nugget, and range of the average N₂O flux were 0.59 mg N₂O-N m⁻² d⁻², 0.37 mg N₂O-N m⁻² d⁻², and 244-m, respectively, while the sill, nugget, and range of the cumulative emissions were 0.7 mg N₂O-N² m⁻², 0.43 mg N₂O-N² m⁻², and 320-m, respectively (data not shown). As a measure of variance, the sill provides a field-scale estimate of spatial uncertainty, while the nugget is an estimate of either measurement uncertainty or microscale variation [Yanai *et al.*, 2003]. Here, a large nugget effect suggests large uncertainty at fine-scales. Observations taken from points separated by a distance greater than the range are no longer spatially autocorrelated, a point identified in the semivariogram where variance becomes asymptotic (i.e. the sill).

During the measurement period, the field emitted on average (SD) 1.4 (0.6) mg N₂O-N m⁻² d⁻¹, with a 43% CV, more than half that of the original chamber data (Figure 5.4). Cumulatively, the OC model predicted that 8.7 kg N₂O-N were emitted over the 42-d measurement (Figure 5.3). This translates to a field-scale mean (SD) cumulative flux of 55.4 (22) mg N₂O-N m⁻². The emission distribution was positively skewed, indicating that the data set was likely affected by hotspots. Because soil samples were not taken at

each individual chamber, OC interpolations of $\text{NO}_3^-_{\text{int}}$ and θ_{int} at each chamber were extracted to assess their relationships with cumulative N_2O emissions. These data show that cumulative N_2O emissions were significantly ($p < 0.01$) correlated with $\text{NO}_3^-_{\text{int}}$ ($r^2 = 0.25$) and θ_{int} ($r^2 = 0.18$) predictions (Figure 5.5).

Using a Getis Ord G_i^* statistical analysis, locations in this field were partitioned into three classes based on their emission strength within the context of neighboring values [Ord and Getis, 2010]. These analyses identified significant clustering of high and low N_2O emissions, characteristic of hotspots and coldspots, respectively (Figure 5.6). The mean (SD) flux from hotspots, intermediate, and coldspot locations was 2.5 (0.4) $\text{mg N}_2\text{O-N m}^{-2} \text{ d}^{-1}$, 1.3 (0.3) $\text{mg N}_2\text{O-N m}^{-2} \text{ d}^{-1}$, and 0.8 (0.05) $\text{mg N}_2\text{O-N m}^{-2} \text{ d}^{-1}$, respectively. Cumulatively, 3.1 kg $\text{N}_2\text{O-N}$, 4.6 kg $\text{N}_2\text{O-N}$, and 0.9 kg $\text{N}_2\text{O-N}$ were emitted from hotspots, intermediate, and coldspot locations, respectively.

These analyses indicate that a disproportionate share of the field-scale emission budget can be attributed to hotspot locations. Here, hotspots were responsible for 36% of the cumulative N_2O emission budget despite occupying only 21% of the field, while coldspots emitted 11% of the cumulative budget from a comparable area (18%). The remaining N_2O emissions (53%) were lost from intermediate locations, largely because 61% of the land surface fell under this emission class. However, the area of a field that qualifies as a hotspot could fluctuate based on meteorology – for instance, a particularly wet spring could increase the surface area of locations that experience prolonged and high moisture exposure. Kruskal-Wallis tests showed that the WPI observed in hotspot locations was greater than the WPI values typically found in the other emission classes,

in part because these locations had low slopes and elevation. A Kruskal-Wallis test revealed that hotspots had statistically different slopes (mean = 1.6%) and elevation (mean = 327.8-m) than intermediate (mean = 3.3%; 331.4-m) or coldspot (mean = 3.7%; 331.1-m) locations (data not shown).

Consequently, the general locations of hotspots were largely static, likely because of the strong relation with topographic indices, including elevation and slope. The positive relations identified here indicate that topography, *via* its controls on nutrient and moisture distributions, can help guide N₂O management practices. Towards this end, the disproportionate strength and stability of N₂O hotspots indicates that targeted management of these sources could efficiently reduce total emissions. For instance, if the average hotspot flux density were reduced from 2.5 mg N₂O-N m⁻² d⁻¹ to 1.3 (0.3) mg N₂O-N m⁻² d⁻¹, a magnitude that is more in step with intermediate areas, the mean field-scale flux density over the entire measurement period could be reduced by up to 14% (10-18). By reducing the cumulative hotspot emissions to 49 (10.4) mg N₂O-N m⁻², the rate observed in intermediate areas, the field-scale budget could be reduced by as much as 17% (12-22). The removal of hotspots through native wetland reclamation could reduce emissions by as much as 36%. Given the strong radiative forcing and other side effects of N₂O, these findings deserve serious consideration, especially if the distribution of potential hotspots is similarly predictable throughout the U.S. Corn Belt.

From a management perspective, emission hotspots were generally collocated with NO₃⁻_{int} hotspots. Consequently, variable rate nitrogen application (VRNA), a recent advancement in precision agriculture, could prove an effective tool to address N₂O

hotspots. This technology translates crop reflectance readings into fine-scale fertilizer decisions and has been shown to increase yield and income while providing promising N uptake results [Scharf *et al.*, 2011]. Better soil N management overall will potentially reduce N₂O emissions; however, the one-size-fits-all approach to fertilizer application may be a contributing factor to hotspots that VRNA can overcome. For instance, because low-lying areas accumulate surplus NO₃⁻ from upland areas and may not require additional N, VRNA can limit over application. Further, easing the NO₃⁻ surplus in upland areas using fine-scale fertilizer decisions could help mitigate the effects of terrain focusing. Alternatively, the selective application of enhanced efficiency N fertilizers (EENFs), which show promising N₂O mitigation results [Halvorson *et al.*, 2014], to hotspots *via* VRNA could minimize their strength. However, extrapolating the effect EENFs may have on hotspots here becomes difficult since EENF results are often specific to soil type and climate.

These data also showed that N₂O and θ_{int} hotspots were collocated, suggesting that N₂O hotspots are most likely to require subsurface drainage to ensure crop success. If conservation wetlands or VRNA were capable of reducing NO₃⁻ losses in tile drainage, either by improving N uptake for target and non-target species (i.e., wetland plants) or by reduced subsurface drainage overall, indirect emissions downstream could also be mitigated [Turner *et al.*, 2016a]. A reduction of offsite nitrate losses, like those from leaching and runoff, would be an important benefit because these can be disproportionately strong sources of N₂O, especially in the Corn Belt [Griffis *et al.*, 2013;

Turner et al., 2015; Chen et al., 2016]. However, little is known about emissions from conservation wetlands or the ultimate N₂O effect from VRNA.

Since our data set only includes six sample dates, these analyses may not include episodic emissions and therefore likely represent a conservative estimate. To resolve this uncertainty, automated soil chambers are an effective means for taking high frequency measurements [*Baker et al., 2014; Turner et al., 2016b*]. However, sampling constraints (e.g., cost, tube length, and on-site power) tether chambers to a central point, limiting their ability to capture the spatial distribution of emissions observed here. Therefore, the potential for terrain artifacts to bias measurements must be considered when selecting chamber placement. For instance, past work in this field explored various N₂O treatment effects using an automated chamber system [*Fassbinder et al., 2013; Baker et al., 2014*]. Although, those experiments were situated in a location that our analyses has classified as an intermediate strength emitter, they highlight the risks of automated chamber clusters in hotspot or coldspot regions.

Conclusions

Our data and analyses have shown that LiDAR DEMs and geospatial techniques can be valuable tools to resolve hotspots and model fine-scale N₂O emissions. Here, hotspots were disproportionately strong sources, responsible for more than a third of the cumulative emissions. Because hotspots are reliant on terrain focusing for nutrients and moisture, they are relatively static features. Consequently, their regularity and

predictability should facilitate targeted management practices that could reduce field-scale emissions by as much as 17%.

Acknowledgements

We thank Jeff Wood, Matt Erickson, Mike Dolan, William Breiter, Ke Xiao, Zichong Chen, and Lucas Rosen for field and laboratory assistance. This work was supported by the US Department of Agriculture (USDA) Grant USDA-NIFA 2013-67019-21364 and the USDA – Agricultural Research Service. We are also appreciative of the private landowner who volunteered their field for our use.

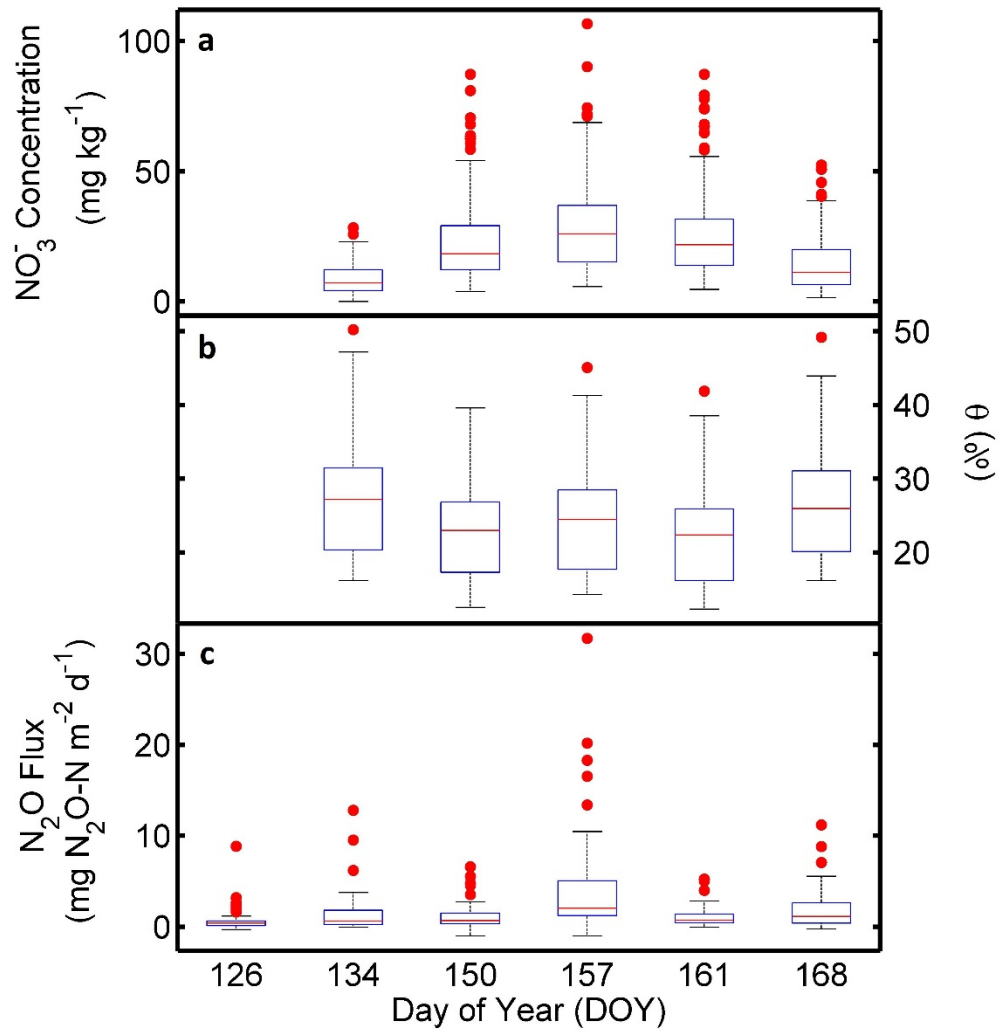


Figure 5.1. Boxplots of a) NO₃⁻ concentration (mg NO₃⁻ kg⁻¹), b) gravimetric moisture content (%), and c) N₂O flux density (mg N₂O-N m⁻² d⁻¹). Red points designate outliers.

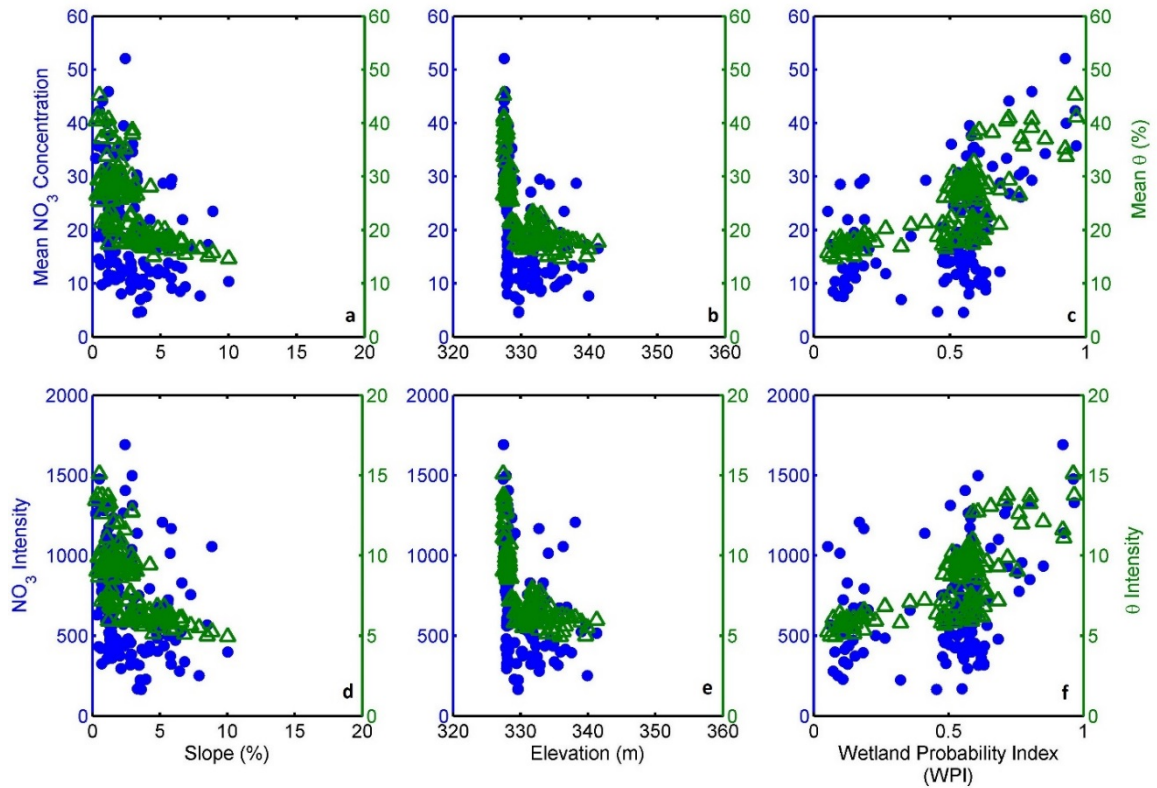


Figure 5.2. Plotted relationships between topographic indices and soil characteristics ($n = 129$). Top row). Mean soil NO_3^- concentration (blue dots); mean gravimetric water content (θ ; green triangles). Bottom row). Integrated soil NO_3^- ($\text{NO}_3^-_{\text{int}}$; blue dots); integrated gravimetric water content (θ_{int} ; green triangles).

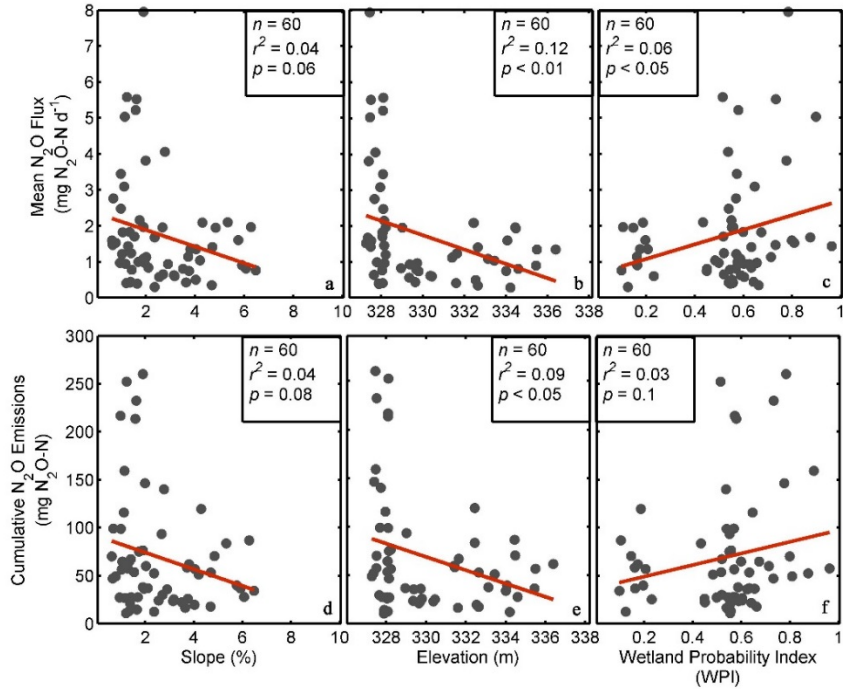


Figure 5.3. Plotted relationships between mean N_2O fluxes (a, b, and c) and cumulative N_2O emissions (d, e, and f) over the measurement period against topographic indices ($n = 60$). Lines of linear best fit (red lines) for each graph are included.

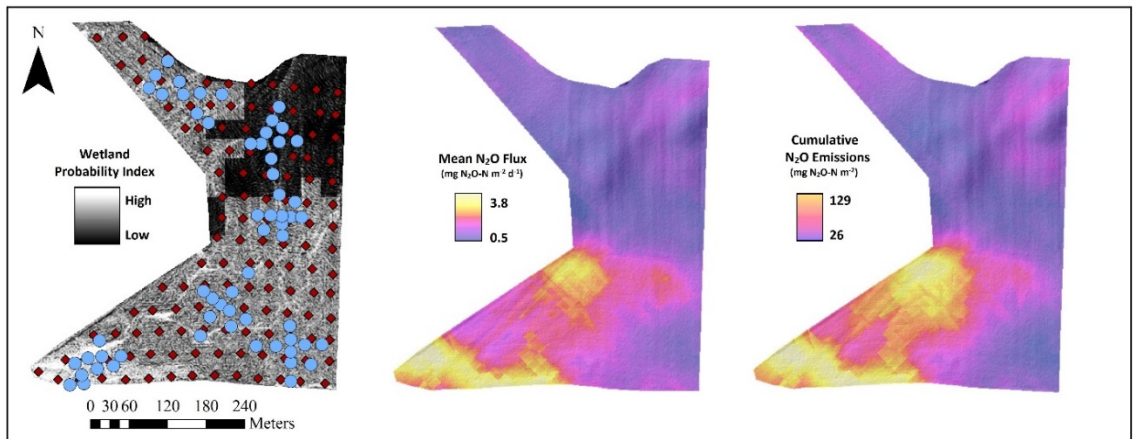


Figure 5.4. The Wetland Probability Index (WPI) overlain with chamber measurements (blue circles) and soil samples (red diamonds). Results are presented from the N₂O ordinary cokriging model, which interpolated mean flux density and cumulative emissions at a 1-m spatial resolution.

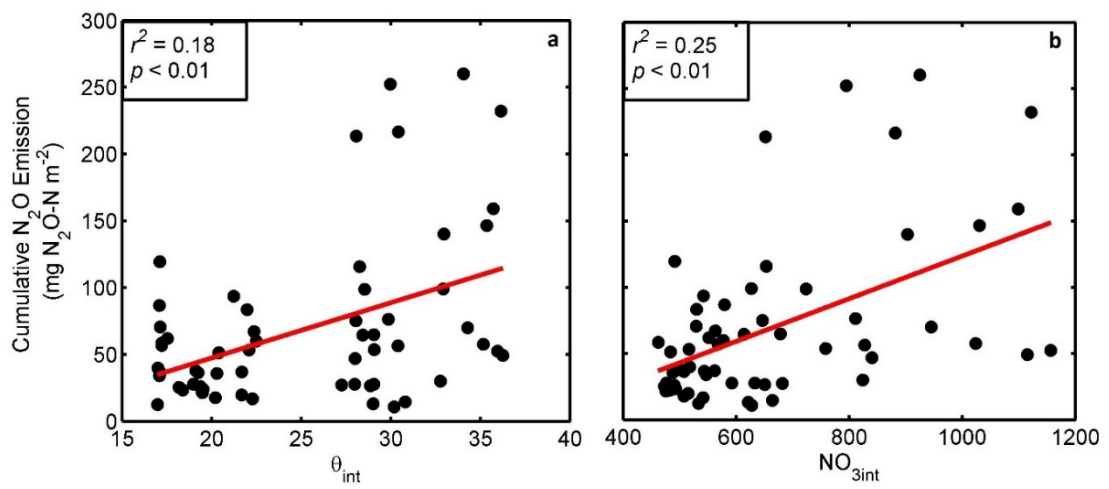


Figure 5.5. The relationship between cumulative N₂O emissions and the soil characteristics, NO₃⁻_{int} and θ_{int}. A linear line of best fit is included (red).

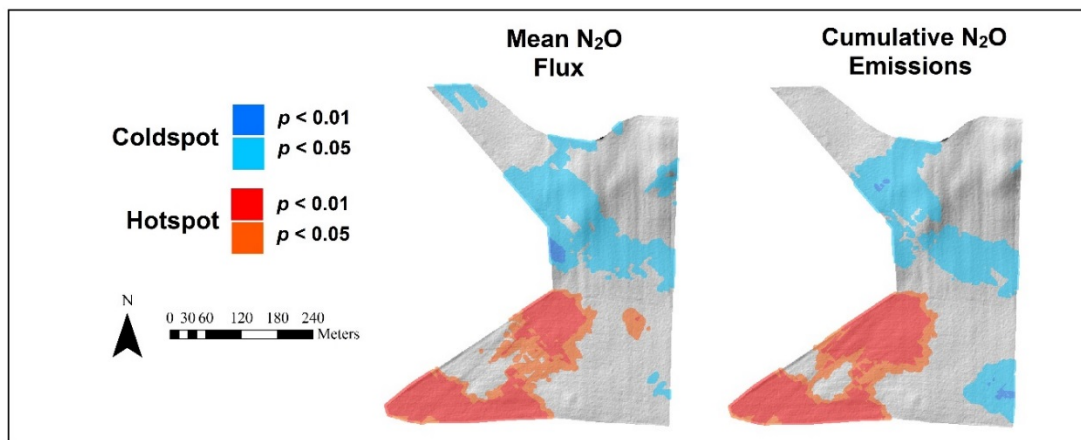


Figure 5.6. Results from the Getis Ord G_i^* statistic that was used to identify the spatial distribution of hotspots and coldspots. Intermediate locations are transparent.

Appendix

Results from the semivariogram and covariance models used to interpolate field-scale N₂O distributions.

Covariance		Partial Sill			Nugget	Range
		Mean Flux	Mean Nitrate	Mean Moisture		
	Mean Flux	0.22			0.37	157
	Mean Nitrate	0.15	0.10		0.14	
	Mean Moisture	0.13	0.09	0.11	0.0001	
Covariance		Partial Sill			Nugget	Range
		Cumulative Emissions	Nitrate Intensity	Moisture Intensity		
	Cumulative Emissions	0.27			0.49	321
	Nitrate Intensity	0.07	0.05		0.19	
	Moisture Intensity	0.08	0.05	0.08	0	
Semivariogram		Partial Sill			Nugget	Range
		Mean Flux	Mean Nitrate	Mean Moisture		
	Mean Flux	0.22			0.37	244
	Mean Nitrate	0.11	0.09		0.16	
	Mean Moisture	0.11	0.07	0.07	0.001	
Semivariogram		Partial Sill			Nugget	Range
		Cumulative Emissions	Nitrate Intensity	Moisture Intensity		
	Cumulative Emissions	0.27			0.43	320
	Nitrate Intensity	0.73	0.05		0.2	
	Moisture Intensity	0.07	0.05	0.08	0	

Chapter 6

Conclusion

This study sought to: 1) quantify the strength of indirect N₂O emissions from leaching and runoff and revise the EF (EF₅) accordingly; and, 2) identify the underlying mechanisms that control direct and indirect emissions in order to help guide N₂O mitigation practices. The findings presented here provide a roadmap for policy makers and farm managers to address and proactively manage agriculturally linked N₂O emissions.

Over the last decade, the indirect emission factor for rivers (EF_{5r}) has emerged as one of the most uncertain components included in bottom-up N₂O emission inventories. This finding can be attributed, in large part, to the broad range of stream morphology types that directly affect the exchange efficiency at the atmosphere – water interface and the rate of nitrogen (N) processing. Yet, a framework that incorporates these differences across a stream network gradient has never been considered. In Chapter 2, static chamber measurements taken longitudinally from a stream network found that N₂O fluxes decline exponentially with the Strahler stream order. When coupled with high-resolution stream network data sets, this exponential function was used to upscale N₂O emissions, which indicated that the EF_{5r} is underestimated by as much as 9-fold in a high-density agricultural region. As a result, bottom-up inventories could be as much as 40% greater than previously reported. Consequently, when our revised EF_{5r} is incorporated, the difference between bottom-up and top-down inventories becomes insignificant. The findings presented in Chapter 2 suggest that either the piston velocity, N processing, or a combination of the two, declines with increasing stream size. From these data alone

however, the instream controls on N₂O production remain unclear and must be identified in order to implement practices designed to mitigate indirect emissions.

Towards this end, Chapter 3 sought to improve understanding of the instream biochemical controls that promote N₂O supersaturation because present N₂O data sets provide limited contextual information. Using a novel gas equilibrator approach, the world's largest freshwater dissolved N₂O data set and the first measurements from the Mississippi River are presented. These data indicate a strong, non-linear relation between dissolved N₂O and NO₃⁻, which suggests that the asymptotic behavior of N₂O at high NO₃⁻ concentrations is caused by environmental limitations on N processing. According to riverine model projections of NO₃⁻ doubling, N₂O emissions from the Upper Mississippi could increase by as much as 40%. However, emissions could be diminished if ancillary variables – including, turbidity were reduced. Therefore, these findings suggest that in addition to reducing NO₃⁻ leaching and runoff, indirect emissions could be curtailed by reducing riverine sediment loading.

Direct emissions from soils are responsible for a significant fraction of N₂O losses and thus, efforts to mitigate emissions from this source deserve serious attention. Practices designed to mitigate direct emissions often focus on traditional nitrogen management, allowing the farmer to play a greater role in climate change mitigation. Increased adoption of alternative management practices, including cover crops that minimize soil erosion and increase pest resilience while fixing N, have created a need to understand how these practices may affect N₂O emissions. In Chapter 4, data are presented from the first study to measure N₂O emissions from a kura clover living mulch

in a rotational corn – soybean system. Analysis of high-resolution data obtained using automated chambers determined that in both the corn and the soybean years, emissions from the kura clover treatment were significantly greater than plots without kura clover. This response was caused by enhanced N₂O emissions from the kura clover during periods of soil disturbance, plant stress, and post-anthesis. These findings suggest that although kura clover does not offer a direct N₂O benefit, indirect emissions might be reduced if NO₃⁻ leaching and sediment losses were minimized.

The results from one-size-fits-all N management practices (e.g., optimizing the placement, source, and timing of fertilizer) designed to mitigate N₂O losses by improving field-scale N use efficiency have been mixed. These findings are promoted by the high spatial variability of N₂O emissions, whereby upscaling exercises are beset with uncertainty. Such variability results from differential soil properties, which cause some locations to produce N₂O at disproportionately high rates (i.e. “hotspots”) and others to have anomalously low production rates (i.e. “coldspots”). Consequently, many studies find that emission frequency distributions are positively skewed by hotspots, which are often discovered in low-lying areas. In Chapter 5, N₂O emissions at a high spatial resolution were resolved using geospatial analyses. Analysis of these data detected hotspots and their relative importance in field-scale emission budgets was quantified. These findings showed that hotspots emitted as much as 38% of the field’s N₂O budget, despite occupying only a fraction (21%) of the field area. As hypothesized, hotspots were concentrated in low-lying areas where terrain focusing ensured ample soil moisture and NO₃⁻ to sustain high rates of denitrification. Further, these data indicate that targeted

management of hotspot locations *via* variable rate nitrogen application or conservation wetlands could substantially reduce direct emissions by as much as 17%.

Future Research Directions

“Legacy” Nitrogen

Mitigation of indirect emissions must also consider the importance of “legacy” N, which has been accumulating in soils over decades of fertilizer application. In the Mississippi River basin, legacy N export models suggest a 35-yr biogeochemical lag [Van Meter *et al.*, 2016] before riverine NO_3^- concentrations are affected by N management practices. Historical data from Pool 8 of the Upper Mississippi River (UMR) provided by the United States Geological Survey (USGS) appears to support that hypothesis. There, dissolved inorganic nitrogen (DIN) concentrations have not changed over the 1991-2013 period ($p = 0.5$) despite the dramatic expansion of the Conservation Reserve Program throughout the watershed. Because Chapter 3 suggests that N_2O is limited in the absence of suspended sediments (lowered nitrification potential), reducing soil erosion could offer an alternative option to mitigate indirect emissions until N management practices offset legacy N. Yet, since long-term N_2O measurements in rivers are non-existent, the effects that conservation policies have had on aquatic N_2O emissions remains uncertain.

Machine Learning Applications

Across the U.S., a water quality network deployed by the USGS has created a long-term, publicly available data set of water chemistry attributes. Using the ensemble

regression model created in Chapter 3 as a training data set, a variety of research directions could be pursued – including, tightening constraints on riverine N₂O emission inventories, assessing policy initiatives by hindcasting N₂O based on historical data, and identifying national aquatic emission trends.

Agricultural Drainage

To sustain the high headwater fluxes described in Chapter 2, a strong water – atmosphere gradient must be maintained by either strong *in-situ* N₂O production or large direct agricultural N₂O inputs from subsurface tile drainage. Because Chapter 3 has shown that dissolved N₂O plateaus at high NO₃⁻ concentrations, strong emissions from headwaters streams may represent a terrestrial signal from tile drainage. These systems act as direct conduits of NO₃⁻ and N₂O laden leachate to headwater streams, but direct measurements of drainage water are sparse. As a result, data are needed to disentangle N₂O that is produced *in-situ* and the terrestrially produced N₂O delivered *via* tile drainage. Further, a recent meta-analysis suggests that the emission factor for N₂O from groundwater should be lowered by nearly an order of magnitude [Sawamoto, 2005], yet measurements from the U.S. Corn Belt or a dense agricultural region were not included in this data set. Because a large fraction of the agricultural landscape is tile drained, emissions from this component could be a large, yet remain a poorly understood source.

Moving Forward

At present, a silver-bullet, broad-scale solution that can reduce N₂O emissions without negatively affecting food security does not exist. However, the data presented

here can develop a roadmap for policy makers and farmers to address and proactively manage agriculturally linked N₂O emissions. A combinatory approach, equivalent to climate stabilization wedges [*Pacala and Socolow, 2008*] levied at the watershed-scale to curtail the N cascade into non-target ecosystems [*Galloway et al., 2003*] would be an effective starting point.

From Chapter 2, the relationship between N₂O flux and stream order implies that indirect emissions can be mitigated most efficiently by targeting low-order, headwater streams. Indeed, NO₃⁻ runoff conservation practices would provide beneficial water and air quality benefits. However, the non-linear N₂O:NO₃⁻ relationship shown in Chapter 3 suggests that such practices would have a minimal effect on N₂O in the NO₃⁻ laden headwater systems prevalent in the U.S. Corn Belt [*Wall et al., 2013*]. Alternatively, measures that reduce both NO₃⁻ and sediment runoff, the latter of which was identified in Chapter 3 as an important driver of riverine N₂O, would likely limit *in-situ* N₂O production. Cover crops are capable of reducing both NO₃⁻ and sediment runoff, and although Chapter 4 did not quantify indirect emissions, it is likely that the broader distribution of cover crops would have a beneficial effect on indirect emissions. Further, as detailed in Chapter 5, farmers can begin to play a more proactive role in N₂O management by expanding the use of fine-scale N application, a technique that can increase farm profits, providing a veritable win-win for farmers and air quality. Cumulatively, these practices could help reduce direct and indirect N₂O emissions and guide effective policies.

References

- Alexander, R. B., R. A. Smith, and G. E. Schwarz (2000), Effect of stream channel size on the delivery of nitrogen to the Gulf of Mexico, *Nature*, 403(February), 758–761.
- Alexander, R. B., E. W. Boyer, R. A. Smith, G. E. Schwarz, and R. B. Moore (2007), The role of headwater streams in downstream water quality, *J. Am. Water Resour. Assoc.*, 43(1), 41–59, doi:10.1111/j.1752-1688.2007.00005.x.
- Alluvione, F., C. Bertora, L. Zavattaro, and C. Grignani (2010), Nitrous oxide and carbon dioxide emissions following green manure and compost fertilization in corn, *Soil Sci. Soc. Am. J.*, 74(2), 384, doi:10.2136/sssaj2009.0092.
- Ambus, P. (1998), Nitrous oxide production by denitrification and nitrification in temperate forest, grassland and agricultural soils, *Eur. J. Soil Sci.*, 49, 495–502.
- Ambus, P., and S. Christensen (1995), Spatial and seasonal nitrous oxide and methane fluxes in danish forest, grassland, and agroecosystems, *Atmos. Pollut. Trace Gases*, 24, 993–1001.
- Anderson, T. R., P. M. Groffman, and M. T. Walter (2015), Using a soil topographic index to distribute denitrification fluxes across a northeastern headwater catchment, *J. Hydrol.*, 522, 123–134, doi:10.1016/j.jhydrol.2014.12.043.
- Arévalo-Martínez, D. L., M. Beyer, M. Krumbholz, I. Piller, A. Kock, T. Steinhoff, A. Körtzinger, and H. W. Bange (2013), A new method for continuous measurements of oceanic and atmospheric N₂O, CO and CO₂: Performance of off-axis integrated cavity output spectroscopy (OA-ICOS) coupled to non-dispersive infrared detection (NDIR), *Ocean Sci.*, 9(6), 1071–1087, doi:10.5194/os-9-1071-2013.
- Arévalo-Martínez, D. L., A. Kock, C. R. Löscher, R. a. Schmitz, and H. W. Bange (2015), Massive nitrous oxide emissions from the tropical South Pacific Ocean, *Nat. Geosci.*, 8, 530–533, doi:10.1038/ngeo2469.
- Baggs, E. M., M. Stevenson, M. Pihlatie, a. Regar, H. Cook, and G. Cadisch (2003), Nitrous oxide emissions following application of residues and fertiliser under zero and conventional tillage, *Plant Soil*, 254(2), 361–370, doi:10.1023/A:1025593121839.
- Baker, J. M. (2012), Vegetative propagation of kura clover: A field-scale test, *Can. J. Plant Sci.*, 92(7), 1245–1251, doi:10.4141/cjps2012-014.
- Baker, J. M., J. Fassbinder, and J. A. Lamb (2014), The impact of corn stover removal on N₂O emission and soil respiration: An investigation with automated chambers, *Bioenergy Res.*, 7, 503–508, doi:10.1007/s12155-014-9412-1.
- Ball, B. C., G. W. Horgan, H. Clayton, and J. P. Parker (1997), Spatial variability of nitrous oxide fluxes and controlling soil and topographic properties, *J. Environ. Qual.*, 26(1992), 1399, doi:10.2134/jeq1997.00472425002600050029x.
- Bange, H. W., S. Rapsomanikis, and M. O. Andreae (1996), Nitrous oxide emissions from the Arabian Sea, *Geophys. Res. Lett.*, 23(22), 3175, doi:10.1029/96GL03072.
- Barton, L., K. Butterbach-Bahl, R. Kiese, and D. V. Murphy (2011), Nitrous oxide fluxes from a grain-legume crop (narrow-leafed lupin) grown in a semiarid climate, *Glob.*

- Chang. Biol.*, 17, 1153–1166, doi:10.1111/j.1365-2486.2010.02260.x.
- Basche, A. D., F. E. Miguez, T. C. Kaspar, and M. J. Castellano (2014), Do cover crops increase or decrease nitrous oxide emissions? A meta-analysis, *J. Soil Water Conserv.*, 69(6), 471–482, doi:10.2489/jswc.69.6.471.
- Baulch, H. M., S. L. Schiff, R. Maranger, and P. J. Dillon (2011), Nitrogen enrichment and the emission of nitrous oxide from streams, *Global Biogeochem. Cycles*, 25(4), 1–15, doi:10.1029/2011GB004047.
- Bavin, T. K., T. J. Griffis, J. M. Baker, and R. T. Venterea (2009), Impact of reduced tillage and cover cropping on the greenhouse gas budget of a maize/soybean rotation ecosystem, *Agric. Ecosyst. Environ.*, 134, 234–242, doi:10.1016/j.agee.2009.07.005.
- Beaulieu, J. J., C. P. Arango, S. K. Hamilton, and J. L. Tank (2008), The production and emission of nitrous oxide from headwater streams in the Midwestern United States, *Glob. Chang. Biol.*, 14, 878–894, doi:10.1111/j.1365-2486.2007.01485.x.
- Beaulieu, J. J., W. D. Shuster, and J. A. Rebolz (2010), Nitrous oxide emissions from a large, impounded river: The Ohio river, *Environ. Sci. Technol.*, 44(19), 7527–7533, doi:10.1021/es1016735.
- Beaulieu, J. J. et al. (2011), Nitrous oxide emission from denitrification in stream and river networks, *Proc. Natl. Acad. Sci. U. S. A.*, 108(1), 214–219, doi:10.1073/pnas.1011464108.
- Beaulieu, J. J., W. D. Shuster, and J. A. Rebolz (2012), Controls on gas transfer velocities in a large river, *J. Geophys. Res. Biogeosciences*, 117(G2), 1–13, doi:10.1029/2011JG001794.
- Beaulieu, J. J., C. T. Nietch, and J. L. Young (2015), Controls on nitrous oxide production and consumption in reservoirs of the Ohio River Basin, *J. Geophys. Res. Biogeosciences*, 1–16, doi:10.1002/2015JG002941. Received.
- Boyer, E. W., R. B. Alexander, W. J. Parton, C. Li, K. Butterbach-Bahl, S. D. Donner, R. W. Skaggs, and S. J. Del Grosso (2006), Modeling denitrification in terrestrial and aquatic ecosystems at regional scales, *Ecol. Appl.*, 16(6), 2123–2142, doi:10.1890/1051-0761(2006)016[2123:MDITAA]2.0.CO;2.
- Brozyna, M. A., S. O. Petersen, N. Chirinda, and J. E. Olesen (2013), Effects of grass-clover management and cover crops on nitrogen cycling and nitrous oxide emissions in a stockless organic crop rotation, *Agric. Ecosyst. Environ.*, 181, 115–126, doi:10.1016/j.agee.2013.09.013.
- Butman, D., and P. A. Raymond (2011), Significant efflux of carbon dioxide from streams and rivers in the United States, *Nat. Geosci.*, 4(12), 839–842, doi:10.1038/ngeo1294.
- Chen, Z. et al. (2016), Partitioning N₂O Emissions within the US Corn Belt using an Inverse Modeling Approach, *Global Biogeochem. Cycles*, doi:10.1002/2015GB005313.
- Christensen, S., P. Ambus, J. R. M. Arah, H. Clayton, B. Galle, D. W. T. Griffith, K. J. Hargreaves, and L. Klemetsson (1996), Nitrous oxide emission from an agricultural field: Comparison between measurements by flux chamber and micrometeorological techniques, *Atmos. Environ.*, 30(24), 4183–4190,

- doi:10.1016/1352-2310(96)00145-8.
- Clough, T. J., J. E. Bertram, R. R. Sherlock, R. L. Leonard, and B. L. Nowicki (2006), Comparison of measured and EF5-r-derived N₂O fluxes from a spring-fed river, *Glob. Chang. Biol.*, 12(2), 352–363, doi:10.1111/j.1365-2486.2005.01089.x.
- Clough, T. J., L. E. Buckthought, F. M. Kelliher, and R. R. Sherlock (2007), Diurnal fluctuations of dissolved nitrous oxide (N₂O) concentrations and estimates of N₂O emissions from a spring-fed river: Implications for IPCC methodology, *Glob. Chang. Biol.*, 13(5), 1016–1027, doi:10.1111/j.1365-2486.2007.01337.x.
- Cole, J. J., and N. F. Caraco (1998), Atmospheric exchange of carbon dioxide in a low-wind oligotrophic lake measured by the addition of SF₆, *Limnol. Oceanogr.*, 43(4), 647–656, doi:10.4319/lo.1998.43.4.0647.
- Cole, J. J., and N. F. Caraco (2001), Emissions of nitrous oxide (N₂O) from a tidal, freshwater river, the Hudson River, New York, *Environ. Sci. Technol.*, (845), 991–996.
- Crawford, J. T., R. G. Striegl, K. P. Wickland, M. M. Dornblaser, and E. H. Stanley (2013), Emissions of carbon dioxide and methane from a headwater stream network of interior Alaska, *J. Geophys. Res. Biogeosciences*, 118(2), 482–494, doi:10.1002/jgrg.20034.
- Crawford, J. T., L. C. Loken, N. J. Casson, C. Smith, A. G. Stone, and L. A. Winslow (2015), High-speed limnology: Using advanced sensors to investigate spatial variability in biogeochemistry and hydrology, *Environ. Sci. Technol.*, 49, 442–450.
- Crawford, J. T., L. C. Loken, E. H. Stanley, E. G. Stets, M. M. Dornblaser, and R. G. Striegl (2016), Basin scale controls on CO₂ and CH₄ emissions from the Upper Mississippi River, *Geophys. Res. Lett.*, 43, 1–7, doi:10.1002/2015GL067599.
- Crews, T. E., and M. B. Peoples (2004), Legume versus fertilizer sources of nitrogen: Ecological tradeoffs and human needs, *Agric. Ecosyst. Environ.*, 102, 279–297, doi:10.1016/j.agee.2003.09.018.
- Crutzen, P. J., A. R. Mosier, K. A. Smith, and W. Winiwarter (2008), N₂O release from agro-biofuel production negates global warming reduction by replacing fossil fuels, *Atmos. Chem. Phys.*, 8(2), 389–395, doi:10.5194/acpd-7-11191-2007.
- Davidson, E. A. (2009), The contribution of manure and fertilizer nitrogen to atmospheric nitrous oxide since 1860, *Nat. Geosci.*, 2(9), 659–662, doi:10.1038/ngeo608.
- Davidson, E. A., and D. Kanter (2014), Inventories and scenarios of nitrous oxide emissions, *Environ. Res. Lett.*, 9(10), 105012, doi:10.1088/1748-9326/9/10/105012.
- De'ath, G., and K. E. Fabricius (2000), Classification and regression trees: A powerful yet simple technique for ecological data analysis, *Ecology*, 81(11), 3178–3192, doi:10.1890/0012-9658(2000)081[3178:CARTAP]2.0.CO;2.
- Decock, C. (2014), Mitigating nitrous oxide emissions from corn cropping systems in the Midwestern U.S.: potential and data gaps, *Environ. Sci. Technol.*, 48, 4247–4256, doi:10.1021/es4055324.
- Dong, L. F., D. B. Nedwell, I. Colbeck, and J. Finch (2004), Nitrous oxide emissions from some English and Welsh rivers and estuaries, *Water. Air. Soil Pollut.*, 4, 127–134.

- Downing, J. A., J. J. Cole, C. M. Duarte, J. J. Middelburg, J. M. Melack, Y. T. Prairie, P. Kortelainen, R. G. Striegl, W. H. McDowell, and L. J. Tranvik (2012), Global abundance and size distribution of streams and rivers, *Inl. Waters*, 2(4), 229–236, doi:10.5268/IW-2.4.502.
- Enache, A. J., and R. D. Ilnicki (1990), Weed control by subterranean clover (*Trifolium subterraneum*) used as a living mulch, *Weed Sci. Soc. Am.*, 4(3), 534–538.
- FAO (2015), FAOSTAT Database, *Food Agric. Organ. United States*. Available from: <http://faostat3.fao.org/> (Accessed 1 January 2016)
- Farahbakhshazad, N., D. L. Dinnes, C. Li, D. B. Jaynes, and W. Salas (2008), Modeling biogeochemical impacts of alternative management practices for a row-crop field in Iowa, *Agric. Ecosyst. Environ.*, 123, 30–48, doi:10.1016/j.agee.2007.04.004.
- Fassbinder, J. J., N. M. Schultz, J. M. Baker, and T. J. Griffis (2013), Automated, low-power chamber system for measuring nitrous oxide emissions., *J. Environ. Qual.*, 42, 606–14, doi:10.2134/jeq2012.0283.
- Fink, C. M., and P. J. Drohan (2016), High Resolution Hydric Soil Mapping using LiDAR Digital Terrain Modeling, *Soil Sci. Soc. Am. J.*, 80, 355–363, doi:10.2136/sssaj2015.07.0270.
- Folorunso, O. A., and D. E. Rolston (1984), Spatial Variability Of Field-measured Denitrification Gas Fluxes, *Soil Sci. Soc. Am. J.*, 48(6), 1214–1219, doi:10.2136/sssaj1984.03615995004800060002x.
- Galloway, J. N., J. D. Aber, J. W. Erisman, S. P. Seitzinger, R. W. Howarth, E. B. Cowling, and B. J. Cosby (2003), The nitrogen cascade, *Am. Inst. Biol. Sci.*, 53(4), 341, doi:10.1641/0006-3568(2003)053[0341:TNC]2.0.CO;2.
- Galzki, J. C., A. S. Birr, and D. J. Mulla (2011), Identifying critical agricultural areas with three-meter LiDAR elevation data for precision conservation, *J. Soil Water Conserv.*, 66(6), 423–430, doi:10.2489/jswc.66.6.423.
- García-Ruiz, R., S. N. Pattinson, and B. A. Whitton (1998), Kinetic parameters of denitrification in a river continuum, *Appl. Environ. Microbiol.*, 64(7), 2533–2538.
- George, T., J. K. Ladha, D. P. Garrity, and R. J. Buresh (1994), Legumes as nitrate catch crops during the dry-to-wet transition in lowland rice cropping systems, *Agron. J.*, 86(2), 267–273.
- Gomes, J., C. Bayer, F. de Souza Costa, M. de Cássia Piccolo, J. A. Zanatta, F. C. B. Vieira, and J. Six (2009), Soil nitrous oxide emissions in long-term cover crops-based rotations under subtropical climate, *Soil Tillage Res.*, 106(1), 36–44, doi:10.1016/j.still.2009.10.001.
- Grefe, I., and J. Kaiser (2014), Equilibrator-based measurements of dissolved nitrous oxide in the surface ocean using an integrated cavity output laser absorption spectrometer, *Ocean Sci.*, 10, 501–512, doi:10.5194/os-10-501-2014.
- Griffis, T. J., J. Zhang, J. M. Baker, N. Kljun, and K. Billmark (2007), Determining carbon isotope signatures from micrometeorological measurements: Implications for studying biosphere-atmosphere exchange processes, *Boundary-Layer Meteorol.*, 123(2), 295–316, doi:10.1007/s10546-006-9143-8.
- Griffis, T. J., X. Lee, J. M. Baker, M. P. Russelle, X. Zhang, R. Venterea, and D. B.

- Millet (2013), Reconciling the differences between top-down and bottom-up estimates of nitrous oxide emissions for the U.S. Corn Belt, *Global Biogeochem. Cycles*, 27(3), 746–754, doi:10.1002/gbc.20066.
- van Groenigen, J. W., G. L. Velthof, O. Oenema, K. J. Van Groenigen, and C. Van Kessel (2010), Towards an agronomic assessment of N₂O emissions: A case study for arable crops, *Eur. J. Soil Sci.*, 61(6), 903–913, doi:10.1111/j.1365-2389.2009.01217.x.
- Groffman, P. M., K. Butterbach-Bahl, R. W. Fulweiler, A. J. Gold, J. L. Morse, E. K. Stander, C. Tague, C. Tonitto, and P. Vidon (2009), Challenges to incorporating spatially and temporally explicit phenomena (hotspots and hot moments) in denitrification models, *Biogeochemistry*, 93, 49–77, doi:10.1007/s10533-008-9277-5.
- Halvorson, A. D., C. S. Snyder, A. D. Blaylock, and S. J. Del Grosso (2014), Enhanced-efficiency nitrogen fertilizers: potential role in nitrous oxide emission mitigation, *Agron. J.*, 106(2), 715, doi:10.2134/agronj2013.0081.
- Harrison, J., and P. Matson (2003), Patterns and controls of nitrous oxide emissions from waters draining a subtropical agricultural valley, *Global Biogeochem. Cycles*, 17(3), 1–13, doi:10.1029/2002GB001991.
- Hartmann, D. L. et al. (2013), *Observations: Atmosphere and surface*, edited by Intergovernmental Panel on Climate Change, Cambridge University Press.
- Hasegawa, K., K. Hanaki, T. Matsuo, and S. Hidaka (2000), Nitrous oxide from the agricultural water system contaminated with high nitrogen, *Chemosph. - Glob. Chang. Sci.*, 2(3-4), 335–345, doi:10.1016/S1465-9972(00)00009-X.
- van den Heuvel, R. N., M. M. Hefting, N. C. G. Tan, M. S. M. Jetten, and J. T. A. Verhoeven (2009), N₂O emission hotspots at different spatial scales and governing factors for small scale hotspots, *Sci. Total Environ.*, 407(7), 2325–2332, doi:10.1016/j.scitotenv.2008.11.010.
- Hinshaw, S. E., and R. A. Dahlgren (2013), Dissolved nitrous oxide concentrations and fluxes from the eutrophic San Joaquin River, California, *Environ. Sci. Technol.*, 47, 1313–1322, doi:10.1021/es301373h.
- Hoben, J. P., R. J. Gehl, N. Millar, P. R. Grace, and G. P. Robertson (2011), Nonlinear nitrous oxide (N₂O) response to nitrogen fertilizer in on-farm corn crops of the US Midwest, *Glob. Chang. Biol.*, 17, 1140–1152, doi:10.1111/j.1365-2486.2010.02349.x.
- Huang, Y., J. Zou, X. Zheng, Y. Wang, and X. Xu (2004), Nitrous oxide emissions as influenced by amendment of plant residues with different C:N ratios, *Soil Biol. Biochem.*, 36(6), 973–981, doi:10.1016/j.soilbio.2004.02.009.
- Jarecki, M. K., T. B. Parkin, A. S. K. Chan, T. C. Kaspar, T. B. Moorman, J. W. Singer, B. J. Kerr, J. L. Hatfield, and R. Jones (2009), Cover crop effects on nitrous oxide emission from a manure-treated Mollisol, *Agric. Ecosyst. Environ.*, 134(1-2), 29–35, doi:10.1016/j.agee.2009.05.008.
- Jin, V. L. et al. (2014), Soil greenhouse gas emissions in response to corn stover removal and tillage management across the US Corn Belt, *Bioenergy Res.*, 7, 517–527,

doi:10.1007/s12155-014-9421-0.

- Jones, J. B., and P. J. Mulholland (1998), Influence of drainage basin topography and elevation on carbon dioxide and methane supersaturation of stream water, *Biogeochemistry*, 40(1), 57–72, doi:10.1023/A:1005914121280.
- Jones, S. K., D. Famulari, C. F. Di Marco, E. Nemitz, U. M. Skiba, R. M. Rees, and M. a. Sutton (2011), Nitrous oxide emissions from managed grassland: A comparison of eddy covariance and static chamber measurements, *Atmos. Meas. Tech.*, 4(10), 2179–2194, doi:10.5194/amt-4-2179-2011.
- Kampschreur, M. J., H. Temmink, R. Kleerebezem, M. S. M. Jetten, and M. C. M. van Loosdrecht (2009), Nitrous oxide emission during wastewater treatment, *Water Res.*, 43(17), 4093–4103, doi:10.1016/j.watres.2009.03.001.
- Kanter, D. et al. (2013), A post-Kyoto partner: Considering the stratospheric ozone regime as a tool to manage nitrous oxide, *Proc. Natl. Acad. Sci. U. S. A.*, 110(41), 4451–4457, doi:10.1073/pnas.1317243110.
- Kennedy, T. L., E. C. Suddick, and J. Six (2013), Reduced nitrous oxide emissions and increased yields in California tomato cropping systems under drip irrigation and fertigation, *Agric. Ecosyst. Environ.*, 170, 16–27, doi:10.1016/j.agee.2013.02.002.
- De Klein, C., R. S. A. Novoa, S. Ogle, K. A. Smith, P. Rochette, and T. C. Wirth (2006), N₂O emissions from managed soils, and CO₂ emissions from lime and urea application, in *2006 IPCC Guidelines for National Greenhouse Gas Inventories*, vol. 4, pp. 11.1–11.54.
- Knowles, R. (1982), Denitrification, *Microbiol. Rev.*, 46(1), 43–70.
- Komatsuzaki, M., and M. G. Wagger (2015), Nitrogen recovery by cover crops in relation to time of planting and growth termination, *J. Soil Water Conserv.*, 70(6), 385–398, doi:10.2489/jswc.70.6.385.
- Kool, D. M., J. Dol, N. Wrage, J. Willem, and V. Groenigen (2011), Soil Biology & Biochemistry Nitrifier denitrification as a distinct and significant source of nitrous oxide from soil, *Soil Biol. Biochem.*, 43, 174–178, doi:10.1016/j.soilbio.2010.09.030.
- Kort, E. A., J. Eluszkiewicz, B. B. Stephens, J. B. Miller, C. Gerbig, T. Nehrkorn, B. C. Daube, J. O. Kaplan, S. Houweling, and S. C. Wofsy (2008), Emissions of CH₄ and N₂O over the United States and Canada based on a receptor-oriented modeling framework and COBRA-NA atmospheric observations, *Geophys. Res. Lett.*, 35, 1–5, doi:10.1029/2008GL034031.
- Lin, X., K. Spokas, R. Venterea, R. Zhang, J. Baker, and G. Feyereisen (2014), Assessing microbial contributions to N₂O impacts following biochar additions, *Agronomy*, 4, 478–496, doi:10.3390/agronomy4040478.
- Lundy, M. E., C. M. Pittelkow, B. a. Linquist, X. Liang, K. J. van Groenigen, J. Lee, J. Six, R. T. Venterea, and C. van Kessel (2015), Nitrogen fertilization reduces yield declines following no-till adoption, *F. Crop. Res.*, 183, 204–210, doi:10.1016/j.fcr.2015.07.023.
- Maharjan, B., and R. T. Venterea (2014), Anhydrous ammonia injection depth does not affect nitrous oxide emissions in a silt loam over two growing seasons, *J. Environ.*

- Qual.*, 43(5), 1527–1535, doi:10.2134/jeq2014.07.0292.
- Maharjan, B., R. T. Venterea, and C. Rosen (2014), Fertilizer and irrigation management effects on nitrous oxide emissions and nitrate leaching, *Agron. J.*, 106, 703–714, doi:10.2134/agronj2013.0179.
- Maier, R. M., I. L. Pepper, and C. P. Gerba (2009), *Environmental Microbiology*, 2nd ed., Elsevier Inc, Burlington, MA.
- Marzadri, A., D. Tonina, A. Bellin, and J. L. Tank (2014), A hydrologic model demonstrates nitrous oxide emissions depend on streambed morphology, *Geophys. Res. Lett.*, 41, 5484–5491, doi:10.1002/2014GL060732.
- Mathieu, O., J. Lévêque, C. Hénault, M. J. Milloux, F. Bizouard, and F. Andreux (2006), Emissions and spatial variability of N₂O, N₂ and nitrous oxide mole fraction at the field scale, revealed with ¹⁵N isotopic techniques, *Soil Biol. Biochem.*, 38(5), 941–951, doi:10.1016/j.soilbio.2005.08.010.
- McClain, M. E. et al. (2003), Biogeochemical hot spots and hot moments at the interface of terrestrial and aquatic ecosystems, *Ecosystems*, 6(4), 301–312, doi:10.1007/s10021-003-0161-9.
- McMahon, P. B., and K. F. Dennehy (1999), N₂O emission from a nitrogen-enriched river, *Environ. Sci. Technol.*, 33(303), 21–25.
- McSwiney, C. P., S. S. Snapp, and L. E. Gentry (2010), Use of N immobilization to tighten the N cycle in conventional agroecosystems, *Ecol. Appl.*, 20(3), 648–662, doi:10.1890/09-0077.1.
- Van Meter, K. J., N. B. Basu, J. J. Veenstra, and C. L. Burras (2016), The nitrogen legacy: Emerging evidence of nitrogen accumulation in anthropogenic landscapes, *Environ. Res. Lett.*, 11(3), 035014, doi:10.1088/1748-9326/11/3/035014.
- Miller, S. M. et al. (2012), Regional sources of nitrous oxide over the United States: Seasonal variation and spatial distribution, *J. Geophys. Res. Atmos.*, 117(D6), 1–13, doi:10.1029/2011JD016951.
- Mitchell, D. C., M. J. Castellano, J. E. Sawyer, and J. Pantoja (2013), Cover crop effects on nitrous oxide emissions: Role of mineralizable carbon, *Soil Sci. Soc. Am. J.*, 77, 1765, doi:10.2136/sssaj2013.02.0074.
- Molodovskaya, M., J. Warland, B. K. Richards, G. Öberg, and T. S. Steenhuis (2011), Nitrous oxide from heterogeneous agricultural landscapes: Source contribution analysis by eddy covariance and chambers, *Soil Sci. Soc. Am. J.*, 75(5), 1829, doi:10.2136/sssaj2010.0415.
- Moore, I. D., P. Gessler, G. A. Nielsen, and G. A. Peterson (1993), Soil attribute prediction using terrain analysis, *Soil Sci. Soc. Am. J.*, 57(2), 443–452, doi:10.2136/sssaj1993.572NPb.
- Mosier, A., C. Kroeze, C. Nevison, O. Oenema, and S. Seitzinger (1998), Closing the global N₂O budget: nitrous oxide emissions through the agricultural nitrogen cycle, *Nutr. Cycl. Agroecosystems*, 52(2-3), 225–248, doi:10.1023/A:1009740530221.
- Mulholland, P. J. et al. (2008), Stream denitrification across biomes and its response to anthropogenic nitrate loading., *Nature*, 452(7184), 202–205, doi:10.1038/nature06686.

- Murphy, P. N. C., J. Ogilvie, and P. Arp (2009), Topographic modelling of soil moisture conditions: A comparison and verification of two models, *Eur. J. Soil Sci.*, 60(1), 94–109, doi:10.1111/j.1365-2389.2008.01094.x.
- Murray, R. H., D. V. Erler, and B. D. Eyre (2015), Nitrous oxide fluxes in estuarine environments: Response to global change, *Glob. Chang. Biol.*, n/a–n/a, doi:10.1111/gcb.12923.
- Nair, A., and V. Lawson (2014), Quantifying nitrogen scavenging benefits of cover crops in the Mississippi River basin, *Iowa State Res. Farm Prog. Rep.*, Paper 2189.
- Nevison, C. (2000), Review of the IPCC methodology for estimating nitrous oxide emissions associated with agricultural leaching and runoff, *Chemosph. - Glob. Chang. Sci.*, 2(3-4), 493–500, doi:10.1016/S1465-9972(00)00013-1.
- NRCS (2012), *Assessment of the effects of conservation practices on cultivated cropland in the Upper Mississippi River basin.*
- O'Reilly, C., I. R. Santons, T. Cyronak, a McMahan, and D. T. Maher (2015), Nitrous oxide and methane dynamics in a coral reef lagoon driven by pore water exchange: Insights from automated high-frequency observations, *Geophys. Res. Lett.*, 42, doi:10.1002/2015GL063126, doi:10.1002/2015GL063126.Received.
- Ochsner, T. E., K. A. Albrecht, T. W. Schumacher, J. M. Baker, and R. J. Berkevich (2010), Water balance and nitrate leaching under corn in kura clover living mulch, *Agron. J.*, 102, 1169–1178, doi:10.2134/agronj2009.0523.
- Ord, J. K., and A. Getis (2010), Local spatial autocorrelation statistics: Distributional issues and an application, *Geogr. Anal.*, 27(4), 286–306, doi:10.1111/j.1538-4632.1995.tb00912.x.
- Outram, F. N., and K. M. Hiscock (2012), Indirect nitrous oxide emissions from surface water bodies in a lowland arable catchment: A significant contribution to agricultural greenhouse gas budgets?, *Environ. Sci. Technol.*, 46, 8156–8163, doi:10.1021/es3012244.
- Owens, N. J. P. (1986), Estuarine nitrification: A naturally occurring fluidized bed reaction?, *Estuar. Coast. Shelf Sci.*, 22, 31–44.
- Pacala, S., and R. Socolow (2008), Stabilization Wedges : Solving the Climate Problem for the Next 50 Years with Current Technologies, *Science (80-.)*, 968(2004), 968–972, doi:10.1126/science.1100103.
- Panno, S. V, K. C. Hackley, W. R. Kelly, and H.-H. Hwang (2006), Isotopic evidence of nitrate sources and denitrification in the Mississippi River, Illinois., *J. Environ. Qual.*, 35(2), 495–504, doi:10.2134/jeq2005.0012.
- Parkin, T. B. (1987), Soil microsites as a source of denitrification variability, *Soil Sci. Soc. Am. J.*, 51, 1194–1199, doi:10.2136/sssaj1987.03615995005100050019x.
- Parkin, T. B., R. T. Venterea, and S. K. Hargreaves (2012), Calculating the detection limits of chamber-based soil greenhouse gas flux measurements, *J. Environ. Qual.*, 41, 705, doi:10.2134/jeq2011.0394.
- Peterson, B. J. et al. (2001), Control of nitrogen export from watersheds by headwater streams., *Science*, 292, 86–90, doi:10.1126/science.1056874.
- van den Pol-van Dasselaar, A., W. J. Corré, A. Priemé, Å. K. Klemetsson, P. Weslien,

- L. Klemetsson, A. Stein, and O. Oenema (1998), Spatial variability of methane, nitrous oxide, and carbon dioxide emissions from drained grasslands, *Soil Sci. Soc. Am. J.*, 62(3), 810–817, doi:10.2136/sssaj1998.03615995006200030039x.
- Potter, P., N. Ramankutty, E. M. Bennett, and S. D. Donner (2011), Global Fertilizer and Manure, Version 1: Nitrogen Fertilizer Application,
- Rabalais, N. (2002), Nitrogen in aquatic ecosystems, *Ambio*, 31(2), 102–112.
- Ravishankara, A. R., J. S. Daniel, and R. W. Portmann (2009), Nitrous oxide (N₂O): The dominant ozone-depleting substance emitted in the 21st century, *Science*, 326, 123–125, doi:10.1126/science.1176985.
- Raymond, P. A., and J. J. Cole (2001), Gas exchange in rivers and estuaries: Choosing a gas transfer velocity, *Estuaries*, 24(2), 312, doi:10.2307/1352954.
- Raymond, P. A., C. J. Zappa, D. Butman, T. L. Bott, J. Potter, P. Mulholland, a. E. Laursen, W. H. McDowell, and D. Newbold (2012), Scaling the gas transfer velocity and hydraulic geometry in streams and small rivers, *Limnol. Oceanogr. Fluids Environ.*, 2(1), 41–53, doi:10.1215/21573689-1597669.
- Raymond, P. A. et al. (2013), Global carbon dioxide emissions from inland waters., *Nature*, 503, 355–359, doi:10.1038/nature12760.
- Reay, D. S., K. A. Smith, and A. C. Edwards (2003), Nitrous oxide emission from agricultural drainage waters, *Glob. Chang. Biol.*, 9(3), 195–203.
- Richardson, W. B., E. A. Strauss, L. A. Bartsch, E. M. Monroe, J. C. Cavanaugh, L. Vingum, and D. M. Soballe (2004), Denitrification in the Upper Mississippi River: Rates, controls, and contribution to nitrate flux, *Can. J. Fish. Aquat. Sci.*, 61(7), 1102–1112, doi:10.1139/f04-062.
- Rochette, P., and H. H. Janzen (2005), Towards a revised coefficient for estimating N₂O emissions from legumes, *Nutr. Cycl. Agroecosystems*, 73(2-3), 171–179, doi:10.1007/s10705-005-0357-9.
- Rosamond, M. S., S. J. Thuss, S. L. Schiff, and R. J. Elgood (2011), Coupled cycles of dissolved oxygen and nitrous oxide in rivers along a trophic gradient in southern Ontario, Canada., *J. Environ. Qual.*, 40, 256–270, doi:10.2134/jeq2010.0009.
- Rosamond, M. S., S. J. Thuss, and S. L. Schiff (2012), Dependence of riverine nitrous oxide emissions on dissolved oxygen levels, *Nat. Geosci.*, 5(10), 715–718, doi:10.1038/ngeo1556.
- Santos, I. R., D. T. Maher, and B. D. Eyre (2012), Coupling automated radon and carbon dioxide measurements in coastal waters, *Environ. Sci. Technol.*, 46, 7685–7691, doi:10.1021/es301961b.
- Sawamoto, T. (2005), Evaluation of emission factors for indirect N₂O emission due to nitrogen leaching in agro-ecosystems, *Geophys. Res. Lett.*, 32, L03403, doi:10.1029/2004GL021625.
- Scharf, P. C., D. K. Shannon, H. L. Palm, K. A. Sudduth, S. T. Drummond, N. R. Kitchen, L. J. Mueller, V. C. Hubbard, and L. F. Oliveira (2011), Sensor-based nitrogen applications out-performed producer-chosen rates for corn in on-farm demonstrations, *Agron. J.*, 103(6), 1683–1691, doi:10.2134/agronj2011.0164.
- Seitzinger, S. P., C. Kroeze, a. F. Bouwman, N. Caraco, F. Dentener, and R. V. Styles

- (2002), Global patterns of dissolved inorganic and particulate nitrogen inputs to coastal systems: Recent conditions and future projections, *Estuaries*, 25(4), 640–655, doi:10.1007/BF02804897.
- Shcherbak, I., N. Millar, and G. P. Robertson (2014), Global metaanalysis of the nonlinear response of soil nitrous oxide (N₂O) emissions to fertilizer nitrogen., *Proc. Natl. Acad. Sci. U. S. A.*, 111(25), 9199–204, doi:10.1073/pnas.1322434111.
- Smil, V. (1999), Nitrogen in crop production : An account of global flows, *Global Biogeochem. Cycles*, 13(2), 647–662.
- Sørensen, R., and J. Seibert (2007), Effects of DEM resolution on the calculation of topographical indices: TWI and its components, *J. Hydrol.*, 347(1-2), 79–89, doi:10.1016/j.jhydrol.2007.09.001.
- Spencer, R. G. M., G. R. Aiken, M. M. Dornblaser, K. D. Butler, R. M. Holmes, G. Fiske, P. J. Mann, and A. Stubbins (2013), Chromophoric dissolved organic matter export from U.S. rivers, *Geophys. Res. Lett.*, 40(April), 1575–1579, doi:10.1002/grl.50357.
- Stehfest, E., and L. Bouwman (2006), N₂O and NO emission from agricultural fields and soils under natural vegetation: Summarizing available measurement data and modeling of global annual emissions, *Nutr. Cycl. Agroecosystems*, 74(3), 207–228, doi:10.1007/s10705-006-9000-7.
- Strauss, E. A., N. L. Mitchell, and G. A. Lamberti (2002), Factors regulating nitrification in aquatic sediments: effects of organic carbon, nitrogen availability, and pH, *Can. J. Fish. Aquat. Sci.*, 59(3), 554–563, doi:10.1139/f02-032.
- Strauss, E. A., W. B. Richardson, L. A. Bartsch, J. C. Cavanaugh, D. A. Bruesewitz, H. Imker, J. A. Heinz, and D. M. Soballe (2004), Nitrification in the Upper Mississippi River: Patterns, controls, and contribution to the NO₃- budget, *J. North Am. Benthol. Soc.*, 23(3), 1–14.
- Strauss, E. A., W. B. Richardson, L. A. Bartsch, and J. C. Cavanaugh (2011), Effect of habitat type on in-stream nitrogen loss in the Mississippi River, *River Syst.*, 19(3), 261–269, doi:10.1127/1868-5749/2011/019-0021.
- Sundqvist, E., A. Persson, N. Kljun, P. Vestin, L. Chasmer, C. Hopkinson, and A. Lindroth (2015), Upscaling of methane exchange in a boreal forest using soil chamber measurements and high-resolution LiDAR elevation data, *Agric. For. Meteorol.*, 214-215, 393–401, doi:10.1016/j.agrformet.2015.09.003.
- Sutton, C. D. (2005), Classification and regression trees, bagging, and boosting, *Handb. Stat.*, 24(04), 303–329, doi:10.1016/S0169-7161(04)24011-1.
- Syakila, A., and C. Kroeze (2011), The global nitrous oxide budget revisited, *Greenh. Gas Meas. Manag.*, 1(1), 17–26, doi:10.3763/ghgmm.2010.0007.
- Trewavas, A. (2002), Malthus foiled again and again, *Nature*, 418(6898), 668–670, doi:10.1038/nature01013.
- Turner, P. A., T. J. Griffis, X. Lee, J. M. Baker, R. T. Venterea, and J. D. Wood (2015), Indirect nitrous oxide emissions from streams within the US Corn Belt scale with stream order, *Proc. Natl. Acad. Sci. U. S. A.*, 112(32), 9839–9843, doi:10.1073/pnas.1503598112.

- Turner, P. A., T. J. Griffis, J. M. Baker, X. Lee, J. T. Crawford, L. C. Loken, and R. T. Venterea (2016a), Regional-scale controls on dissolved nitrous oxide in the Upper Mississippi River, *Geophys. Res. Lett.*, *43*(9), 4400–4407, doi:10.1002/2013GL058740.
- Turner, P. A., J. M. Baker, T. J. Griffis, and R. T. Venterea (2016b), The impact of kura clover living mulch on nitrous oxide emissions in a corn/soybean system, *J. Environ. Qual.*, doi:10.2134/jeq2016.01.0036.
- Turner, R. E., and N. N. Rabalais (1991), Changes in Mississippi River water quality this century: Implications for coastal food webs, *Am. Inst. Biol. Sci.*, *41*(3), 140–147.
- US Department of State (2014), 2014 United States Climate Action Report,
- USEPA (2015), *Inventory of U.S. Greenhouse Gas Emissions and Sinks: 1990 - 2013*.
- Vauclin, M., S. R. Vieira, G. Vachaud, and D. R. Nielsen (1983), The Use of Cokringing with Limited Field Soil Observations, *Soil Sci. Soc. Am. J.*, *47*(2), 175–184.
- Velthof, G. L., J. W. van Groenigen, G. Gebauer, S. Pietrzak, S. C. Jarvis, M. Pinto, W. Corré, and O. Oenema (2000), Temporal stability of spatial patterns of nitrous oxide fluxes from sloping grassland, *J. Environ. Qual.*, *29*(5), 1397, doi:10.2134/jeq2000.00472425002900050005x.
- Venkiteswaran, J. J., M. S. Rosamond, and S. L. Schiff (2014), Nonlinear response of riverine N₂O fluxes to oxygen and temperature, *Environ. Sci. Technol.*, *48*(2), 1566–1573, doi:10.1021/es500069j.
- Venterea, R. T. (2013), Theoretical comparison of advanced methods for calculating nitrous oxide fluxes using non-steady state chambers, *Soil Sci. Soc. Am. J.*, *77*, 709, doi:10.2136/sssaj2013.01.0010.
- Venterea, R. T., and J. A. Coulter (2015), Split application of urea does not decrease and may increase nitrous oxide emissions in rainfed corn, *Agron. J.*, *107*, 337, doi:10.2134/agronj14.0411.
- Venterea, R. T., M. Bijesh, and M. S. Dolan (2011), Fertilizer source and tillage effects on yield-scaled nitrous oxide emissions in a corn cropping system., *J. Environ. Qual.*, *40*, 1521–1531, doi:10.2134/jeq2011.0039.
- Venterea, R. T., T. J. Clough, J. a. Coulter, and F. Breuillin-Sessoms (2015), Ammonium sorption and ammonia inhibition of nitrite-oxidizing bacteria explain contrasting soil N₂O production, *Sci. Rep.*, *5*(April), 12153, doi:10.1038/srep12153.
- Venterea, R. T., J. A. Coulter, and M. S. Dolan (2016), Evaluation of Intensive “4R” Strategies for Decreasing Nitrous Oxide Emissions and Nitrogen Surplus in Rainfed Corn, *J. Environ. Qual.*, doi:10.2134/jeq2016.01.0024.
- Wagner-Riddle, C., and G. W. Thurtell (1998), Nitrous oxide emissions from agricultural fields during winter and spring thaw as affected by management practices, *Nutr. Cycl. Agroecosystems*, *52*(2-3), 151–163, doi:10.1023/A:1009788411566.
- Wall, D., D. Mulla, S. Weiss, D. Wasley, T. E. Pearson, and B. Henningsgaard (2013), Nitrogen in Minnesota surface waters, , (Minnesota Pollution Control Agency).
- Wall, G. J., E. A. Pringle, and R. W. Sheard (1991), Intercropping red clover with silage corn for soil erosion control, *Can. J. Soil Sci.*, *71*(2), 137–145, doi:10.4141/cjss91-013.

- Wallin, M. B., M. G. Öquist, I. Buffam, M. F. Billett, J. Nisell, and K. H. Bishop (2011), Spatiotemporal variability of the gas transfer coefficient (k_{CO_2}) in boreal streams: Implications for large scale estimates of CO_2 evasion, *Global Biogeochem. Cycles*, 25(3), 1–14, doi:10.1029/2010GB003975.
- Wan, H., D. J. Mulla, and J. C. Galzki (2014), Using LiDAR and geographic information system data to identify optimal sites in southern Minnesota for constructed wetlands to intercept nonpoint source nitrogen, *J. Soil Water Conserv.*, 69(4), 115A–120A, doi:10.2489/jswc.69.4.115A.
- Wang, S., C. Liu, K. M. Yeager, G. Wan, J. Li, F. Tao, Y. Lü, F. Liu, and C. Fan (2009), The spatial distribution and emission of nitrous oxide (N_2O) in a large eutrophic lake in eastern China: Anthropogenic effects, *Sci. Total Environ.*, 407(10), 3330–3337, doi:10.1016/j.scitotenv.2008.10.037.
- Wanninkhof, R. (1992), Relationship between wind speed and gas exchange over the ocean, *J. Geophysical Res.*, 97(92), 7373–7382, doi:10.1029/92JC00188.
- Weintraub, S. R., P. G. Taylor, S. Porder, C. C. Cleveland, G. P. Asner, and A. R. Townsend (2014), Topographic controls on soil nitrogen availability in a lowland tropical forest, *Ecology*, 96(6), 1561–1574, doi:10.1890/14-0834.1.
- Weiss, R. F., and B. A. Price (1980), Nitrous oxide solubility in water and seawater, *Mar. Chem.*, 8, 347–359, doi:10.1016/0304-4203(80)90024-9.
- Xia, Y., Y. Li, C. Ti, X. Li, Y. Zhao, and X. Yan (2013), Is indirect N_2O emission a significant contributor to the agricultural greenhouse gas budget? A case study of a rice paddy-dominated agricultural watershed in eastern China, *Atmos. Environ.*, 77(2013), 943–950, doi:10.1016/j.atmosenv.2013.06.022.
- Yanai, J., T. Sawamoto, T. Oe, K. Kusa, K. Yamakawa, K. Sakamoto, T. Naganawa, K. Inubushi, R. Hatano, and T. Kosaki (2003), Atmospheric Pollutants and Trace Gases Factors in an Agricultural Field, *J. Environ. Qual.*, 32, 1965–1977.
- Yoon, T. K., H. Jin, N.-H. Oh, and J.-H. Park (2016), Technical note: Applying equilibration systems to continuous measurements of pCO_2 in inland waters, *Biogeosciences Discuss.*, (February), 1–34, doi:10.5194/bg-2016-54.
- Yu, Z., H. Deng, D. Wang, M. Ye, Y. Tan, Y. Li, Z. Chen, and S. Xu (2013), Nitrous oxide emissions in the Shanghai river network: Implications for the effects of urban sewage and IPCC methodology, *Glob. Chang. Biol.*, 19(3), 2999–3010, doi:10.1111/gcb.12290.
- Zemenchik, R. A., K. A. Albrecht, C. M. Boerboom, and J. G. Lauer (2000), Corn production with kura clover as a living mulch, *Agron. J.*, 92, 698–705, doi:10.2134/agronj2000.924698x.
- Zhang, W., and D. R. Montgomery (1994), Digital elevation model grid size, landscape representation, and hydrologic simulations, , 30(4), 1019–1028.
- Zhang, X., X. Lee, T. J. Griffis, A. E. Andrews, J. M. Baker, M. D. Erickson, N. Hu, and W. Xiao (2014), Quantifying nitrous oxide fluxes on multiple spatial scales in the Upper Midwest, USA, *Int. J. Biometeorol.*, 59(3), 299–310, doi:10.1007/s00484-014-0842-4.
- Zhong, Z., R. L. Lemke, and L. M. Nelson (2009), Nitrous oxide emissions associated

with nitrogen fixation by grain legumes, *Soil Biol. Biochem.*, 41(11), 2283–2291,
doi:10.1016/j.soilbio.2009.08.009.